ABSTRACT

Title of dissertation: WAVEFORM DESIGN
AND NETWORK SELECTION
IN WIDEBAND SMALL CELL NETWORKS

Yu-Han Yang, Doctor of Philosophy, 2013

Dissertation directed by: Professor K. J. Ray Liu
Department of Electrical and Computer Engineering

The explosion in demand for wireless data traffic in recent years has triggered rapid development and pervasive deployment of wireless communication networks. To meet the exponentially increasing demand, a promising solution is the concept of wideband small cells, which is based on the idea of using broader frequency bandwidth and employing more efficient radio frequency resource reuse by dense deployment of wideband, short-range, low cost and low power base-stations. Broader bandwidth provides substantial degrees of freedom as well as challenges for system design due to the abundant multipaths and thus interference in high speed systems under large delay spread channels. Reducing the transmission range and increasing the number of cells permit better spatial reuse of spectrum. With the proliferation of wideband small cells, the strategy of selection among multiple networks has significant impacts to the performance of users and to the load balance of the system. In this dissertation, we address these problems with a focus on waveform design and network selection.

In time-reversal communication systems, the time-reversal transmit waveform can boost the signal-to-noise ratio at the receiver with simple single-tap detection by utilizing channel reciprocity with very low transmitter complexity. However, the large delay spread gives rise to severe inter-symbol interference when the data rate is high, and the achievable transmission rate is further degraded in the multiuser downlink due to the inter-user interference. We study the weighted sum rate optimization problem by means of waveform design in the time-reversal multiuser downlink. We propose a new power allocation algorithm, which is able to achieve comparable sum rate performance to that of globally optimal power allocation. Further, we study the joint waveform design and interference pre-cancellation by exploiting the symbol information to further improve the performance by utilizing the information of previous symbols. In the proposed joint design, the causal interference is subtracted using interference pre-cancellation and the anti-causal interference can be further suppressed by waveform design with more degrees of freedom.

The second part of this dissertation is concerned with the wireless access network selection problem considering the negative network externality, i.e, the influence of subsequent users' decisions on an individual's throughput due to the limited available resources. We formulate the wireless network selection problem as a stochastic game with negative network externality and show that finding the optimal decision rule can be modelled as a multi-dimensional Markov decision process. A modified value iteration algorithm is proposed to efficiently obtain the optimal decision rule with a simple threshold structure, which enables us to reduce the storage space of the strategy profile. We further investigate the mechanism design problem

with incentive compatibility constraints, which enforce the networks to reveal the truthful state information. We analyze a data set of wireless LAN traces collected from campus networks, from which we observe that the number of user arrivals is approximately Poisson distributed; the session time and the waiting time to switch network can be approximated by exponential distributions. Based on the analysis, we formulate a wireless access network association game with both arriving strategy and switching strategy and validate the effectiveness of the proposed best response strategy.

WAVEFORM DESIGN AND NETWORK SELECTION IN WIDEBAND SMALL CELL NETWORKS

by

Yu-Han Yang

Dissertation submitted to the Faculty of the Graduate School of the
University of Maryland, College Park in partial fulfillment
of the requirements for the degree of
Doctor of Philosophy
2013

Advisory Committee:
Professor K. J. Ray Liu, Chair/Advisor
Professor Min Wu
Professor Michael C. Rotkowitz
Dr. Zoltan Safar
Professor Lawrence C. Washington

Dedication

To my Family —

Yue-Jiao Kao, De-Siang Yang,

and Wei-Fang Yang.

Acknowledgments

First and foremost, I would like to express my most esteemed gratitude to my advisor, Prof. K. J. Ray Liu for his patient guidance and continuous support during my Ph.D. study. I would not have been able to afford studying abroad without his help in applying scholarships in the very beginning. His constant enthusiasm and inspiration lead me to innovative research and contributing to the advance of wireless communications. I appreciate his influence in my motivation, attitude, and my professional and personal development. I will always remember his advice — broaden your vision, open your mind, and collaborate with people — which is the best thing I have learned throughout my graduate career.

I would also like to thank all members in my dissertation committee. I am specially grateful to Prof. Michael Rotkowitz for kind guidance on my research work and enormous help when I served as his TA, and thankful to Dr. Zoltan Safar for enlightening discussions on research and for generously sharing with me his invaluable industry experience. I also thank Prof. Min Wu and Prof. Lawrence Washington for their time and efforts serving on my dissertation committee and reviewing my thesis.

I would like to thank all members in Signal and Information Group for their pleasant friendship and assistance. I have learned so much from Wan-Yi Lin, Beibei Wang, and Yan Chen for their mentorship and collaboration on research. Special thanks to Feng Han, Yang Gao, Chunxiao Jiang, Zhenzhen Gao, Yi Han, and Ma Hang for various thoughtful discussions and the wonderful time during the past few

years.

I thank all my friends for the moments we shared, which gave me rest and reinvigoration to overcome the stresses of life. Thanks to Chen-Hung Wu for encouraging me to study abroad and the continuing cheering support. Special thanks to Angelina Y.-F. Ho for her companionship and love, which enriched and lightened my daily life during the past years.

Most importantly, I give my most sincere appreciation to my parents, Yue-Jiao Kao and De-Siang Yang, and my sister, Wei-Fang Yang. Without their endless love, encouragement, and emotional support, I would not have been able to walk through my graduate study to this important achievement. This dissertation is dedicated to them.

Table of Contents

List of Tables

List of Figures

Chapter 1

Introduction

1.1 Motivation

In recent years, the exponential increase of wireless devices such as smartphones and tablets has created an explosion of demand in indoor wireless data traffic. To meet such an expanding demand, a promising solution is the concept of wideband small cells, which is based on the idea of using broader frequency bandwidth and employing more efficient radio frequency resource reuse by dense deployment of wideband, short-range, low cost and low power base-stations.

It is well known that cell-size reduction is the simplest and most effective way to increase system capacity [51]. Moreover, transmission in a short distance evidently allows lower power-consumption at both base-stations and user equipments, and hence increases the battery life of mobile handset devices. Wideband small cells can further extend the coverage of macro-cells in indoor areas through the deployment by users. Wideband small cells offer high quality data services to indoor equipments by using prevailing broadband data access services (e.g., Digital Subscriber Lines (DSL), cable, etc.) as a backhaul for users to connect to the Internet, and therefore offload the traffic of indoor users from macro-cells. The traffic

offload based on users' deployment of small cells is not only beneficial to end-users due to better user experience, but also favorable for network operators because of the potential enhancement of system capacity. Therefore, wideband small cells as small-sized base-stations deployed in indoor environments are expected as the next major performance expansion in the evolution of wireless communications.

Broader bandwidth provides substantial degrees of freedom as well as challenges for system design due to the severe interference in high speed communications under large delay spread channels. The traditional time-reversal (TR) waveform [103] is able to boost the signal-to-noise ratio at the receiver with very low transmitter complexity in a severe multipath channel. Such a waveform is simply the time-reverse of the channel impulse response which is transmitted by propagating back through each multipath with channel reciprocity. In essence, the environment is performing deconvolution on the fly for the system. It can collect most energy of the multipaths to a single tap. The receiver complexity is hence very low due to the one-tap detection, that is, the receiver detects the received signal using only one sample instead of more complicated receive equalization.

The traditional time-reversal technique can be viewed as a simple matched-filter of the multipath channel which maximizes the signal-to-noise ratio (SNR) at the receiver when using single-tap detection. Such a waveform is optimal if only one symbol is transmitted. However, when the symbol duration is smaller than the channel delay spread, the symbol waveforms are overlapped and thus interfere with each other. When the symbol rate is very high, such inter-symbol interference (ISI) can be notably severe and causes crucial performance degradation [33,122]. Further,

in multi-user downlink scenarios, the time-reversal base-station uses each user's channel impulse response as the user's symbol waveform to modulate the symbols intended for that user. Despite the inherent randomness of the channel impulse responses, as long as they are not orthogonal to each other, which is almost always the case, these waveforms will inevitably interfere with each other when transmitted concurrently. Hence, the performance of TR transmission can be impaired and even limited by the inter-user interference (IUI). Moreover, interference can also be caused by incorporating multiple transmit antenna in the TR systems.

In a wideband environment, substantial degrees of freedom are available for the transmitted waveforms to be designed to combat the interference. Based on design criteria such as system performance, quality-of-service (QoS) constraints, or fairness among users, the waveform design can be formulated as an optimization problem with the transmitted waveforms as the optimization valuables. The basic idea of waveform design is to delicately adjust the amplitude and phase of each tap of the waveform based on the channel information, such that after convolving with the channel, the received signal at the receiver retains most of the intended signal strength and rejects or suppresses the interference as much as possible.

As to radio frequency reuse, reducing the network size and increasing the number of networks is effective in spatial reuse of spectrum [4]. With the recent proliferation of wireless devices and the ubiquity of wireless networks, users can connect to WiFi wireless networks through hot-spots or access points (APs) in most public areas. As the cellular networks usually have a broader range of coverage, the WiFi networks are smaller in its reachable range but more densely deployed. More-

over, the development of femtocells [19] also arouses more choices for cellular service subscribers. Therefore, when a user attempts to access a wireless network, oftentimes he/she may encounter a decision to choose one of multiple wireless networks. From a user's viewpoint, the decision of network association can lead to different quality of service during the session. From the perspective of a service provider, better allocation of users can provide more efficient utilization of resources such as signal power, temporal and spatial bandwidth.

In most current practical systems, the network association decision is often made based on the instantaneous signal-to-noise ratio (SNR) criterion, i.e., a user simply connects to the wireless network with the highest SNR. Such a strategy may be a good heuristic but is not optimal due to following reasons. First, SNR does not take into account the influence caused by other users, i.e., the *negative network externality* [35, 83], which means the negative effect on a user caused by other users with the same strategy in a network. For example, the traffic congestion caused by the vehicles that choose the same route delays each vehicle's traveling time. Thus, instead of SNR, the signal-to-interference-plus-noise ratio (SINR) should be considered. However, these instantaneous criteria only reflect the current condition without considering the future utility, which can be significantly degraded if subsequent users make the same decision. The wireless access network association problem is becoming more and more important due to its frequent occurrence in our daily life and the influence to efficient resource utilization.

1.2 Dissertation Outline and Contributions

From the above discussions, we can see that as wideband small cells are deployed more and more to meet the growing demand of wireless data traffic, there are many new challenges to the optimal system design. In this dissertation, we address these problems with a focus on waveform design and network selection. The first part of this dissertation is concerned with waveform design in time-reversal communication systems from the perspective of base-stations. The second part, from the perspective of users, is on the optimal strategy in wireless access network selection considering other users' strategies. The rest of this dissertation is organized as follows.

1.2.1 Near-Optimal Waveform Design for Sum Rate Optimization in Time-Reversal Multiuser Downlink Systems (Chapter 2)

In this chapter, we study the weighted sum rate optimization problem by means of waveform design in the time-reversal multiuser downlink where the receiver processing is based on a single sample. Power allocation has a significant impact on the waveform design problem. We propose a new power allocation algorithm named Iterative SINR Waterfilling, which is able to achieve comparable sum rate performance to that of globally optimal power allocation.

We further propose another approach called Iterative Power Waterfilling for multiple data streams. Iterative SINR Waterfilling provides better performance than Iterative Power Waterfilling in the scenario of high interference, while Itera-

tive Power Waterfilling can work under multiple data streams. Simulation results show the superior performance of the proposed algorithms in comparison with other waveform designs such as zero-forcing and conventional time-reversal waveform.

1.2.2 Joint Waveform Design and Interference Pre-Cancellation for Time-Reversal Systems (Chapter 3)

In Chapter 2, it is shown that waveform design can significantly improve the system performance of TR systems. However, when the symbol rate is very high, the severe ISI still limits the performance at high power region.

In this chapter, we study the joint waveform design and interference pre-cancellation by exploiting the symbol information to further improve the performance. In the proposed joint design, the causal ISI is subtracted by interference pre-cancellation and the anti-causal ISI can be further suppressed by the waveform design with the more abundant degrees of freedom. The transmitter utilizes the information of previous symbols to enhance the signal quality while the receiver structure remains simple. In the multi-user scenario, both the IUI and ISI can be similarly categorized by its causality, and then be tackled accordingly by the proposed joint design.

The resulting multi-user waveform design is a non-convex optimization problem, for which two iterative algorithms are proposed and both are guaranteed to converge to suboptimal solutions. Simulation results validate the convergence behavior and demonstrate the remarkable performance improvement over the non-joint

waveform design in Chapter 2.

1.2.3 Wireless Access Network Selection Game with Negative Network Externality (Chapter 4)

A key problem in wireless access network selection is to study the rational strategy considering the negative network externality, i.e, the influence of subsequent users' decisions on an individual's throughput due to the limited available resources. In this chapter, we formulate the wireless network selection problem as a stochastic game with negative network externality and show that finding the optimal decision rule can be modelled as a multi-dimensional Markov decision process (M-MDP). A modified value iteration algorithm is proposed to efficiently obtain the optimal decision rule with a simple threshold structure, which enables us to reduce the storage space of the strategy profile.

Further, we also investigate a mechanism design problem with incentive compatibility constraints, which enforce the networks to reveal the truthful state information. The formulated problem is a mixed integer programming problem which in general lacks an efficient solution. Exploiting the optimality of substructures, we propose a dynamic programming algorithm that can optimally solve the problem in the two-network scenario. For the multi-network scenario, the proposed algorithm can outperform the heuristic greedy approach in a polynomial-time complexity. Finally, simulation results are shown to validate the analysis and demonstrate the effectiveness of the proposed algorithms.

1.2.4 Wireless Network Association Game with Data-Driven Statistical Modelling (Chapter 5)

In this chapter, we analyze a data set of wireless LAN traces collected from campus networks, from which we observe that the user arrival distribution is approximately Poisson distributed; the session time and the waiting time to switch network can be approximated by exponential distributions. Based on the data analysis, we formulate a wireless access network association game as an M-MDP with both arriving strategy and switching strategy, where the best response strategy is an approximate Nash equilibrium.

A modified value iteration algorithm is proposed to search the best response strategy profile. Applying the proposed algorithm to the data-driven stochastic model, the best response strategy is shown to achieve a better individual expected utility while satisfying the individual rationality, and attain a near-optimal social welfare performance compared to other strategies such as the centralized method and the greedy algorithm.

Chapter 2

Near-Optimal Waveform Design for Sum Rate Optimization in Time-Reversal Multiuser Downlink Systems

As introduced in Chapter 1, the traditional time-reversal (TR) waveform [103] is able to boost the signal-to-noise ratio at the receiver with very low transmitter complexity in a severe multipath channel. Such a waveform is simply the time-reverse of the channel impulse response which is transmitted by propagating back through each multipath with channel reciprocity. The traditional TR waveform is optimal if only one symbol is transmitted. When the symbol rate is high, large delay spreads of the traditional TR waveform result in severe inter-symbol interference (ISI) [31, 33].

Several approaches have been proposed to suppress ISI. In [31], a zero-forcing (ZF) waveform can be adopted to minimize the ISI, but ZF does not take the noise into account. In [33], Emami *et. al.* improved the traditional time-reversal waveform with the minimum mean squared error (MMSE) waveform which suppresses both the ISI and noise.

Although the ZF and MMSE waveforms can successfully suppress the ISI and hence improve the performance of TR systems, they only consider the single-user scenario. In multiuser downlink communications, one transmitter broadcasts differ-

ent data streams to many receivers at the same time. Since each receiver is only interested in its own data stream, the unintended data streams introduce inter-user interference (IUI) to each receiver. In multiuser communications, due to the low complexity compared to nonlinear methods, linear transmit waveform design can be adopted to enhance the intended signal and suppress the IUI to maximize the transmission rate. Weighted sum rate is an important design criterion since weighting coefficients provide prioritization among different users in various applications. For example, the weights can be chosen as queue lengths to minimize the risk of buffer overflows [14], and the equal weights can be used to maximize the achievable sum rate corresponding to the system capacity.

In the literature, there are some prior works on sum rate optimization for MIMO broadcast channels with linear preprocessing. Some of these works [25,43,94] directly optimize the sum rate in the downlink, and some works [43, 91, 98] exploit the uplink-downlink duality [17, 52, 87, 100] to iteratively optimize the sum rate. Such an iterative solution based on virtual uplink first appeared in [80, 81]. In [87], the joint beamforming and power control solutions to the max-min SINR problem are developed. Cai *et. al.* further consider the max-min SINR problem subject to a weighted-sum power constraint in multi-cell downlink networks [17]. The approaches in [43] optimize the weighted sum rate under linear zero-forcing constraints and greedy algorithms are proposed to allocate data streams to users. In [91], the receiver is assumed to know the transmit power allocation, and thus, the receiver is able to normalize the received signal with the transmit power allocation and the resulting problem is shown to be convex. In [98], the weighted sum rate maximization

is modelled into minimizing the product of MSE, and sequential quadratic programming is used to locate a local optimum of the minimization. Most previous works on beamforming for multiuser MIMO downlink channels assume flat fading and do not consider the ISI introduced by multipath. ISI degrades the user's achievable rate as a self-interfering term proportional to its own transmit power. To the best of our knowledge, the systems with single-tap detection considering ISI and IUI have not been considered before. In order to tackle this problem, we propose a near-optimal waveform design to maximize the weighted sum rate by simultaneously suppressing the ISI and IUI. Pre-equalization for ISI and IUI is proposed in [2], where the design criterion is MSE and thus the problems they considered are convex. In this chapter, the waveform design in the multiuser downlink systems where the receiver processing is based on a single tap is formulated and shown to be similar to the downlink beamforming problem. Beamforming problems with the max-min SINR criteria are convex [17, 87] and thus can be solved optimally, but beamforming for weighted sum rate maximization is known to be a non-convex optimization problem. In tackling the non-convex sum rate maximization problem, d.c. (difference of convex functions) programming has been applied in recent literature (e.g., [34, 56]) by exploiting the fact that the sum rate can be written as difference of convex functions. In [56], Kha *et. al.* proposed an iterative algorithm in which the solution to a convex optimization problem is calculated at each iteration, which is accomplished by another iterative algorithm such as the interior point method. Thus, the overall complexity of such a method is quite high. Other d.c. programming approaches (e.g., [34]) claimed to be able to obtain the global optimum are mostly based on

combinatorial optimization such as branch-and-bound global search and usually require demanding computational complexity. A practical approach is provided in [57] to maximize weighted sum rate for MIMO-OFDM systems but each user has only a single data stream. In this chapter, we further provide an efficient solution to the weighted sum rate maximization problem for multiple data streams. For single data stream, the proposed algorithm is shown to perform better than [57] in the scenario of high interference.

The proposed algorithms are based on the well-known uplink-downlink duality, i.e., the waveform design for the downlink can be obtained using virtual uplink, given any power allocation. However, the power allocation problem for sum rate optimization is non-convex for either uplink or downlink. By exploiting the relation between the allocated power and the SINR targets, we propose a power allocation algorithm called *Iterative SINR Waterfilling* which can achieve comparable performance to the globally-optimal power allocation. The essential idea of the proposed scheme is to first allocate the SINRs to the users to maximize the weighted sum rate, and with the allocated target SINRs, the corresponding power allocation can easily be determined. For multiple data streams, we also propose an iterative power allocation algorithm called *Iterative Power Waterfilling* which is the multiple-data-stream extension of the *modified iterative waterfilling* in [124]. Simulation results show that both the proposed approaches significantly outperform traditional waveform designs such as zero-forcing and time-reversal waveforms.

This chapter is organized as follows. In Section 2.1, the system model and problem formulation are described. In Section 2.2, we introduce the proposed wave-

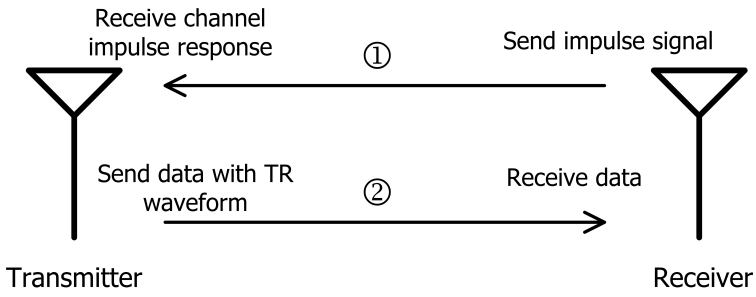

Figure 2.1: The schematic diagram of the time reversal system.

form design which alternately optimizes between calculating the waveform and the power allocation vector. The waveform design for multiple data streams is proposed in Section 2.3. Finally, the numerical simulation in Section 2.4 illustrates the performance compared with traditional methods, and conclusion is drawn in Section 2.5.

2.1 System Model and Problem Formulation

In the time reversal system [103], the receiver first sends an impulse signal, which is then received by the transmitter as a channel impulse response. Utilizing the channel impulse response, the transmitter forms the TR waveform and sends data symbols using the TR waveform. Figure 2.1 shows the schematic diagram of the time reversal system. In this chapter, we consider multiuser downlink multipath channels with one transmitter and K users. The receive signal of the kth user at time m, $y_k[m]$, can be written as

$$y_k[m] = \sum_l h_k[m-l]s[l] + n_k[m], \tag{2.1}$$

where $s[m]$ is the transmit signal and $h_k[m]$ denotes the channel impulse response of user k. The channel length of $h_k[m]$ is denoted by L_k, i.e., $h_k[m] = 0$ for $m < 0$ and $m \geq L_k$. Writing (2.1) in a matrix form, we have the receive signal vector of the kth user as

$$\mathbf{y}_k = \mathbf{H}_k \mathbf{s} + \mathbf{n}_k = \mathbf{H}_k \left(\sum_{j=1}^{K} \mathbf{u}_j \sqrt{p_j} x_j \right) + \mathbf{n}_k, \tag{2.2}$$

where $\mathbf{y}_k$ is a $(2L-1) \times 1$ vector with $L = \max_k L_k$, $\mathbf{u}_j$ is the transmit waveform, p_j is the transmit power allocated to user j, x_j is the intended signal for user j, and $\mathbf{n}_k$ is the additive white Gaussian noise (AWGN) with mean zero and variance σ^2. In (2.2), $\mathbf{H}_k$ is a $(2L-1) \times L$ Toeplitz matrix with each column vector being the shifted version of $\{h_k[m]\}_{m=1}^{L}$, .

In the time-reversal communication system, user k estimates the received signal by only $y_k[L]$. Let $\mathbf{H}_k^{(l)}$ denote the lth row of $\mathbf{H}_k$, the symbol at time slot l for user k as $x_k(l)$, and $[\mathbf{n}_k]_L$ as the Lth element of $\mathbf{n}_k$. The complete characterization of the signal with ISI and IUI is given by

$$\begin{aligned} y_k[L] = \mathbf{H}_k^{(L)} \mathbf{u}_k \sqrt{p}_k x_k(L) + \mathbf{H}_k^{(L)} \left(\sum_{j=1, j \neq k}^{K} \mathbf{u}_j \sqrt{p_j} x_j(L) \right) \\ + \sum_{l=1, l \neq L}^{2L-1} \mathbf{H}_k^{(l)} \left(\sum_{j=1}^{K} \mathbf{u}_j \sqrt{p_j} x_j(l) \right) + [\mathbf{n}_k]_L. \end{aligned} \tag{2.3}$$

Assume that user k only decodes its own current symbol $x_k(L)$ and considers the interferences (IUI and ISI) as noise. Then the SINR of user k is given as

$$\mathrm{SINR}_k^{\mathrm{DL}} = \frac{\mathbf{u}_k^H \mathbf{R}_k^{(1)} \mathbf{u}_k p_k}{\mathbf{u}_k^H \mathbf{R}_k^{(0)} \mathbf{u}_k p_k + \sum_{j=1, j \neq k}^{K} \mathbf{u}_j^H \mathbf{R}_k \mathbf{u}_j p_j + \sigma^2}, \tag{2.4}$$

where $\mathbf{R}_k^{(1)} = \mathbf{H}_k^{(L)H} \mathbf{H}_k^{(L)}$, $\mathbf{R}_j = \mathbf{H}_j^H \mathbf{H}_j$, and $\mathbf{R}_k^{(0)} = \mathbf{R}_k - \mathbf{R}_k^{(1)}$. The superscript

DL denotes the downlink. The first term and the second term in the denominator denote ISI and IUI, respectively.

In this chapter, we jointly design the waveform $\mathbf{U} = [\mathbf{u}_1, ..., \mathbf{u}_K]$ and power allocation vector $\mathbf{p} = [p_1, ..., p_K]^T$ to maximize the weighted sum rate subject to a total power constraint $P_{\max}$, i.e.,

$$\begin{aligned} \boldsymbol{\mathcal{P}}_{\text{Rate}}^{\text{DL}}: \quad \max_{\mathbf{p},\mathbf{U}} \quad & \sum_{k=1}^{K} \alpha_k \log\left(1 + \text{SINR}_k^{\text{DL}}\right) \\ \text{s.t.} \quad & \mathbf{1}^T\mathbf{p} \leq P_{\max}, \mathbf{u}_i^H\mathbf{u}_i = 1, p_i \geq 0, \forall i, \end{aligned} \tag{2.5}$$

where α_k denotes the rate weighting coefficient for user k, and $\mathbf{1}$ is an all-one vector with K elements.

2.2 Iterative Algorithm for the Weighted Sum Rate Optimization

In this section, we develop an iterative algorithm for the weighted sum rate optimization in multiuser downlink time-reversal system. Since the waveform design structure is decoupled in the virtual uplink system and the uplink-downlink duality [52, 87, 100] builds a bridge between the two systems, the proposed algorithm first solves the waveform design and power allocation in the virtual uplink system, and then transforms the solution into the original downlink problem.

The optimal power allocation problem for sum rate maximization is non-convex either in downlink or virtual uplink. In general, solving the global optimum for a non-convex problem requires an exhaustive search, which is computationally impractical. Hence, we propose an algorithm to efficiently attain a satisfactory near-optimal solution for the non-convex power allocation problem. We will show in

Section 2.4 by simulations that the proposed algorithm can reach a solution which is very closed to global optimum.

2.2.1 Uplink-Downlink Duality

As shown in (2.4), the SINR of every user depends on the waveforms of all users, so all users' waveforms have to be jointly designed at the same time. Thus, the waveform design is complicated in the downlink system. With the uplink-downlink duality [52, 87, 100], the downlink optimal waveform can be individually decided in the virtual uplink with fixed power allocation.

The virtual uplink problem is constructed as follows.

$$\begin{aligned} \boldsymbol{\mathcal{P}}_{\text{Rate}}^{\text{UL}}: \quad \max_{\mathbf{q},\mathbf{U}} \quad & \sum_{k=1}^{K} \alpha_k \log\left(1+\text{SINR}_k^{\text{UL}}\right) \\ \text{s.t.} \quad & \mathbf{1}^T\mathbf{q} \leq P_{\max}, \mathbf{u}_i^H\mathbf{u}_i = 1, q_i \geq 0, \forall i, \end{aligned} \tag{2.6}$$

where $\mathbf{q} = [q_1, ..., q_K]^T$ is the power allocation in the virtual uplink, the downlink transmit waveform $\{\mathbf{u}_j\}_{j=1}^K$ becomes the uplink receive waveform, and the uplink SINR for user k is

$$\text{SINR}_k^{\text{UL}} = \frac{\mathbf{u}_k^H\mathbf{R}_k^{(1)}\mathbf{u}_k q_k}{\mathbf{u}_k^H\mathbf{R}_k^{(0)}\mathbf{u}_k q_k + \sum_{j=1,j\neq k}^{K}\mathbf{u}_k^H\mathbf{R}_j\mathbf{u}_k q_j + \sigma^2}, \tag{2.7}$$

where q_k is the transmit power of user k in the virtual uplink, and the superscript UL denotes the virtual uplink. Examining the difference between (2.4) and (2.7), we can see that $\text{SINR}_k^{\text{UL}}$ only depends on one user's waveform $\mathbf{u}_k$, and thus the waveform design structure is decoupled in the uplink with the solution given by the generalized eigenvalue problem [95].

By exploiting the fact that the SINR achievable regions are the same [100] for the two dual problems, we develop an iterative algorithm to solve $\boldsymbol{\mathcal{P}}_{\text{Rate}}^{\text{DL}}$ by first solving $\boldsymbol{\mathcal{P}}_{\text{Rate}}^{\text{UL}}$. It is now well-known [87] that for given SINR targets $\{\gamma_k\}_{k=1}^K$, the minimum required total power for the downlink and its virtual uplink are the same. On the other hand, given a sum-power constraint $P_{\max}$, the achievable SINR region is the same for both the downlink and its virtual uplink. Therefore, the solution for $\boldsymbol{\mathcal{P}}_{\text{Rate}}^{\text{UL}}$ is also the solution for $\boldsymbol{\mathcal{P}}_{\text{Rate}}^{\text{DL}}$. Because the transmit waveforms $\{\mathbf{u}_j\}_{j=1}^K$ in $\boldsymbol{\mathcal{P}}_{\text{Rate}}^{\text{DL}}$ cannot be directly solved, the proposed algorithm iterates between computing the waveforms $\{\mathbf{u}_j\}_{j=1}^K$ and solving for the uplink power vector $\mathbf{q}$. After the iteration for virtual uplink is completed, the downlink power vector $\mathbf{p}$ is then calculated using the waveforms $\{\mathbf{u}_j\}_{j=1}^K$ and the virtual uplink power vector $\mathbf{q}$.

Given a fixed power allocation, the optimal waveform design of $\{\mathbf{u}_j\}_{j=1}^K$ can be directly derived by leveraging the uplink-downlink duality. Based on this, we can then focus on the design of power allocation. We propose a power allocation algorithm to be employed in the iterative sum rate optimization algorithm. Due to the non-convexity of the problem, to obtain the global optimum in general requires exhaustive search. The proposed algorithm can attain a sub-optimum that is very close to the global optimum in terms of weighted sum rate performance and thus much better than traditional methods such as zero-forcing and time-reversal waveforms. In the following two subsections, we describe the waveform design and the power allocation algorithm in detail.

2.2.2 Individual Waveform Design

The $\mathrm{SINR}_k^{\mathrm{UL}}$ in (2.7) can also be written as

$$\mathrm{SINR}_k^{\mathrm{UL}} = \frac{q_k \mathbf{u}_k^H \mathbf{R}_k^{(1)} \mathbf{u}_k}{\mathbf{u}_k^H \left(q_k \mathbf{R}_k^{(0)} + \sum_{j \neq k} q_j \mathbf{R}_j + \sigma^2 \mathbf{I} \right) \mathbf{u}_k}, \tag{2.8}$$

where only $\mathbf{u}_k$ is involved and thus $\mathrm{SINR}_k^{\mathrm{UL}}$ can be optimized by choosing $\mathbf{u}_k$ to be the principle eigenvector of the generalized eigenvalue problem,

$$q_k \mathbf{R}_k^{(1)} \mathbf{u}_k = \mathrm{SINR}_k^{\mathrm{UL}} \left(q_k \mathbf{R}_k^{(0)} + \sum_{j \neq k} q_j \mathbf{R}_j + \sigma^2 \mathbf{I} \right) \mathbf{u}_k, \tag{2.9}$$

This SINR-maximizing waveform turns out to be the MMSE waveform

$$\mathbf{u}_k^{\mathrm{MMSE}} = c_k^{\mathrm{MMSE}} \left(\sum_{j=1}^{K} q_j \mathbf{R}_j + \sigma^2 \mathbf{I} \right)^{-1} \mathbf{H}_k^{(1)H}. \tag{2.10}$$

Here, c_k^{MMSE} is a constant such that the norm of $\mathbf{u}_k^{\mathrm{MMSE}}$ is normalized to unit. This can be easily verified by substituting (2.10) into (2.9), and the corresponding eigenvalue can be obtained as $\mathrm{SINR}_k^{\mathrm{UL}} = \mathbf{H}_k^{(1)} \left(q_k \mathbf{R}_k^{(0)} + \sum_{j \neq k} q_j \mathbf{R}_j + \sigma^2 \mathbf{I} \right)^{-1} \mathbf{H}_k^{(1)H}$.

2.2.3 Power Allocation: Iterative SINR Waterfilling

Given fixed $\{\mathbf{u}_j\}_{j=1}^K$, the problem $\boldsymbol{\mathcal{P}}_{\mathrm{Rate}}^{\mathrm{UL}}$ becomes solving the power allocation vector $\mathbf{q}$ given a sum power constraint $P_{\max}$. It can be verified that this problem is non-convex so the global optimal solution is difficult to search. Instead, our objective of the power allocation algorithm is to efficiently obtain a near-optimal solution.

We propose a new power allocation algorithm called *Iterative SINR Waterfilling*. The key feature of the proposed algorithm is that, instead of directly allocating the power $\{q_k\}_{k=1}^K$, we first allocate the SINRs $\{\gamma_k\}_{k=1}^K$ to maximize the weighted

sum rate under the sum power constraint. And then with the allocated SINRs, the power allocation of $\{q_k\}_{k=1}^K$ can be easily established. The conversion to SINR waterfilling changes the objective function to be convex and the feasible region to be non-convex. In the following, it will be seen that such conversion can better capture the structure of interference. The SINR is expressed in terms of the power by

$$\gamma_k = \mathrm{SINR}_k^{\mathrm{UL}} = \frac{\mathbf{u}_k^H \mathbf{R}_k^{(1)} \mathbf{u}_k q_k}{\mathbf{u}_k^H \mathbf{R}_k^{(0)} \mathbf{u}_k q_k + \sum_{j \neq k} \mathbf{u}_k^H \mathbf{R}_j \mathbf{u}_k q_j + \sigma^2}. \tag{2.11}$$

Let $\mathbf{D}$ be a diagonal matrix with $[\mathbf{D}]_{kk} = \gamma_k / \mathbf{u}_k^H \mathbf{R}_k^{(1)} \mathbf{u}_k$, and

$$[\mathbf{\Phi}]_{kj} = \begin{cases} \mathbf{u}_j^H \mathbf{R}_k \mathbf{u}_j, & k \neq j \\ \mathbf{u}_k^H \mathbf{R}_k^{(0)} \mathbf{u}_k, & k = j \end{cases}. \tag{2.12}$$

On the other hand, rewriting (2.11), we can represent the power allocation vector $\mathbf{q}$ in terms of $\{\gamma_k\}_{k=1}^K$ by

$$\mathbf{q} = \left(\mathbf{I} - \mathbf{D}\mathbf{\Phi}^T\right)^{-1} \mathbf{D}\boldsymbol{\sigma}, \tag{2.13}$$

where $\boldsymbol{\sigma}$ is a $K \times 1$ vector of all elements equal to σ^2. With (2.13), the power allocations $\{q_k\}_{k=1}^K$ can be obtained from the SINR targets $\{\gamma_k\}_{k=1}^K$.

Then the weighted sum rate optimization problem in terms of $\{\gamma_k\}_{k=1}^K$ can be reformulated as

$$\max_{\gamma_1,\ldots,\gamma_K} \quad \sum_{k=1}^K \alpha_k \log\left(1+\gamma_k\right), \tag{2.14}$$

$$\text{s.t.} \quad \mathbf{1}^T \left(\mathbf{I} - \mathbf{D}\mathbf{\Phi}^T\right)^{-1} \mathbf{D}\boldsymbol{\sigma} \leq P_{\max}, \tag{2.15}$$

$$\rho\left(\mathbf{D}\mathbf{\Phi}^T\right) < 1, \tag{2.16}$$

where $\rho(\cdot)$ denotes the spectral radius. Inequality (2.15) denotes the sum power constraint in terms of $\{\gamma_k\}_{k=1}^K$. The feasibility condition (2.16) and the constraint

that the obtained power $\{q_k\}_{k=1}^K$ are all non-negative are equivalent to each other. The detailed proof can be found in [13, Theorem 2]. One direction can be shown by observing that in (2.13), $\left(\mathbf{I}-\mathbf{D}\mathbf{\Phi}^T\right)^{-1}=\sum_{i=0}^{\infty}(\mathbf{D}\mathbf{\Phi}^T)^i$ if $\rho\left(\mathbf{D}\mathbf{\Phi}^T\right)<1$ (cf. [49, p.301]), and the matrix $\mathbf{D}\mathbf{\Phi}^T$ is element-wise positive.

According to the Karush-Kuhn-Tucker (KKT) conditions, the optimum γ_k must satisfy

$$\gamma_k=\left(\frac{\alpha_k}{\lambda t_k}-1\right)^+, \tag{2.17}$$

$$\mathbf{1}^T\left(\mathbf{I}-\mathbf{D}\mathbf{\Phi}^T\right)^{-1}\mathbf{D}\boldsymbol{\sigma}=P_{\max}, \tag{2.18}$$

$$\rho\left(\mathbf{D}\mathbf{\Phi}^T\right)<1, \tag{2.19}$$

where λ is the KKT multiplier and

$$t_k=\frac{\mathbf{u}_k^H\mathbf{R}_k^{(1)}\mathbf{u}_k}{\gamma_k^2}\mathbf{1}^T\left(\mathbf{I}-\mathbf{D}\mathbf{\Phi}^T\right)^{-1}\mathbf{D}\mathbf{e}_k\mathbf{e}_k^T\left(\mathbf{I}-\mathbf{D}\mathbf{\Phi}^T\right)^{-1}\mathbf{D}\boldsymbol{\sigma}, \tag{2.20}$$

and $\mathbf{e}_k$ is the kth column of a $K\times K$ identity matrix. The term t_k is a function of $\{\gamma_k\}_{k=1}^K$, i.e., it implicitly captures the interference introduced by the SINR allocation. Next, in order to solve λ, we show the monotonicity of λ in the left hand side of (2.18) and (2.19).

Lemma 1 *Let $\mathbf{\Lambda}$ be a square diagonal matrix with positive diagonal elements, and $\mathbf{S}$ be a square matrix with positive elements. Then $\rho(\mathbf{\Lambda}\mathbf{S})\leq\rho(\mathbf{\Lambda})\rho(\mathbf{S})$.*

Proof: Let $\mathbf{x}$ and $\mathbf{y}$ be the eigenvectors corresponding to the maximum eigenvalues of $\mathbf{\Lambda}\mathbf{S}$ and $\mathbf{\Lambda}^{1/2}\mathbf{S}\mathbf{\Lambda}^{-1/2}$, respectively, with $\|\mathbf{x}\|=1$, and $\|\mathbf{y}\|=\|\mathbf{\Lambda}^{1/2}\mathbf{x}\|$. We

have $\|\mathbf{y}\|^2 \leq \rho(\mathbf{\Lambda})\|\mathbf{x}\|^2$. Then,

$$\begin{aligned}\rho(\mathbf{\Lambda S}) = \mathbf{x}^T(\mathbf{\Lambda S})\mathbf{x} &\leq \rho(\mathbf{\Lambda}^{1/2}\mathbf{S}\mathbf{\Lambda}^{-1/2})\|\mathbf{y}\|^2 \\ &\leq \rho(\mathbf{S})\rho(\mathbf{\Lambda}). \end{aligned} \tag{2.21}$$

□

Proposition 1 *$\rho(\mathbf{D\Phi}^T)$ is monotonically decreasing with λ. $\mathbf{1}^T\left(\mathbf{I}-\mathbf{D\Phi}^T\right)^{-1}\mathbf{D}\boldsymbol{\sigma}$ is also monotonically decreasing with λ if $\rho(\mathbf{D\Phi}^T) < 1$.*

Proof: Assume $\hat{\lambda} > \lambda$. From (2.17), we have $\hat{\gamma_k} \leq \gamma_k$ and $\rho(\hat{\mathbf{D}}\mathbf{D}^{-1}) \leq 1$. With *Lemma 1*,

$$\begin{aligned}\rho(\hat{\mathbf{D}}\mathbf{\Phi}^T) = \rho(\hat{\mathbf{D}}\mathbf{D}^{-1}\mathbf{D}\mathbf{\Phi}^T) &\leq \rho(\hat{\mathbf{D}}\mathbf{D}^{-1})\rho(\mathbf{D}\mathbf{\Phi}^T) \\ &\leq \rho(\mathbf{D}\mathbf{\Phi}^T). \end{aligned} \tag{2.22}$$

Thus, $\rho(\mathbf{D\Phi}^T)$ is monotonically decreasing with λ.

If $\rho(\mathbf{D\Phi}^T) < 1$, then $\left(\mathbf{I}-\mathbf{D\Phi}^T\right)^{-1} = \sum_{r=0}^{\infty}\left(\mathbf{D\Phi}^T\right)^r$ (cf. [49, p.301]). We have

$$\begin{aligned}\mathbf{1}^T\left(\mathbf{I}-\mathbf{D\Phi}^T\right)^{-1}\mathbf{D}\boldsymbol{\sigma} &= \mathbf{1}^T\sum_{r=0}^{\infty}\left(\mathbf{D\Phi}^T\right)^r\mathbf{D}\boldsymbol{\sigma} \\ &\geq \mathbf{1}^T\sum_{r=0}^{\infty}\left(\hat{\mathbf{D}}\mathbf{\Phi}^T\right)^r\hat{\mathbf{D}}\boldsymbol{\sigma}. \end{aligned} \tag{2.23}$$

Thus, $\mathbf{1}^T\left(\mathbf{I}-\mathbf{D\Phi}^T\right)^{-1}\mathbf{D}\boldsymbol{\sigma}$ is also monotonically decreasing with λ if $\rho(\mathbf{D\Phi}^T) < 1$.

□

Since the γ_k in (2.17), $\rho(\mathbf{D\Phi}^T)$, and $\mathbf{1}^T\left(\mathbf{I}-\mathbf{D\Phi}^T\right)^{-1}\mathbf{D}\boldsymbol{\sigma}$ are all monotonic with λ, the bisection search can be applied to efficiently compute the λ such that the power constraint is satisfied. In the one dimensional bisection search, the initial

upper bound of λ can be set as $\max_k \alpha_k/t_k$ since the SINR targets $\{\gamma_k\}_{k=1}^K$ are all zero for λ higher than this value. The lower bound can be set as a small positive number, which corresponds to very large values of $\{\gamma_k\}_{k=1}^K$.

Eqn. (2.17) is a waterfilling-like solution with a feasibility constraint (2.19) and a nonlinear power constraint (2.18). The t_k can be considered as a modification term to the water level due to the effect of the interference. In solving the optimum γ_k, we can first fix t_k, and then SINR target γ_k is found by using bisection search for λ and substituting λ into (2.17). The new γ_k is then used to update t_k as in (2.20). The procedure is repeated until convergence. The proposed Iterative SINR Waterfilling is summarized in Table 2.1.

We can incorporate a memory term for γ_k to slow down the update and the convergence can be improved. In the nth iteration, the $\gamma_k(n)$ can be calculated by $\gamma_k(n) = \beta\gamma_k^{\text{new}}(n) + (1-\beta)\gamma_k(n-1)$, where $\gamma_k^{\text{new}}(n)$ is the one obtained after the bisection search and β is the forgetting factor with $0 < \beta < 1$.

2.2.4 Iterative Sum Rate Optimization

The iterative sum rate optimization algorithm iterates between calculating the waveforms $\{\mathbf{u}_j\}_{j=1}^K$ using (2.10) and the power allocation $\mathbf{q}$ using Table 2.1 in the virtual uplink. The iterative algorithm is not guaranteed to converge. However, very fast convergence is almost always observed in the numerical simulation. When the algorithm converges, the obtained solution is a fixed point of (2.17)-(2.20), i.e., the solution satisfies the KKT conditions. In case it does not converge or it takes a

Table 2.1: Iterative SINR Waterfilling

(i) Given $\mathbf{q}$, initialize γ_k with (2.11).

(ii) **Loop**:

1. Calculate t_k using (2.20).
2. Bisection search λ with (2.17)-(2.19), i.e.,
   (a) Set bisection upper bound $\lambda^{\max} = \max_k \alpha_k/t_k$,
   and lower bound $\lambda^{\min} = \delta > 0$.
   (b) **Loop**:
   Set $\lambda = \frac{1}{2}(\lambda^{\max} + \lambda^{\min})$.
   Compute $\gamma_k = \left(\frac{\alpha_k}{\lambda t_k} - 1\right)^+$.
   If $\rho\left(\mathbf{D}\mathbf{\Phi}^T\right) < 1$ **then**
   If $\mathbf{1}^T\left(\mathbf{I} - \mathbf{D}\mathbf{\Phi}^T\right)^{-1}\mathbf{D}\boldsymbol{\sigma} < P_{\max}$ **then**
   $\lambda^{\max} = \lambda$.
   else
   $\lambda^{\min} = \lambda$.
   else
   $\lambda^{\min} = \lambda$.
   Until $|\mathbf{1}^T\left(\mathbf{I} - \mathbf{D}\mathbf{\Phi}^T\right)^{-1}\mathbf{D}\boldsymbol{\sigma} - P_{\max}| < \epsilon$.
3. With γ_k obtained in last step, compute $\mathbf{q}$ by (2.13).

Until $\mathbf{q}$ converges or the max. number of iterations is reached.

Table 2.2: Iterative Weighted Sum Rate Optimization Algorithm for Single Data Stream

(i) Initialize $q_k = P_{\max}/K$.

(ii) **Loop** (uplink optimization):

1. Calculate $\{\mathbf{u}_j\}_{j=1}^K$ by (2.10).
2. Calculate $\mathbf{q}$ using *Iterative SINR Waterfilling*.

Until $\mathbf{q}$ and $\{\mathbf{u}_j\}_{j=1}^K$ converges or the max. number of iterations is reached.

(iii) Compute γ_k by (2.11).

(iv) Obtain downlink power vector $\mathbf{p}$ by (2.24).

long time to converge, the algorithm stops when the maximum number of iterations is reached. The solution obtained in each iteration is always feasible regardless of convergence. Hence, after convergence or the maximum number of iterations is reached, we can compute the corresponding achievable SINR targets $\{\gamma_k\}_{k=1}^K$ and the downlink power allocation $\mathbf{p}$ can then be obtained similar to (2.13), i.e.,

$$\mathbf{p} = (\mathbf{I} - \mathbf{D}\boldsymbol{\Phi})^{-1}\mathbf{D}\boldsymbol{\sigma}. \tag{2.24}$$

The proposed algorithm for the weighted sum rate optimization algorithm is summarized in Table 2.2. After convergence or maximum number of iterations is reached, we take the variables obtained at the last iteration as the solution. The performance may be better if the iterative algorithm keeps track of all passing solutions and chooses the best solution when the maximum number of iterations is reached. However, keeping track of all passing solutions requires a heavy overhead of space complexity but does not contribute much to the averaged performance due to the rareness of the non-converging cases. We have conducted simulations and verified that the performance difference is not perceivable. Hence, concerning the complexity and performance tradeoff, we choose to use the variables obtained at the last iteration instead of keeping track of all passing solutions.

The accuracy of using the virtual uplink to compute the solution of the downlink is commented as follows. Given fixed transmit waveforms $\{u_j\}_{j=1}^K$, the power allocation problems to minimize the required sum power in the uplink and the downlink for achieving certain SINR targets are dual problems [87, 100]. As a consequence, the achievable weighted sum rates of the uplink and the downlink under

the same sum power constraint are exactly the same. The solution in the uplink can be transformed into the downlink using (2.13), where the SINR targets are calculated by the uplink powers using (2.11), to achieve exactly identical SINRs and thus exactly the same weighted sum rate.

2.3 Multiuser MIMO Downlink with Multiple Data Streams

In MIMO time-reversal systems where multiple data streams are transmitted to each user, the transmit waveforms of different data streams have a significant impact on the achievable rates of all users. The proposed Iterative SINR Waterfilling can only work for systems with single data streams. In this section, we first describe the system model and then also develop an iterative algorithm for the waveform design.

2.3.1 System Model

The transmitter is now equipped with N_t transmit antennas. Each of the K users has $N_{r,k}$ receive antennas. The transmitter is transmitting M_k data streams to user k. The $N_{r,k} \times 1$ receive signal vector of the kth user at time m, $\mathbf{y}_k[m]$, can be written as $\mathbf{y}_k[m] = \sum_l \mathbf{H}_k[m-l]\mathbf{s}[l] + \mathbf{n}_k[m]$, where the $N_t \times 1$ vector $\mathbf{s}[m]$ is the transmit signal at time m and the $N_{r,k} \times N_t$ matrices $\{\mathbf{H}_k[m]\}_{m=0}^{L-1}$ denote the MIMO channel impulse response of user k at time m. We assume each channel is

L-tap. In a matrix form, the receive signal vector of the kth user is given by

$$\begin{aligned}\mathbf{y}_k &= \mathbf{H}_k\mathbf{s} + \mathbf{n}_k \\ &= \mathbf{H}_k\left(\mathbf{U}_k\sqrt{\mathbf{P}_k}\mathbf{x}_k + \sum_{j\neq k}\mathbf{U}_j\sqrt{\mathbf{P}_j}\mathbf{x}_j\right) + \mathbf{n}_k,\end{aligned} \tag{2.25}$$

where $\mathbf{y}_k = [\mathbf{y}_k^T[1], ..., \mathbf{y}_k^T[2L-1]]^T \in \mathbb{C}^{(2L-1)N_{r,k}}$, and the $M_k \times 1$ vector $\mathbf{x}_k$ comprises M_k data streams intended for user k. The matrix $\mathbf{U}_k = [\mathbf{U}_k^T[1], ..., \mathbf{U}_k^T[L]]^T \in \mathbb{C}^{LN_t \times M_k}$ is the transmit waveform for user k. The diagonal matrix $\mathbf{P}_k = diag\{p_{k1}, ..., p_{kM_k}\}$ is the power allocated to the M_k data streams of user k. $\mathbf{n}_k \in \mathbb{C}^{(2L-1)N_{r,k}}$ denotes the additive white Gaussian noise and each element of $\mathbf{n}_k$ is with zero mean and variance σ_k^2. The channel $\mathbf{H}_k \in \mathbb{C}^{(2L-1)N_{r,k}\times LN_t}$ is a block-Toeplitz matrix in which each sub-block $\mathbf{H}_k[m] \in \mathbb{C}^{N_{r,k}\times N_t}$ is the channel matrix of receiver k at time m, i.e.,

$$\mathbf{H}_k = \begin{bmatrix} \mathbf{H}_k[1] & \mathbf{0} & ... & \mathbf{0} \\ \mathbf{H}_k[2] & \mathbf{H}_k[1] & ... & \mathbf{0} \\ \vdots & \vdots & \ddots & \vdots \\ \mathbf{0} & \mathbf{0} & ... & \mathbf{H}_k[1] \end{bmatrix}, \tag{2.26}$$

In the MIMO time-reversal system, users perform the single-tap detection by considering only the receive signal vector at time L, i.e., $\mathbf{y}_k[L]$. Let $\mathbf{H}_k^{(l)}$ denote the lth sub-block row of $\mathbf{H}_k$, e.g., $\mathbf{H}_k^{(L)} = [\mathbf{H}_k[L], ..., \mathbf{H}_k[1]]$. After processing $\mathbf{y}_k[L]$ with receive filter $\mathbf{V}_k$, the complete characterization of the signal, ISI and IUI is given by

$$\begin{aligned}\hat{\mathbf{x}}_k(L) &= \mathbf{V}_k^H\mathbf{y}_k[L] \\ &= \mathbf{V}_k^H\mathbf{H}_k^{(L)}\mathbf{U}_k\sqrt{\mathbf{P}_k}\mathbf{x}_k(L) + \mathbf{V}_k^H\mathbf{H}_k^{(L)}\left(\sum_{j\neq k}\mathbf{U}_j\sqrt{\mathbf{P}_j}\mathbf{x}_j(L)\right) \\ &\quad + \sum_{l\neq L}\mathbf{V}_k^H\mathbf{H}_k^{(l)}\left(\sum_j\mathbf{U}_j\sqrt{\mathbf{P}_j}\mathbf{x}_j(l)\right) + \mathbf{V}_k^H\mathbf{n}_k[L].\end{aligned} \tag{2.27}$$

Assume that user k only decodes its own current symbol $\mathbf{x}_k(L)$ and considers the interferences (IUI and ISI) as noise. Then the rate of user k is given as

$$R_k^{\mathrm{DL}} = \log\det\left(\mathbf{I} + \mathbf{V}_k^H \mathbf{H}_k^{(L)} \mathbf{U}_k \mathbf{P}_k \mathbf{U}_k^H \mathbf{H}_k^{(L)H} \mathbf{V}_k \mathbf{X}_k^{-1}\right), \tag{2.28}$$

where the superscript DL denotes downlink and the interference matrix

$$\begin{aligned}\mathbf{X}_k = \sigma_k^2 \mathbf{V}_k^H \mathbf{V}_k + \sum_{l \neq L} \mathbf{V}_k^H \mathbf{H}_k^{(l)} \mathbf{U}_k \mathbf{P}_k \mathbf{U}_k^H \mathbf{H}_k^{(l)H} \mathbf{V}_k \\ + \sum_{j \neq k} \sum_{l} \mathbf{V}_k^H \mathbf{H}_k^{(l)} \mathbf{U}_j \mathbf{P}_j \mathbf{U}_j^H \mathbf{H}_k^{(l)H} \mathbf{V}_k.\end{aligned} \tag{2.29}$$

The second term of (2.29) is the ISI of user k, and the third term is the IUI from other users' signals.

In the following, we will jointly design the transmit waveforms of the K users $\mathbf{U} = [\mathbf{U}_1, ..., \mathbf{U}_K]$ and power allocation $\mathbf{P} = diag\{\mathbf{P}_1, ..., \mathbf{P}_K\}$ to maximize the weighted sum rate $\sum_{k=1}^{K} \alpha_k R_k^{\mathrm{DL}}$ subject to a total power constraint $P_{\max}$, i.e.,

$$\begin{aligned}\boldsymbol{\mathcal{P}}_{\mathrm{Rate}}^{\mathrm{DL}}: \quad \max_{\mathbf{P},\mathbf{U}} \quad & \sum_{k=1}^{K} \alpha_k R_k^{\mathrm{DL}} \\ \text{s.t.} \quad & \mathrm{tr}(\mathbf{P}) \leq P_{\max},\end{aligned} \tag{2.30}$$

where α_k denotes the rate weighting coefficient for user k.

2.3.2 Uplink-Downlink Duality for Multiple Data Streams

In (2.28) and (2.29), all the waveforms $\{\mathbf{U}_j\}_{j=1}^{K}$ are involved in R_k, so the waveform design is complicated in the downlink. With the uplink-downlink duality for multiple data streams [52], the downlink optimal waveform can be found in the

virtual uplink with fixed power allocation. The sum rate optimization problem in the virtual uplink is constructed as follows.

$$\boldsymbol{\mathcal{P}}_{\text{Rate}}^{\text{UL}}: \quad \max_{\mathbf{Q},\mathbf{U}} \quad \sum_{k=1}^{K} \alpha_k R_k^{\text{UL}}$$
$$\text{s.t.} \quad \text{tr}\left(\mathbf{Q}\right) \leq P_{\max} \tag{2.31}$$

where $\mathbf{Q} = diag\left\{\mathbf{Q}_1, ..., \mathbf{Q}_K\right\}$ is the power allocation in the virtual uplink, the downlink transmit waveform $\mathbf{U}$ is equivalent to the uplink receive waveform, and the uplink transmission rate for user k is

$$R_k^{\text{UL}} = \log\det\left(\mathbf{I} + \mathbf{U}_k^H \mathbf{H}_k^{(L)H} \mathbf{V}_k \mathbf{Q}_k \mathbf{V}_k^H \mathbf{H}_k^{(L)H} \mathbf{U}_k \mathbf{Y}_k^{-1}\right), \tag{2.32}$$

where the superscript UL denotes the virtual uplink, and the interference matrix

$$\mathbf{Y}_k = \sigma_k^2 \mathbf{U}_k^H \mathbf{U}_k + \sum_{l \neq L} \mathbf{U}_k^H \mathbf{H}_k^{(l)H} \mathbf{V}_k \mathbf{Q}_k \mathbf{V}_k^H \mathbf{H}_k^{(l)} \mathbf{U}_k$$
$$+ \sum_{j \neq k} \sum_{l} \mathbf{U}_k^H \mathbf{H}_k^{(l)H} \mathbf{V}_j \mathbf{Q}_j \mathbf{V}_j^H \mathbf{H}_k^{(l)} \mathbf{U}_k. \tag{2.33}$$

By exploiting the fact that under MMSE receive filtering the SINR achievable regions of the two dual problems are the same for multiple data streams [52], we develop an iterative algorithm to compute the transmit waveform $\mathbf{U}$ and the uplink power $\mathbf{Q}$ in the virtual uplink, and calculate the receive waveform $\mathbf{V}$ and the downlink power $\mathbf{P}$ in the downlink. In the following two subsections, we describe the waveform design and the power allocation algorithm in detail.

2.3.3 Individual Waveform Design for Multiple Data Streams

As mentioned in Section 2.3.2, under MMSE receive filtering the SINR achievable regions of the two dual problems are the same [52]. Therefore, in this subsection

we briefly introduce the MMSE receive filter.

Given the power allocation matrix $\mathbf{P}$ and transmit waveform $\mathbf{U}$, the MMSE receive filter for the downlink can be derived as

$$\mathbf{V}_k = \left(\mathbf{H}_k^{(L)}\mathbf{U}_k\mathbf{P}_k\mathbf{U}_k^H\mathbf{H}_k^{(L)H} + \mathbf{X}_k\right)^{-1}\mathbf{H}_k^{(L)}\mathbf{U}_k\sqrt{\mathbf{P}_k}. \tag{2.34}$$

Similarly, for the virtual uplink, given the power allocation $\mathbf{Q}$ and transmit filter $\mathbf{V}$, the MMSE receive filter is given by

$$\mathbf{U}_k = \left(\mathbf{H}_k^{(L)H}\mathbf{V}_k\mathbf{Q}_k\mathbf{V}_k^H\mathbf{H}_k^{(L)} + \mathbf{Y}_k\right)^{-1}\mathbf{H}_k^{(L)H}\mathbf{V}_k\sqrt{\mathbf{Q}_k}. \tag{2.35}$$

2.3.4 Power Allocation for Multiple Data Streams: Iterative Power Waterfilling

We introduce the proposed power allocation algorithm for multiple data streams. This algorithm is the multiple-data-stream extension of the *modified iterative waterfilling* in [124]. For multiple data streams, we cannot obtain the power allocation vector by allocating the SINR targets since there may be multiple solutions satisfying the same SINR targets. Thus, we directly allocate the power allocation vector.

Given the transmit waveforms $\mathbf{U}_k$, the power allocation problem can be written as

$$\begin{aligned} \max_{\{\mathbf{P}_k\}} \quad & \sum_{k=1}^{K}\alpha_k R_k \\ \text{s.t.} \quad & \sum_{k=1}^{K}\mathrm{tr}\left(\mathbf{P}_k\right) \le P_{\max}, \mathbf{P}_k \ge 0, \forall k. \end{aligned} \tag{2.36}$$

Taking derivative on the Lagrangian with respect to p_{kl}, $1 \leq l \leq M_k$, we have

$$\frac{\alpha_k}{z_{kl}^{-1} + p_{kl}} - t_{kl} = \lambda - \mu_{kl}. \tag{2.37}$$

where

$$z_{kl} = \mathbf{e}_l^T \mathbf{\Phi}_{k,k,L}^H \left(\mathbf{X}_k + \sum_{m=1, m \neq l}^{L_k} p_{km} \mathbf{\Phi}_{k,k,L} \mathbf{e}_m \mathbf{e}_m^T \mathbf{\Phi}_{k,k,L}^H \right)^{-1} \mathbf{\Phi}_{k,k,L} \mathbf{e}_l, \tag{2.38}$$

and

$$\begin{aligned} t_{kl} = & \alpha_k \sum_{i \neq L} \mathbf{e}_l^T \mathbf{\Phi}_{k,k,i}^H \left(\mathbf{X}_k + \mathbf{\Phi}_{k,k,L} \mathbf{P}_k \mathbf{\Phi}_{k,k,L}^H \right)^{-1} \mathbf{\Phi}_{k,k,L} \mathbf{P}_k \mathbf{\Phi}_{k,k,L}^H \mathbf{X}_k^{-1} \mathbf{\Phi}_{k,k,i} \mathbf{e}_l \\ & + \sum_{j \neq k} \alpha_j \sum_i \mathbf{e}_l^T \mathbf{\Phi}_{j,k,i}^H \left(\mathbf{X}_j + \mathbf{\Phi}_{j,j,L} \mathbf{P}_j \mathbf{\Phi}_{j,j,L}^H \right)^{-1} \mathbf{\Phi}_{j,j,L} \mathbf{P}_j \mathbf{\Phi}_{j,j,L}^H \mathbf{X}_j^{-1} \mathbf{\Phi}_{j,k,i} \mathbf{e}_l, \end{aligned} \tag{2.39}$$

where the $M_k \times M_k$ matrix $\mathbf{\Phi}_{k,j,i}$ is defined as $\mathbf{V}_k^H \mathbf{H}_k^{(i)} \mathbf{U}_j$.

According to the Karush-Kuhn-Tucker (KKT) conditions for (2.36), the optimum p_{kl} satisfies

$$p_{kl} = \left(\frac{\alpha_k}{\lambda + t_{kl}} - z_{kl}^{-1} \right)^+, \tag{2.40}$$

$$\sum_{k=1}^{K} \sum_{l=1}^{L_k} p_{kl} \leq P_{\max}. \tag{2.41}$$

From the complementary slackness, either $\sum_{k=1}^{K} \sum_{l=1}^{L_k} p_{kl} = P_{\max}$, $\lambda > 0$ or $\sum_{k=1}^{K} \sum_{l=1}^{L_k} p_{kl} < P_{\max}$, $\lambda = 0$ should be satisfied. Since λ is monotonic with respect to $\sum_{k,l} p_{kl}$, we can first check whether $\sum_{k=1}^{K} \sum_{l=1}^{L_k} p_{kl} > P_{\max}$ is satisfied for $\lambda = 0$. If so, the value of λ satisfying $\sum_{k,l} p_{kl} = P_{\max}$ can be obtained via a one dimensional bisection search, where the upper bound of λ can be set as $\max_{k,l} \{\alpha_k z_{kl} - t_{kl}\}$, and we choose a small positive value for the lower bound. Similar procedures can be done for the case when $\lambda = 0$ and $\sum_{k,l} p_{kl} < P_{\max}$. The proposed Iterative Power Waterfilling is summarized in Table 2.3.

Table 2.3: Iterative Power Waterfilling for Multiple Data Streams

(i) Given $\mathbf{P}$

(ii) **Loop**:

1. Calculate t_{kl} and z_{kl} using (2.39) and (2.38).
2. Bisection search λ with (2.40) and (2.41), i.e.,

   If $\sum_{k,l}\left(\alpha_k t_{kl}^{-1} - z_{kl}^{-1}\right)^+ < P_{\max}$ **then**

   $p_{kl} = \left(\alpha_k t_{kl}^{-1} - z_{kl}^{-1}\right)^+$.

   else

   (a) Set bisection upper bound $\lambda^{\max} = \max_{k,l}\{\alpha_k z_{kl} - t_{kl}\}$,

   and lower bound $\lambda^{\min} = \delta > 0$.

   (b) **Loop**:

   Set $\lambda = \frac{1}{2}(\lambda^{\max} + \lambda^{\min})$.

   Compute $p_{kl} = \left(\frac{\alpha_k}{\lambda + t_{kl}} - z_{kl}^{-1}\right)^+$.

   If $\sum_{k,l} p_{kl} < P_{\max}$ **then**

   $\lambda^{\max} = \lambda$.

   else

   $\lambda^{\min} = \lambda$.

   Until $|\sum_{k,l} p_{kl} - P_{\max}| < \epsilon$.

Until $\mathbf{P}$ converges or the max. number of iterations is reached.

Table 2.4: Iterative Weighted Sum Rate Optimization Algorithm for Multiple Data Streams

(i) Initialize $\mathbf{Q}_k = \frac{P_{\max}}{\sum_j M_j}\mathbf{I}_{M_k}$, $\mathbf{U}_k$ = some random matrix.

(ii) **Loop** :

1. Calculate $\mathbf{V}$ by (2.34).
2. Calculate $\mathbf{Q}$ using *Iterative Power Waterfilling*.
1. Calculate $\mathbf{U}$ by (2.35).
1. Calculate $\mathbf{P}$ using *Iterative Power Waterfilling*.

Until $(\mathbf{U}, \mathbf{Q}, \mathbf{V}, \mathbf{P})$ converges or the max. number of iterations is reached.

2.3.5 Iterative Sum Rate Optimization for Multiple Data Streams

For multiple data streams, the sum rate optimization algorithm iterates between the virtual uplink ($\mathbf{U}$ and $\mathbf{Q}$) and downlink ($\mathbf{V}$ and $\mathbf{P}$). When computing one of $(\mathbf{U}, \mathbf{Q}, \mathbf{V}, \mathbf{P})$, the other three variables are considered constant. Table 2.3 is applied for calculating the power allocation $\mathbf{P}$, and the algorithm for computing $\mathbf{Q}$ is similar. Different from the proposed algorithm for single data stream (Table 2.2), where the receive filter is simply a scalar and does not need to be updated, for multiple data streams the calculation of $\mathbf{P}$ or $\mathbf{U}$ relies on $\mathbf{V}$, and the calculation of $\mathbf{Q}$ or $\mathbf{V}$ relies on $\mathbf{U}$. Therefore, the algorithm has to iterate between the virtual uplink and the downlink. After convergence or maximum number of iterations is reached, we take the variables obtained at the last iteration as the solution and compute the achievable sum rate accordingly. The algorithm is summarized in Table 2.4.

The global optimum of a non-convex problem can be obtained by exhaustive search which, however, requires prohibitively high computational complexity. The

solution of the proposed iterative waveform design is suboptimal since we tradeoff the optimality with complexity. Simulation results show that such sub-optima can still achieve a much better weighted sum rate performance than traditional methods such as Block-Diagonalization (BD) [93] and ZF.

2.4 Numerical Simulation

In this section, we use numerical simulations to demonstrate the performance of the proposed iterative sum rate optimization algorithms. In the simulation, each path of the channel is assumed to be an i.i.d. complex Gaussian random variable with zero mean and variance of $\frac{1}{2L}$ per dimension.

The amount of ISI depends on the symbol rate. Thus, we introduce the decimation ratio D, which represents the ratio of the symbol duration to the signal sampling duration. Each element in $\mathbf{y}$ is a signal sample, and the data symbols are transmitted every D signal samples. Clearly, higher D results in less ISI but lower symbol rate. In other words, one symbol induces ISI to at most $\lfloor 2(L-1)/D \rfloor$ other symbols. Therefore, with decimation ratio D, the channel matrix $\mathbf{H}$ can be decimated by keeping only $\lfloor 2(L-1)/D \rfloor + 1$ rows and deleting the other rows for simplicity.

For example, if $L = 3$ and $D = 2$, the decimated $\mathbf{H}$ then becomes

$$\mathbf{H} = \begin{bmatrix} h[0] & 0 & 0 \\ h[2] & h[1] & h[0] \\ 0 & 0 & h[2] \end{bmatrix}.$$

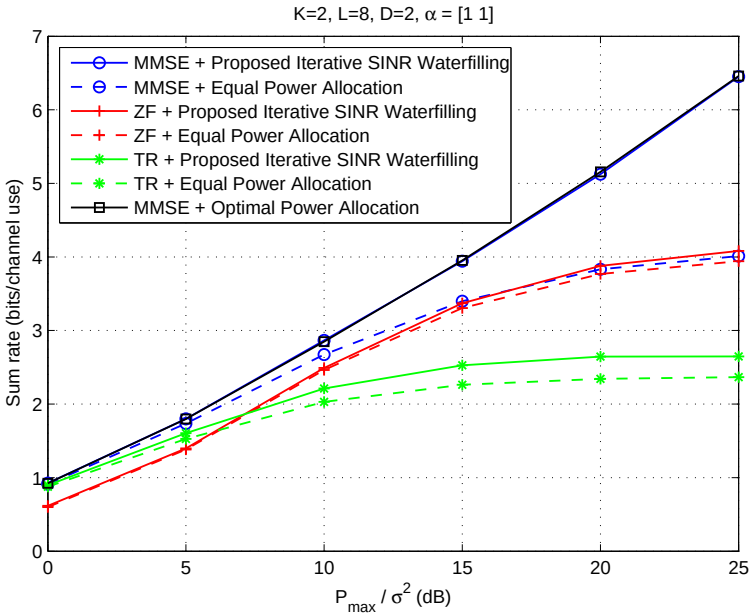

Figure 2.2: Sum rate performance comparison for a 2-user system with $L = 8$, $D = 2$, $\alpha_1 = \alpha_2 = 1$, and $M_1 = M_2 = 1$.

Figure 2.2 shows the sum rate performance of a 2-user system with $L = 8$, $D = 2$, $\alpha_1 = \alpha_2 = 1$. Each rate is averaged over 1000 channel realizations. TR denotes the traditional time-reversal filter, i.e., $\mathbf{u}_k^{\mathrm{TR}} = c_k^{\mathrm{TR}} \mathbf{H}_k^{(1)H}$, where c_k^{TR} is a normalization constant such that $\|\mathbf{u}_k^{\mathrm{TR}}\|_2 = 1$; ZF denotes the zero-forcing waveform, i.e., $\mathbf{u}_k^{\mathrm{ZF}} = c_k^{\mathrm{ZF}}([\mathbf{H}_1^T, \ldots, \mathbf{H}_K^T]^T)^\dagger \tilde{\mathbf{e}}_k$, where $(\cdot)^\dagger$ denotes the Moore-Penrose pseudo-inverse operator, and $\tilde{\mathbf{e}}_k = \left[\mathbf{0}^T, \mathbf{0}^T, \ldots, \mathbf{0}^T, \mathbf{e}_L^T, \mathbf{0}^T, \ldots, \mathbf{0}^T\right]^T$, which is a $K(2L-1)\times 1$ vector with its kth vector as $\mathbf{e}_L$. Here with a slight abuse of notation, we denote $\mathbf{e}_L$ to be the Lth column of a $(2L-1) \times (2L-1)$ identity matrix. The $\mathbf{0}$ denotes a $(2L-1) \times 1$ all zero vector. Therefore, $\tilde{\mathbf{e}}_k$ has only one non-zero value at its $((2L-1)(k-1)+L)$th element. c_k^{ZF} is chosen to normalize the norm of $\mathbf{u}_k^{\mathrm{ZF}}$ to be 1.

We compare the proposed Iterative SINR Waterfilling with equal power allocation and optimal power allocation in Figure 2.2. For the proposed algorithms, the forgetting factor β is set to be $1/K$. The maximum iteration number of Iterative SINR Waterfilling is set to be 20. In this chapter, since we focus on demonstrating the performance advantage of the proposed power allocation scheme, some parameters of the proposed algorithms, such as the maximum number of iterations and the forgetting factor β, are empirically chosen and the performance is already promising. Thus, we do not aim to further optimize these parameters. The equal power allocation is to split the total power equally to each user, i.e., $p_k = P_{\max}/K$. The optimal power allocation is simulated by exhaustive search of the discretized power variables, where the number of discrete levels of each power variable is set as 10^3. The exhaustive search requires very high computational complexity, which is exponentially increasing in the number of variables as the number of discrete levels increases.

From the figure, the proposed power allocation can improve the performance of equal power allocation for all waveform designs, since the proposed Iterative SINR Waterfilling is able to find sub-optima by taking into consideration the channel gains. The improvement for the MMSE waveform is especially significant at high power region. The MMSE waveform with the proposed Iterative SINR Waterfilling performs almost the same as the globally-optimal power allocation. We also observe that even with the MMSE waveform, which is optimal given any power allocation for single data stream, the equal power allocation still saturates at high power region.

Note that since the sub-optimal waveforms TR and ZF do not change un-

der different power allocation, these methods do not require iterations between the waveform design and power allocation. For the MMSE with equal power allocation, since the power allocation remains the same, the MMSE waveform does not need to be updated accordingly. Therefore, these methods are not iterative and thus require lower computational complexity compared to the proposed algorithm, which has two levels of iterations.

It is well-known [32] that since TR only maximizes the received signal power without considering the interference, it saturates at a lower rate, as shown in both figures. ZF cancels the interference but sacrifices the received signal power resulting in worse performance at low power region. MMSE can strike a balance between the two by reducing the interference including ISI and IUI, while keeping a high received signal power.

In Figure 2.3, the proposed Iterative SINR Waterfilling is compared with the convex approximation using geometric programming (GP) [24], which approximates the rate function $\log(1 + \mathrm{SINR}_k)$ as $\log(\mathrm{SINR}_k)$ in high SINR regime. With such an approximation, the weighted sum rate function can be shown to be a posynomial and the optimization problem becomes a geometric program, which can be optimally solved via standard convex programming techniques. In the figure, for $K = 2$, $L = 8$, and $D = 3$, since the interference is low and $\mathrm{SINR}_k \gg 1$, the sum rate optimization problem can be well approximated using the convex objective function, and the performance of the proposed method is very close to the globally optimal solution of the approximated convex optimization problem. For $K = 4$, $L = 8$, $D = 4$, and $K = 4$, $L = 8$, $D = 3$, the higher interference from more

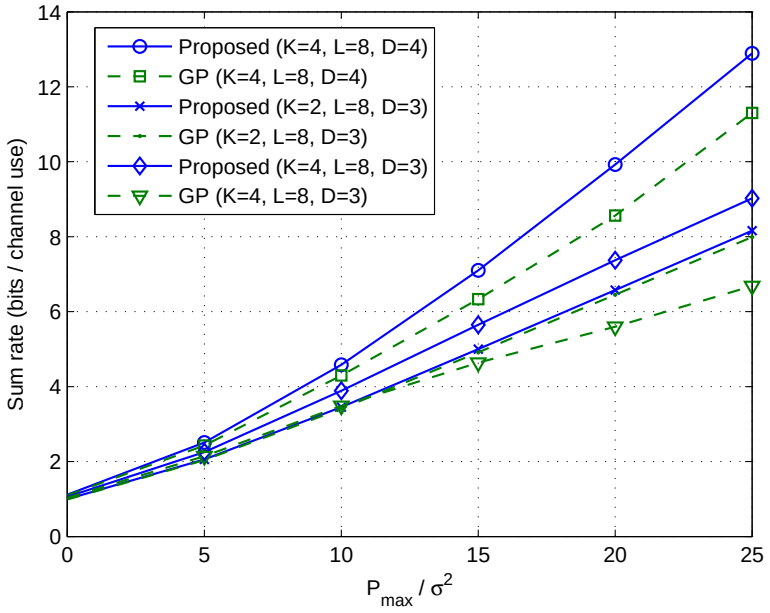

Figure 2.3: Sum rate performance comparison of the proposed algorithm in Table 2.2 and the convex approximation using geometric programming (GP).

users causes more performance degradation to the GP method. This is because the approximate objective function $\sum_k \log(\mathrm{SINR}_k)$ can be seen as the proportional fairness criterion for SINRs and it deters some SINR_k from being very small and significantly decreasing the approximate objective function. On the contrary, the original sum rate $\sum_k \log(1 + \mathrm{SINR}_k)$ is not impaired as much if some SINR_k are small, because most power can be allotted to other users with lower interference and still makes good contribution to the sum rate. In other words, if some users' interference is high, the original sum rate maximization can abandon these users and allocate most power to the others. Such a consequence cannot arise in the GP method. Hence, only when the interference is low for all users, the sum rate optimization problem can be well approximated with the convex objective function.

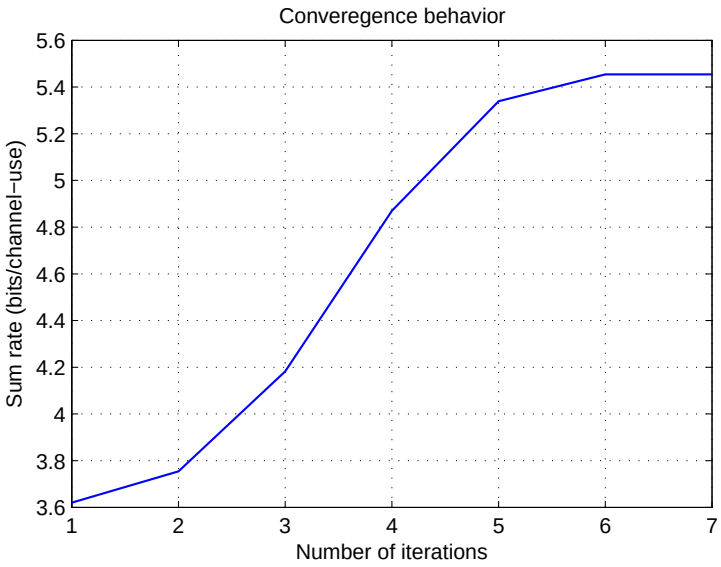

Figure 2.4: Convergence behaviors of the proposed sum rate optimization algorithm.

The performance gap between the proposed method and the GP method becomes larger as $P_{\max}/\sigma^2$ increases. This seems not to comply with the intuition that the GP method can obtain higher accuracy of approximation with high $P_{\max}/\sigma^2$. Instead, the GP approximation is less accurate when the available power is higher since the interference is also higher. When $P_{\max}/\sigma^2$ is low, the noise is more dominant than the interference, so the interference mitigation from power allocation has less prominent influence on the sum rate. As $P_{\max}/\sigma^2$ increases, the interference also increases. In a high interference scenario, the proposed algorithm can make better use of the available power compared with the GP method, which is based on a less accurate approximation. Therefore, the resulting advantage of the proposed algorithm is more significant as $P_{\max}/\sigma^2$ increases. In this figure, we can also observe that the performance gap for $K = 4$, $L = 8$, $D = 3$ between the two algorithms is larger than the gap for $K = 4$, $L = 8$, $D = 4$ since the GP method allocates power

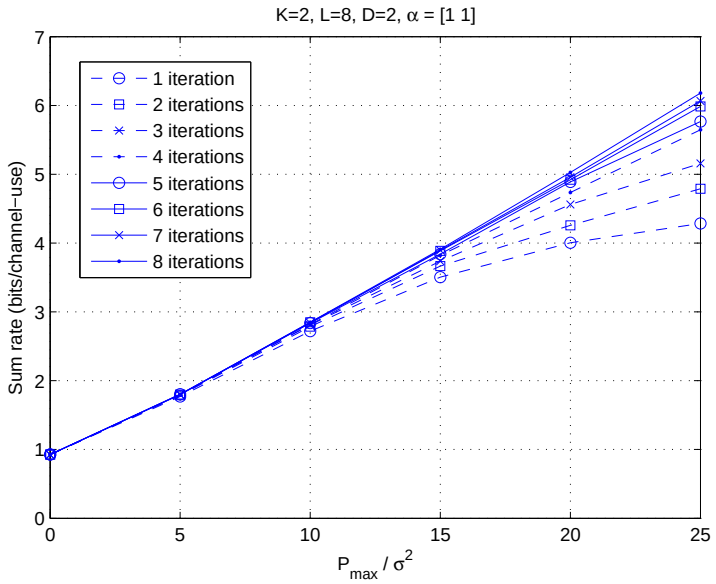

Figure 2.5: Sum rate performance for difference maximum numbers of iterations.

based on a less accurate approximation when the interference is higher. Comparing between $K = 4$, $L = 8$, $D = 3$ and $K = 2$, $L = 8$, $D = 3$, the proposed algorithm can achieve a better sum rate performance when K increases, whereas GP instead performs worse, which is again due to the ineffective approximation.

Figure 2.4 shows a typical convergence behavior of the proposed sum rate optimization algorithm (Table 2.2). Monotonicity and very fast convergence are almost always observed (typically about 3 to 12 iterations). The proposed sum rate optimization algorithms with different maximum numbers of iterations are compared in Figure 2.5. It can be seen that the sum rate performance is improved with more iterations. The improvement is more significant for smaller maximum numbers of iterations and becomes less noticeable for higher maximum numbers of iterations. We have performed extensive (10,000 channel realizations) simulations to inspect the convergence of the proposed algorithm. Over 99% of them converge within 100

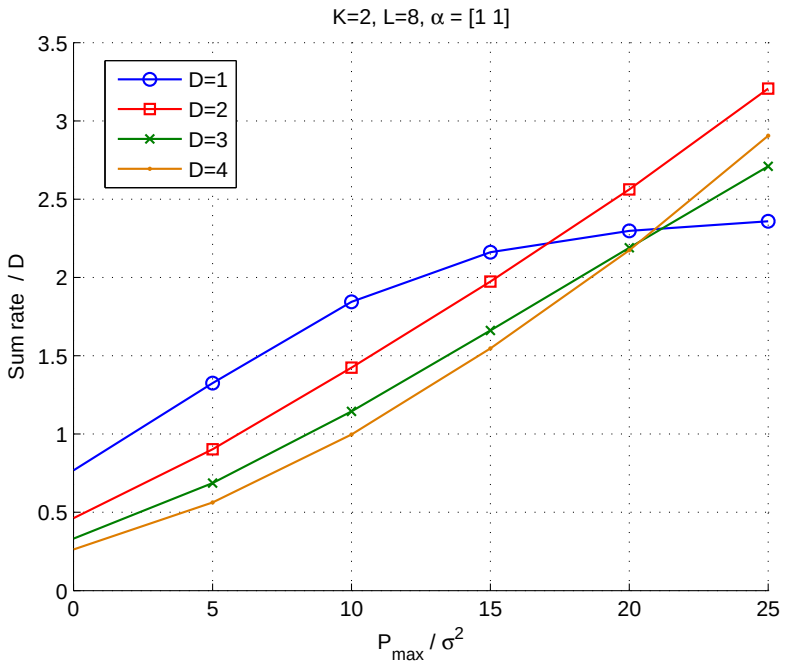

Figure 2.6: Sum rate performance comparison for different decimation ratio D using the proposed algorithm in Table 2.2. The performance is normalized by D.

iterations, while the remaining less than 1% converge more slowly. Note that we define the convergence as the rate improvement between two consecutive iterations being within 10^{-6}, i.e., $\left|(R^{(n+1)} - R^{(n)})/R^{(n)}\right| < 10^{-6}$. We observed that for those cases with slow convergence, the rate still monotonically increases but the increase is just too slow to converge within 100 iterations. Since we assume L-path multipath channel with each path being a Gaussian, the complexity to locate the peculiarity of these channels is very high.

In Figure 2.6, we compare the sum rate performance with different decimation ratio D. Note that for fair comparison, the performance is normalized by $1/D$ which reflects the frequency of channel usage. For smaller D, the transmission is conducted more frequently but severer interference may occur due to the ISI. Similarly for

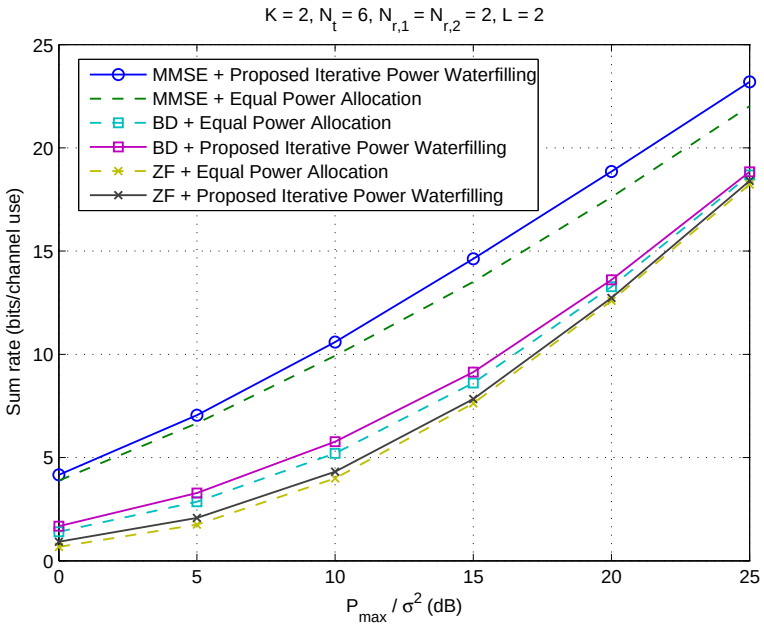

Figure 2.7: Sum rate performance comparison for a 2-user system with $N_t = 6$, $N_{r,1} = N_{r,2} = 2$, $L = 2$, and $M_1 = M_2 = 2$.

higher D, the ISI is reduced but the channel is utilized less frequently. From the figure, we can see that at low SNR region, $D = 1$ attains the highest normalized performance since at low SNR, the ISI is less prominent and the channel utilization is more important to the normalized sum rate. On the other hand, at high SNR, the ISI has a dominant effect and higher D can provide a better normalized sum rate performance despite less frequent channel usage.

Figure 2.7 shows the sum rate performance of a 2-user system with $L = 2$, $\alpha_1 = \alpha_2 = 1$, $N_t = 6$, $N_{r,1} = N_{r,2} = 2$, and $M_1 = M_2 = 2$. The proposed algorithm (Table 2.4) is compared with BD [93] and ZF. For BD, the signal space of each user is orthogonal to each other, i.e., $\mathbf{U}_k$ is in the null space of ISI and IUI. Thus, in order for BD to find a feasible solution, the simulation parameters are chosen to satisfy

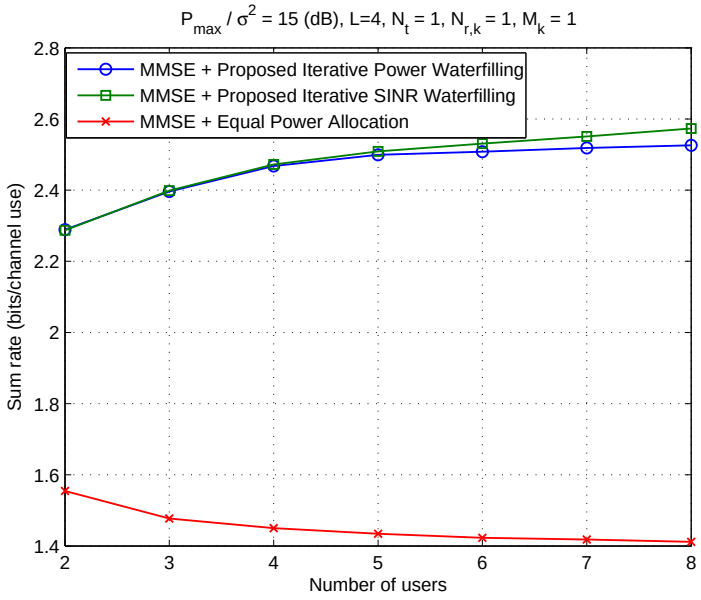

Figure 2.8: Comparison of the two proposed algorithms with different number of users. $L = 4$, $N_t = 1$, $N_{r,k} = 1, \forall k$, $M_k = 1, \forall k$, and $P_{\max}/\sigma^2 = 15$ (dB).

$LN_t - (2L-1)\sum_{j \neq k} N_{r,j} - (2L-1)N_{r,k} \geq M_k, \forall k$. As to ZF, the signal space of each data stream is orthogonal to each other. Hence, ZF also has similar constraint on the dimensions.

We compare the Iterative Power Waterfilling as in Section 2.3.4 with equal power allocation in Figure 2.7. The equal power allocation is to split the total power equally to each data stream, i.e., $\mathbf{P}_k = \frac{P_{\max}}{\sum_j M_j}\mathbf{I}_{M_k}$. From the figure, it is clear that the proposed power allocation outperforms equal power allocation for MMSE, BD, and ZF. It is well-known that interference cancellation based methods, such as BD and ZF, suffer from the noise enhancement and thus result in worse performance than MMSE.

We compare the two proposed power allocation algorithms for single data

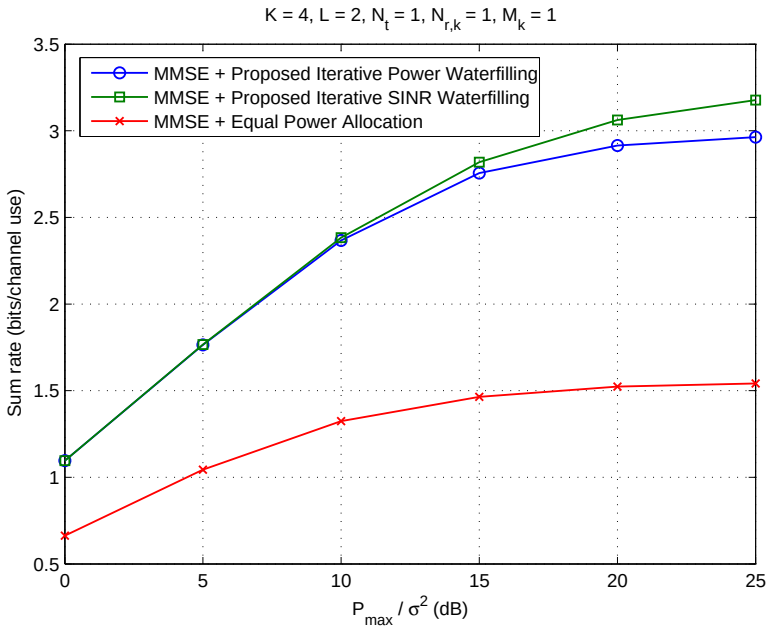

Figure 2.9: Comparison of the two proposed algorithms. $K = 4$, $L = 2$, $N_t = 1$, $N_{r,k} = 1, \forall k$, and $M_k = 1, \forall k$.

stream with different number of users in Figure 2.8. The parameters are chosen as $N_t = 1$, $N_{r,k} = 1, \forall k$, $L = 4$, and $\alpha_k = 1, \forall k$. From the figure, Iterative SINR Waterfilling outperforms the Iterative Power Waterfilling when the number of users is large. Figure 2.9 shows that Iterative SINR Waterfilling can achieve superior sum rate at high SNR, where the parameters are chosen as $K = 4$, $L = 2$, $N_t = 1$, $N_{r,k} = 1, \forall k$, and $\alpha_k = 1, \forall k$. From Figures 2.8 and 2.9, it can be seen that Iterative SINR Waterfilling outperforms Iterative Power Waterfilling in the scenario of high interference. Intuitively, the SINR targets have direct influence on the sum rate and allocating the SINR can better capture the impact of interference compared to allocating the power.

In Figure 2.10, the proposed Iterative SINR Waterfilling is compared with

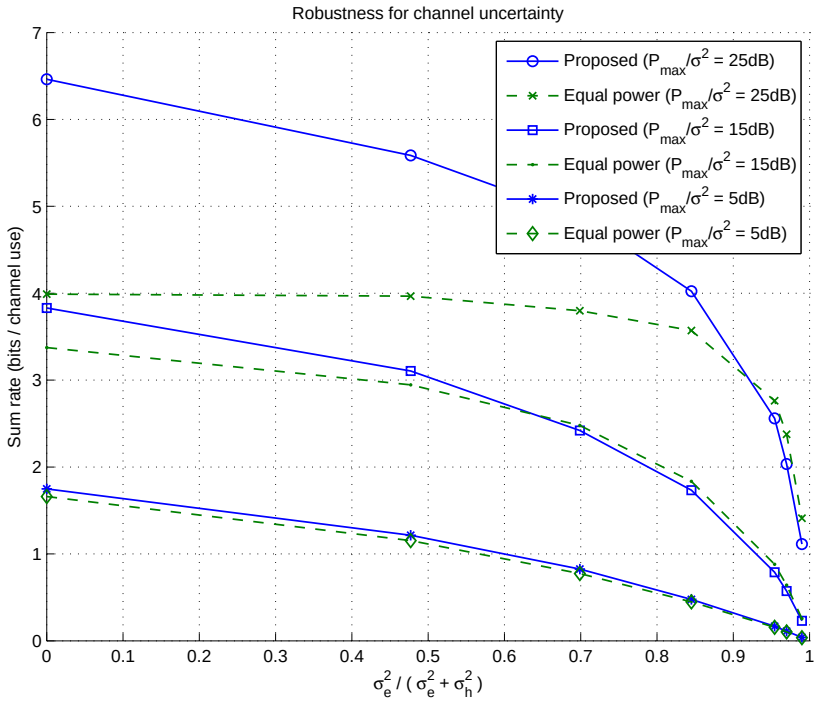

Figure 2.10: Comparison of the proposed algorithm and equal power allocation for sum rate versus channel uncertainty.

equal power allocation. The channel uncertainty model for the kth user at time m is given by $\hat{h}_k[m] = h_k[m] + e_k[m]$, where $\hat{h}_k[m]$ denotes the estimated channel coefficient, $h_k[m]$ denotes the true channel with variance σ_h^2, and $e_k[m]$ is the estimation error with variance σ_e^2. In this figure, we can see that when the channel uncertainty is small, the proposed method can still outperform the equal power allocation. As the channel uncertainty increases, the benefit of the proposed method over the equal power allocation reduces, since the proposed method relies on the perfect channel information to allocate the available power. When the channel uncertainty is very high, the equal power allocation performs better because the proposed method allocates the power according to the coefficients almost uncorrelated to the true channel.

Finally, we note that although we cannot prove the proposed iterative algorithms converge to the global optimum, the simulation results show that the proposed Iterative SINR Waterfilling still results in comparable performance to that of the globally-optimal power allocation and thus outperforms other traditional methods.

2.5 Conclusion

In this chapter, we explored the weighted sum rate optimization problem by transmit waveform design for the MIMO time-reversal multiuser downlink communication systems where the receiver processing is based on a single sample. The waveform design problem is shown to have a structure similar to the downlink beamforming problem with a self-interfering term induced by the ISI. In order to tackle the

problem, we proposed a new power allocation scheme called Iterative SINR Waterfilling which, instead of directly allocating the power, the SINRs are first allocated to maximize the weighted sum rate. With the allocated target SINRs, the corresponding power allocation can be easily determined. For multiple data streams, Iterative Power Waterfilling is further proposed. Iterative algorithms alternately optimize the transmit waveform and the power allocation for each user. Both of the proposed sum rate optimization algorithms significantly outperform other traditional approaches such as zero-forcing and time-reversal waveforms. We also demonstrated that Iterative SINR Waterfilling outperforms Iterative Power Waterfilling in the scenario of high interference, e.g., large number of users or high SNR region. With the MMSE waveform, Iterative SINR Waterfilling is shown to achieve near-optimal performance by comparing with exhaustively-searched global optimum.

Chapter 3

Joint Waveform Design and Interference Pre-Cancellation for Time-Reversal Systems

In basic time-reversal (TR) communication systems [44,105], the time-reversed channel impulse response serving as the transmit waveform is able to boost the signal strength in a large delay spread channel in broadband communication. After the transmitted TR waveform convolves with the multi-path channel, the temporal focusing effect [36,75] of the TR waveform re-collects the most of signal energy into a single tap. Utilizing the channel reciprocity, such a time-reversed waveform is essentially the matched-filter [78], which guarantees the optimal performance by virtue of its capability of maximizing the signal-to-noise ratio (SNR). The TR transmission technique only requires a very low complexity at the receiver since a simple one-tap symbol estimation is performed. Thus, the TR transmission techniques have been shown to be a promising solution to the energy-efficient and low-complexity green wireless communication [44, 105].

As introduced in Chapter 1, the basic idea of waveform design is to delicately adjust the amplitude and phase of each tap of the waveform based on the channel information, such that after convolving with the channel, the received signal at the receiver retains most of the intended signal strength and rejects or suppresses the

interference as much as possible. It can be shown that the mathematical structure of waveform design is analogous to that of the precoder design in MISO systems, since the taps in waveform design act as the beamforming coefficients of the transmit antenna in the precoder design. In the literature, there have been many studies investigating the problems of designing advanced waveforms to suppress the interference [2, 16, 31, 33, 55, 63, 122]. In [33], a minimum mean-square-error (MMSE) waveform was proposed to suppress ISI and noise for a single-user scenario without taking into account the rate back-off factor in the optimization and thus the waveform is suboptimal. A zero-forcing waveform for minimizing the sidelobes (ISI) was considered in [31]. In [122], multi-user joint power allocation and waveform design for sum rate optimization was investigated in downlink TR systems.

Besides the channel information, another important side information the transmitter can exploit in the waveform design is the transmitted symbol information. Theoretically, if the receiver interference is known to the transmitter, it is possible to completely remove the interference by means of complicated coding techniques [29]. The interference is known to the transmitter since it can be derived from the transmit waveforms, the multipath channels, and the information bits. For example, in a single-user scenario, when a signal arrives at the receiver, the waveform of a symbol induces ISI to the previous symbols as well as the following symbols. Given the transmitted symbols, the causal part of ISI can be cancelled in advance in designing the waveform of the current symbol. Such a design is analogous to the transmitter-based interference pre-subtraction [114, 128] in the nonlinear precoding literature. A notable distinction for TR communication systems is that only the causal part

of interference can be cancelled while the anti-causal part of interference cannot be cancelled and needs to be suppressed by the waveform design based on the channel information.

In this chapter, we propose a joint waveform design and interference pre-cancellation for TR communication systems. The single-user scenario permits a closed-form solution of the joint waveform design. It is shown that the resulting design pre-cancels the causal ISI and suppresses the anti-causal ISI. For the multi-user scenario, similarly the interference (ISI and IUI) is categorized into causal interference and anti-causal interference. The pre-cancellation filter design can be easily determined once the multi-user waveform design is settled. Since the resulting multi-user waveform design is non-convex, we propose two iterative algorithms to suboptimally tackle the optimization problem. One approach is based on the alternating optimization and the other is a gradient method [15]. We show that both iterative algorithms are guaranteed to converge to local optimal solutions. Numerical simulation is conducted to validate the convergence behavior of the proposed iterative algorithms and demonstrate the performance of the joint design.

The rest of the chapter is organized as follows. In Section 3.1, the system model of the TR communication system is introduced in detail. The joint waveform design and interference pre-cancellation for the single-user scenario is described in Section 3.2, and the multi-user scenario is further depicted in Section 3.3, where the two iterative algorithms are proposed. In Section 3.4, simulation results are shown to demonstrate the performance. Finally, we draw the conclusion in Section 3.5.

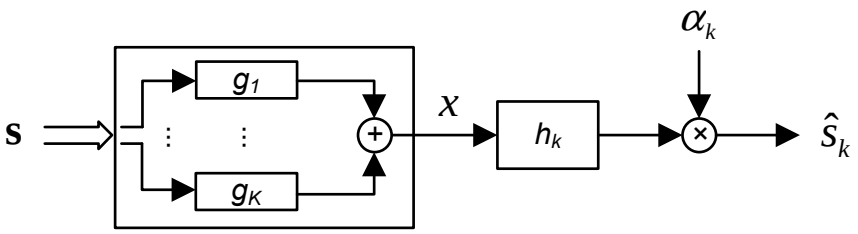

Figure 3.1: Block diagram of waveform design for the multi-user downlink TR system.

3.1 System Model

In the basic time-reversal system [44, 105], a user periodically sends a known sequence of waveforms to the base-station, which then estimates the channel impulse response using the received signal. Based on the channel impulse response, the base-station simply uses the time-reversed version of the channel as the symbol waveform to transmit data symbols. After receiving the signal, the user estimates the transmitted symbol by looking at one sample of the received signal for each symbol. As a consequence, the complexity at the user end can be very low while most of the computational burden is shifted to the base-station. In this chapter, we focus on the joint waveform design and interference pre-cancellation. Hence, for simplicity perfect channel estimation and perfect synchronization are assumed, and the extensions to the more general cases are possible but beyond the scope of this chapter.

A multi-user downlink TR system consists of a base-station and K users. The multipath channel between the base-station and the k-th user is denoted by $\mathbf{h}_k$, a column vector of L elements where L is the maximum channel length among the K

channels. Let s_k denote an information symbol and $\mathbf{g}_k$ be the transmit waveform for user k, which can be a basic TR waveform or a more advanced waveform [122]. The length of $\mathbf{g}_k$ is also L. As shown in Figure 3.1, the received signal $\mathbf{y}_k$ at user k is given by

$$\mathbf{y}_k = \mathbf{H}_k \sum_{j=1}^{K} \mathbf{g}_j s_j + \mathbf{n}_k, \tag{3.1}$$

where $\mathbf{H}_k$ is the Toeplitz matrix of size $(2L-1) \times L$ with the first column being $[\mathbf{h}_k^T \ \mathbf{0}_{1\times(L-1)}]^T$, and $\mathbf{n}_k$ denotes the additive white Gaussian noise (AWGN). The user estimates the symbol s_k by scaling the sample $y_k[L]$ by α_k, which corresponds to the gain control at the receiver. Note that (3.1) represents the received signal when symbols are transmitted further apart, i.e., with a symbol rate being at most $1/L$ times sampling rate $1/T_s$. When the symbol rate is $1/(DT_s)$ where D denotes the rate back-off factor [33] and $D < L$, the received waveforms of different symbols overlap with each other and give rise to the inter-symbol interference (ISI). Here D is the rate back-off factor introduced to adjust the symbol rate in TR systems [33, 44, 105]. To characterize the effect of ISI, the decimated channel matrix of size $(2L_D - 1) \times L$, where $L_D = \lfloor \frac{L-1}{D} \rfloor + 1$, is defined as

$$\tilde{\mathbf{H}}_k = \sum_{i=-L_D+1}^{L_D-1} \mathbf{e}_{L_D+i} \mathbf{e}_{L+iD}^T \mathbf{H}_k, \tag{3.2}$$

where $\mathbf{e}_l$ is the l-th column of a $(2L-1) \times (2L-1)$ identity matrix. In other words, $\tilde{\mathbf{H}}_k$ is obtained by decimating the rows of $\mathbf{H}_k$ by D, i.e., centering at the L-th row, every D-th row of $\mathbf{H}_k$ is kept in $\tilde{\mathbf{H}}_k$ while the other rows are discarded. The center

row index of $\tilde{\mathbf{H}}_k$ is L_D. Then the sample for symbol estimation can be written as

$$y_k[L] = \mathbf{h}_{kL}^H \mathbf{g}_k s_k[L_D] + \mathbf{h}_{kL}^H \sum_{j \neq k} \mathbf{g}_j s_j[L_D] + \sum_{l=1, l \neq L_D}^{2L_D-1} \mathbf{h}_{kl}^H \sum_{j=1}^{K} \mathbf{g}_j s_j[l] + n_k[L], \quad (3.3)$$

where the $\mathbf{h}_{kl}^H = \mathbf{e}_l^T \tilde{\mathbf{H}}_k$ denotes the l-th row of $\tilde{\mathbf{H}}_k$, and $s_j[l]$ denotes user j's l-th symbol. It can be seen from (3.3) that the symbol $s_k[L_D]$, the L_D-th symbol of user k, is interfered by the previous $L_D - 1$ symbols and the later $L_D - 1$ symbols as well as other users' $K(2L_D - 1)$ symbols, and also corrupted by the noise. The design of waveforms $\{\mathbf{g}_k\}$ has critical influence to the symbol estimation and thus the system performance. If the basic TR waveforms are adopted, i.e., $\mathbf{g}_k = \mathbf{h}_{kL}$, then the intended signal power for each user is maximized but without considering the interference caused by other symbols. As such, the performance is limited by the interference when the transmit power is high. Another possible waveform design is zero-forcing (ZF) [64], which minimizes all the interference signal power but without taking into account the intended signal power. Thus, the resulting SNR can be very low and causes severe performance degradation especially when the transmit power is relatively low. In our previous work [122], it has been shown that well-designed waveforms can strike a balance between enhancing the intended signal power and suppressing the interference power.

3.2 Single-User Joint Waveform Design and Interference Pre-cancellation

In this section, we discuss the joint waveform design and interference pre-cancellation for the single-user case, which allows a closed form solution and provides an insight to the joint design in the multi-user scenario. To simplify the notations,

the user index for the single-user scenario is omitted. For example, the channel, the waveform, and the gain are denoted as $\mathbf{h}$, $\mathbf{g}$, and α, respectively. In [122], a waveform design is proposed to suppress the ISI by designing the transmit waveform $\mathbf{g}$ based on the criterion of maximizing the signal-to-interference-plus-noise ratio (SINR). Such a formulation usually involves solving an eigenvalue problem. In this chapter, we consider minimizing mean-square error (MSE) as the design criterion. It can be shown that in the single-user case, a closed form solution to the joint design can be derived, and the minimum MSE waveform without interference pre-cancellation also achieves the maximum SINR [42,122]. In the following, we will first discuss the waveform design for minimizing MSE without interference pre-cancellation, and then the pre-cancelling filter design. Finally, the joint waveform design and interference pre-cancellation is analyzed and the closed form solution is derived.

3.2.1 Waveform Design without Interference Pre-Cancellation

The estimated symbol is obtained by scaling the sample $y[L]$ by the gain α, i.e., $\hat{s}[L_D] = \alpha y[L]$. Let the l-th row of the decimated channel matrix $\tilde{\mathbf{H}}$ be denoted by $\mathbf{h}_l^H$. The estimation MSE defined as $E[\|\hat{s}[L_D] - s[L_D]\|^2]$ is expressed as

$$\begin{aligned}
\mathrm{MSE}(\alpha, \mathbf{g}) &= E\left[\|\alpha y[L] - s[L_D]\|^2\right] \\
&= E[\| \left(\alpha \mathbf{h}_{L_D}^H \mathbf{g} - 1\right) s[L_D] + \alpha n[L] + \sum_{l=1, l\neq L_D}^{2L_D-1} \alpha \mathbf{h}_l^H \mathbf{g} s[l]\|^2] \\
&= |\alpha \mathbf{h}_{L_D}^H \mathbf{g} - 1|^2 P_S + \sum_{l=1, l\neq L_D}^{2L_D-1} |\alpha \mathbf{h}_l^H \mathbf{g}|^2 P_S + |\alpha|^2 P_N, \qquad (3.4)
\end{aligned}$$

where $s[l], l = 1, \ldots, L_D-1, L_D+1, \ldots, 2L_D-1$, denote the interfering symbols transmitted adjacent to the intended symbol $s[L_D]$. The symbol power $P_S = E[\|s[l]\|^2]$, $\forall l$, is assumed to be unity for normalization. The noise is i.i.d. Gaussian distributed and hence $P_N = E[\|n[l]\|^2]$, $\forall l$. To derive the minimum MSE (MMSE) waveform $\mathbf{g}$, we formulate the problem as minimizing MSE subject to a power constraint $\mathbf{g}^H\mathbf{g} = P_{\max}$ to rule out the trivial solution $\mathbf{g} = \mathbf{0}$, the all-zero vector. The Lagrangian function is given by

$$\mathcal{L}(\alpha, \mathbf{g}, \lambda) = \mathrm{MSE}(\alpha, \mathbf{g}) + \lambda(\mathbf{g}^H\mathbf{g} - P_{\max}). \tag{3.5}$$

Note that the optimization problem is nonconvex, and hence the KKT conditions are necessary but may not be sufficient for the global optimal solution. However, it can be shown that the solution to the KKT conditions is unique, which means the unique solution is the global optimal solution. Taking the derivative of $\mathcal{L}$ with respect to $\mathbf{g}$ and α, respectively, we have

$$\frac{\partial \mathcal{L}}{\partial \alpha} = 0 \Rightarrow \alpha = \left(\sum_{l=1}^{2L_D-1} |\mathbf{h}_l\mathbf{g}|^2 + P_N \right)^{-1} \mathbf{g}^H\mathbf{h}_{L_D}, \tag{3.6}$$

and

$$\frac{\partial \mathcal{L}}{\partial \mathbf{g}} = 0 \Rightarrow \mathbf{g} = \alpha^* \left(\sum_{l=1}^{2L_D-1} |\alpha|^2\mathbf{h}_l\mathbf{h}_l^H + \lambda\mathbf{I} \right)^{-1} \mathbf{h}_{L_D}, \tag{3.7}$$

where $(\cdot)^*$ denotes conjugation. From (3.7), we have

$$\alpha^*\mathbf{g}^H\mathbf{h}_{L_D} = \mathbf{g}^H \left(\sum_{l=1}^{2L_D-1} |\alpha|^2\mathbf{h}_l\mathbf{h}_l^H + \lambda\mathbf{I} \right) \mathbf{g}. \tag{3.8}$$

Also from (3.6), we have

$$\mathbf{g}^H\mathbf{h}_{L_D} = \alpha\mathbf{g}^H \left(\sum_{k=1}^{2L-1} \mathbf{h}_k\mathbf{h}_k^H + \frac{P_N}{P_{\max}}\mathbf{I} \right) \mathbf{g} \tag{3.9}$$

Thus, by comparing (3.8) and (3.9), we can solve the Lagrangian multiplier $\lambda = |\alpha|^2 \frac{P_N}{P_{\max}}$. Substituting λ into (3.7) and using the power constraint $\mathbf{g}^H\mathbf{g} = P_{\max}$, we can have

$$\alpha^{\mathrm{SU}} = \sqrt{P_{\max}^{-1}\mathbf{h}_{L_D}^H \left(\sum_{l=1}^{2L_D-1} \mathbf{h}_l\mathbf{h}_l^H + \frac{P_N}{P_{\max}}\mathbf{I} \right)^{-2} \mathbf{h}_{L_D}}, \tag{3.10}$$

where the superscript SU denotes the single-user scenario. Substituting λ and (3.10) into (3.7), we can obtain the optimal waveform

$$\mathbf{g}^{\mathrm{SU}} = \alpha^{\mathrm{SU}-1} \left(\sum_{l=1}^{2L_D-1} \mathbf{h}_l\mathbf{h}_l^H + \frac{P_N}{P_{\max}}\mathbf{I} \right)^{-1} \mathbf{h}_{L_D}. \tag{3.11}$$

The resulting minimum MSE in the TR system is given by

$$\mathrm{MSE}^{\mathrm{SU}} = 1 - \mathbf{h}_{L_D}^H \left(\sum_{l=1}^{2L_D-1} \mathbf{h}_l\mathbf{h}_l^H + \frac{P_N}{P_{\max}}\mathbf{I} \right)^{-1} \mathbf{h}_{L_D}. \tag{3.12}$$

Note that the phase of α can be chosen arbitrarily without altering the MSE. Therefore, we choose a real-valued α^{SU} as in (3.10). From the derivation above, we can obtain the closed-form solution to the waveform design without interference pre-cancellation given the channel matrix and the signal power to noise power ratio.

3.2.2 Interference Pre-cancellation

In TR systems, a user estimates the intended symbol by the sample of the central peak of the receive signal. Therefore, the ISI can be identified as two parts: the causal ISI and the anti-causal ISI. Due to the overlapping of the received signals of consecutive symbols, one symbol can have influence to the 'previous' transmitted symbols and also to the 'future' transmitted symbols. To compensate for the interference caused by the previous symbols, the current symbol can be subtracted by

the interference before convolving with the transmit waveform, that is,

$$v[k] = s[k] - (\mathbf{h}_{L_D}^H \mathbf{g})^{-1} \sum_{l=1}^{L_D-1} (\mathbf{h}_{L_D+l}^H \mathbf{g}) v[k-l]. \tag{3.13}$$

The operation in (3.13) can be considered as passing the symbols $s[\cdot]$ through a feedback filter $\mathbf{b}^{\mathrm{ZF}} = (\mathbf{h}_{L_D}^H \mathbf{g})^{-1}[\mathbf{0}_{1\times L_D}, -\mathbf{h}_{L_D+1}^H \mathbf{g}, \ldots, -\mathbf{h}_{2L_D-1}^H \mathbf{g}]$, where $\mathbf{0}_{1\times L_D}$ denotes a $1 \times L_D$ zero vector. The resulting MSE is then given by

$$\mathrm{MSE}^{\mathrm{IPC}} = |\alpha \mathbf{h}_{L_D}^H \mathbf{g} - 1|^2 P_V + \sum_{l=1}^{L_D-1} |\alpha \mathbf{h}_l^H \mathbf{g}|^2 P_V + |\alpha|^2 P_N, \tag{3.14}$$

where P_V, the average power of $v[\cdot]$, usually requires more power than P_S since additional power is needed for the second term in (3.13) even though the causal interference part $\sum_{l=L_D+1}^{2L_D-1} |\alpha \mathbf{h}_l^H \mathbf{g}|^2$ can be completely cancelled. Thus, the benefit of performing interference pre-cancellation can be impaired by the performance degradation caused by the additional power. Especially when the noise power is more dominant than the interference power, the interference pre-cancellation cannot provide much performance improvement and much of the transmit power would be wasted in performing the pre-cancellation.

The problem of the increase of the transmit power can be resolved by applying the Tomlinson-Harashima Precoding (THP) [71, 99], which is to incorporate a modulo-A component after the interference-precancellation at the transmitter, and a modulo-A component before the symbol estimation at the receiver. The resulting block diagram is depicted in Figure 3.2(a). The modulo-A operation, denoted as $\mathrm{mod}_A(\cdot)$, is to subtract element-wise the nearest integral multiple of A from the

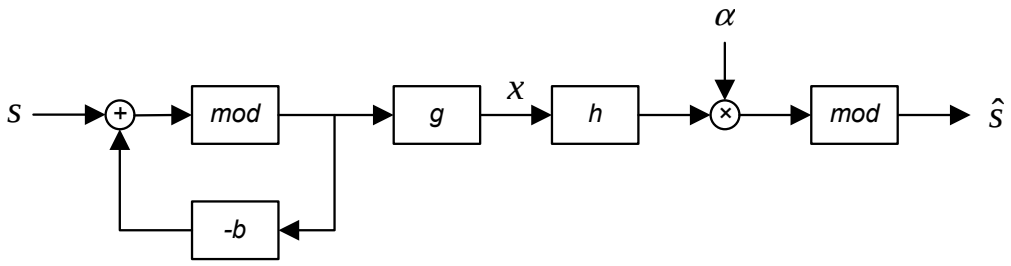

(a) Block diagram of joint waveform design and interference pre-cancellation for a single-user TR system.

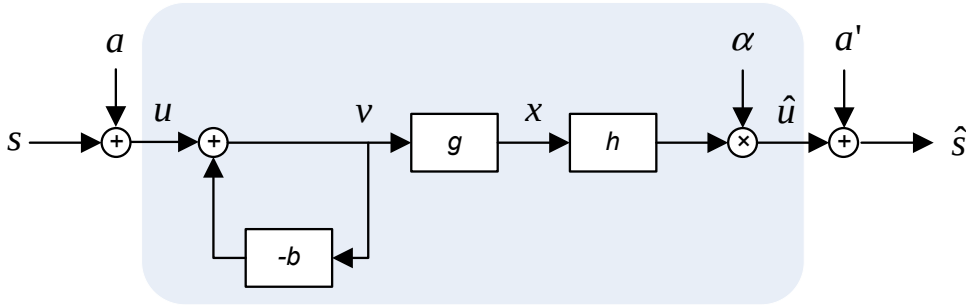

(b) Equivalent block diagram of (a).

Figure 3.2: Block diagrams of joint waveform design and interference pre-cancellation for a single-user TR system.

input such that each element of the output is in $[-\frac{A}{2}, \frac{A}{2})$, i.e., for an input v,

$$\mathrm{mod}_A(v) = v - A\left\lfloor \frac{v}{A} + \frac{1}{2} \right\rfloor, \tag{3.15}$$

where $\lfloor \cdot \rfloor$ is the floor operator, which returns the highest integer that is lower or equal to the input value. Note that for complex value, the modulo-A operator applies to both the real and the imaginary parts independently. With different constellation size of the symbol modulation (e.g., QPSK, 16-QAM, or 64-QAM), the parameter A can be chosen accordingly to minimize the modulo loss which will be explained in detail in Section 3.2.4.

3.2.3 Joint Waveform Design and Interference Pre-cancellation

The modulo-A component imposes nonlinearity to the design of the feedback filter $\mathbf{b}$. The nonlinear part can be moved to the outermost of the system design such that the converted system in Figure 3.2(b) is equivalent to the original system in Figure 3.2(a) [30, 85, 112], where a and a' denote integral multiples of A such that the outputs of the modulo components are within the proper range. We can focus on minimizing the MSE of the linear part of the system, i.e., $\text{MSE}^{\text{IPC}} = E[\|\hat{u} - u\|^2]$, where the superscript IPC denotes interference pre-cancellation, u denotes the symbol after adding a to the original input s, and $\hat{u}$ is the symbol before adding a' for the estimated symbol $\hat{s}$. The MSE is given by

$$\begin{aligned}\text{MSE}^{\text{IPC}}(\mathbf{g}, \mathbf{b}, \alpha) = |\alpha|^2 \sum_{l=1}^{L_D-1} |\mathbf{h}_l^H \mathbf{g}|^2 P_V + |\alpha \mathbf{h}_{L_D}^H \mathbf{g} - 1|^2 P_V \\ + \sum_{l=L_D+1}^{2L_D-1} |\alpha \mathbf{h}_l^H \mathbf{g} - b[l]|^2 P_V + |\alpha|^2 P_N, \end{aligned} \tag{3.16}$$

where P_V is the average power of the modulo output. The first term, $|\alpha|^2 \sum_{l=1}^{L_D-1} |\mathbf{h}_l^H \mathbf{g}|^2 P_V$, is the anti-causal interference caused by the symbols transmitted after the current symbol. The third term, $\sum_{l=L_D+1}^{2L_D-1} |\alpha \mathbf{h}_l^H \mathbf{g} - b[l]|^2 P_V$, is the causal interference caused by the symbols transmitted before the current symbol. Our goal of the joint waveform design and interference pre-cancellation is to jointly determine the parameters $\mathbf{b}$, $\mathbf{g}$ and α such that the MSE is minimized. It is clear that the optimal $b[l]$ should be chosen such that

$$b[l] = \begin{cases} \alpha \mathbf{h}_l^H \mathbf{g}, & l = L_D + 1, \ldots, 2L_D - 1, \\ 0, & \text{otherwise.} \end{cases} \tag{3.17}$$

Substituting (3.17) into (3.16) and setting $P_V = 1$ for normalization, we can solve the problem of MSE minimization subject to a transmit power constraint by a similar analysis as in (3.5)-(3.10). The optimal α and $\mathbf{g}$ is given by

$$\alpha^{\mathrm{IPC}} = \sqrt{P_{\max}^{-1}\mathbf{h}_{L_D}^H \left(\sum_{l=1}^{L_D-1} \mathbf{h}_l \mathbf{h}_l^H + \frac{P_N}{P_{\max}}\mathbf{I} \right)^{-2} \mathbf{h}_{L_D}}, \tag{3.18}$$

$$\mathbf{g}^{\mathrm{IPC}} = \alpha^{-1} \left(\sum_{l=1}^{L_D-1} \mathbf{h}_l \mathbf{h}_l^H + \frac{P_N}{P_{\max}}\mathbf{I} \right)^{-1} \mathbf{h}_{L_D} \tag{3.19}$$

The resulting minimum MSE is given by

$$\mathrm{MSE}^{\mathrm{IPC}} = 1 - \mathbf{h}_{L_D}^H \left(\sum_{l=1}^{L_D-1} \mathbf{h}_l \mathbf{h}_l^H + \frac{P_N}{P_{\max}}\mathbf{I} \right)^{-1} \mathbf{h}_{L_D}. \tag{3.20}$$

Examining the difference between (3.11) and (3.19), we can see that $\mathbf{g}^{\mathrm{IPC}}$ takes into account only the anti-causal ISI, which comprises the 1st to the $(L_D - 1)$-th rows of the decimated channel matrix $\tilde{\mathbf{H}}$. The causal ISI, i.e., the $(L_D + 1)$-th to the $(2L_D - 1)$-th rows, are not considered in $\mathbf{g}^{\mathrm{IPC}}$ since they can be pre-cancelled by the feedback filter $\mathbf{b}$. The difference between the resulting MMSEs in (3.12) and (3.20) also demonstrates such an effect.

The design of the optimal parameters can be summarized as follows. First, the receiver gain α^{IPC} is determined by (3.18). Then the waveform $\mathbf{g}^{\mathrm{IPC}}$ is designed to suppress the anti-causal interference using (3.19) given α^{IPC}. Finally, the coefficients of the feedback filter $\mathbf{b}$ for interference pre-cancellation is obtained by (3.17) given $\mathbf{g}^{\mathrm{IPC}}$ and α^{IPC}.

3.2.4 Bit Error Rate Analysis

The performance of the joint waveform design and interference pre-cancellation can be analyzed by considering several losses of incorporating the THP, including power loss, modulo loss, and shaping loss [37,127]. The power loss is due to the fact that the modulo output still requires higher power P_V than the symbol power P_S. Since the modulo operation changes the constellation to be repeated over the whole space and such a change shrinks the decision region of those symbols at the boundary of the constellation, when those boundary symbols are transmitted, the received symbols may be misinterpreted as wrong symbols and modulo loss occurs. Finally, the shaping loss happens when the distribution of the transmit signal becomes non-Gaussian since information-theoretically the optimal input distribution is Gaussian while the modulo operation generally produces a uniform distributed signal. In the TR system, the output of the modulo operation is passed though the transmit waveform, which considerably randomizes the distribution and tends to give rise to a Gaussian-like distribution. Hence, in the following analysis, we neglect the shaping loss and focus on the power loss and modulo loss.

The output of the modulo operation is uniformly distributed when the interference to be pre-cancelled is large enough. Considering both in-phase and quadrature components of $v[\cdot]$, we can have $P_V = \frac{2A^2}{3}$, where A is the modulo operation size. The optimal choice of A depends on the constellation size [96]. For example, $A = \sqrt{2}$ for QPSK and the power loss is $4/3 \approx 1.25$dB. As discussed above, the modulo loss occurs when the boundary symbols are transmitted, and thus depends

on the constellation size. The bit error rate for QPSK can be approximated by

$$P_b^{\text{QPSK}} \approx 2Q\left(\sqrt{\frac{\frac{1}{\sqrt{2}}P_{\text{loss}}^{-1}}{P_{\text{ISI}}+\sigma^2}}\right) - Q\left(3\sqrt{\frac{\frac{1}{\sqrt{2}}P_{\text{loss}}^{-1}}{P_{\text{ISI}}+\sigma^2}}\right) + Q\left(5\sqrt{\frac{\frac{1}{\sqrt{2}}P_{\text{loss}}^{-1}}{P_{\text{ISI}}+\sigma^2}}\right) - \ldots, \tag{3.21}$$

where $P_{\text{ISI}} = P_V \sum_{l=1}^{L_D-1} |\mathbf{h}_l^H \mathbf{g}|^2$. For higher order constellation such as 16-QAM or 64-QAM, the analysis can be derived similarly.

3.3 Multi-User Joint Waveform Design and Interference Pre-cancellation

In the joint waveform design and interference pre-cancellation for the single-user TR system, the causal ISI is pre-cancelled by the feedback filter and anti-causal ISI is suppressed by the waveform design. In the multi-user downlink TR system, we can leverage a similar idea of pre-cancelling both the causal ISI and the causal IUI by feedback filters, and suppressing both the anti-causal ISI and the anti-causal IUI by the multi-user waveform design.

Figure 3.3(a) depicts the block diagram of a multi-user TR system with interference pre-cancellation. The wide arrows denote the flow of a vector of data streams as the extension of Figure 3.2. The feedback filter takes a vectored input and turns out a vectored output. In the waveform part, each data stream is convolved with its waveform $\mathbf{g}_k$ and the outputs are additively aggregated together to be the transmit signal.

To determine the causality of IUI and ISI, the ordering of users for interference pre-cancellation has to be settled. Finding the optimal ordering requires exhaustive search over all possible permutations and is computationally prohibitive.

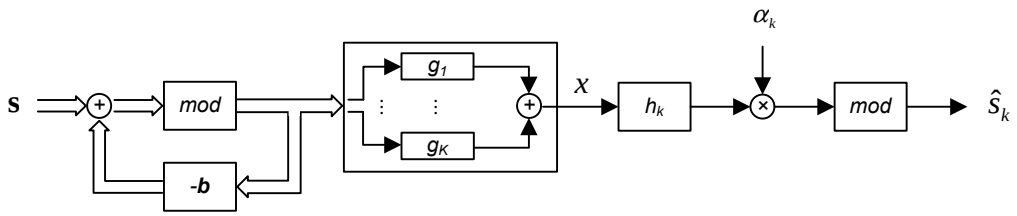

(a) Block diagram of joint waveform design and interference pre-cancellation for a multi-user TR system.

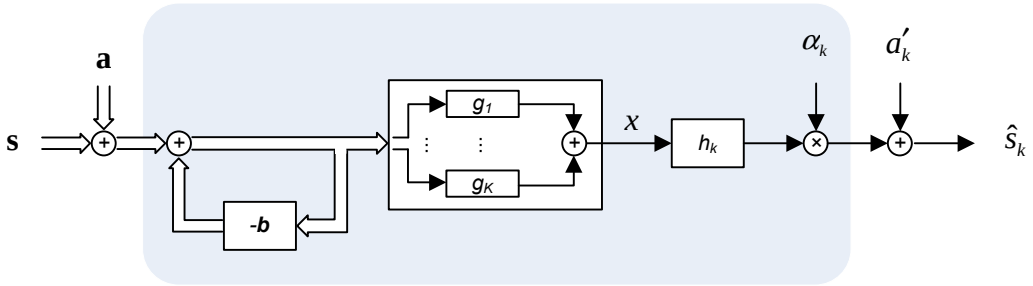

(b) Equivalent block diagram of (a).

Figure 3.3: Block diagrams of joint waveform design and interference pre-cancellation for a multi-user TR system.

Moreover, as will be shown in Section 3.4, the overhead of searching may not be worthy since the amount of interference with different orderings differs only in the current symbols, which contribute a relatively small portion to the overall interference. In the following, we denote the index of a user as its ordering. For user k's L_D-th symbol, $s_k[L_D]$, the causal interference is caused by the symbols including $\{s_j[l], l < L_D, \forall j\}$ and $\{s_j[L_D], j < k\}$; the anti-causal interference is caused by the symbols $\{s_j[l], l > L_D, \forall j\}$ and $\{s_j[L_D], j > k\}$. Figure 3.4 illustrates the causality of interference for a multi-user system with $K = 5$ and $L_D = 5$, and different causalities are separated by dash lines. When the current symbol is $s_3[5]$, the symbols in the bottom left part of Figure 3.4 serve as the causal interference to be pre-cancelled by the feedback filter, and the symbols in the top right part of Figure 3.4 are the anti-causal interference to be suppressed by the waveform design.

Similar to the single-user case, we consider the linear part of the equivalent system in Figure 3.3(b). The MSE of user k in can be expressed as

$$\begin{aligned}\text{MSE}_k = &\sum_{j=1}^{K}\sum_{l=1}^{L_D-1} |\alpha_k \mathbf{h}_{kl}^H \mathbf{g}_j|^2 P_V + \sum_{j>k} |\alpha_k \mathbf{h}_{kL_D}^H \mathbf{g}_j|^2 P_V + |\alpha_k \mathbf{h}_{kL_D}^H \mathbf{g}_k - 1|^2 P_V \\ &+ \sum_{j<k} |\alpha_k \mathbf{h}_{kL_D}^H \mathbf{g}_j - b_{kj}[L_D]|^2 P_V + \sum_{j=1}^{K}\sum_{l=1}^{L_D-1} |\alpha_k \mathbf{h}_{kl}^H \mathbf{g}_j - b_{kj}[l]|^2 P_V + |\alpha_k|^2 P_N,\end{aligned} \tag{3.22}$$

where $b_{kj}[\cdot]$ denotes the feedback filter of user k for pre-cancelling the interference of user j's data stream. In the following, we aim to jointly design the waveforms $\{\mathbf{g}_k\}$, the feedback filters $\{\mathbf{b}_k\}$, and the the gains $\{\alpha_k\}$ such that the total MSE is minimized. It is clear that the optimal coefficients of the feedback filter are given

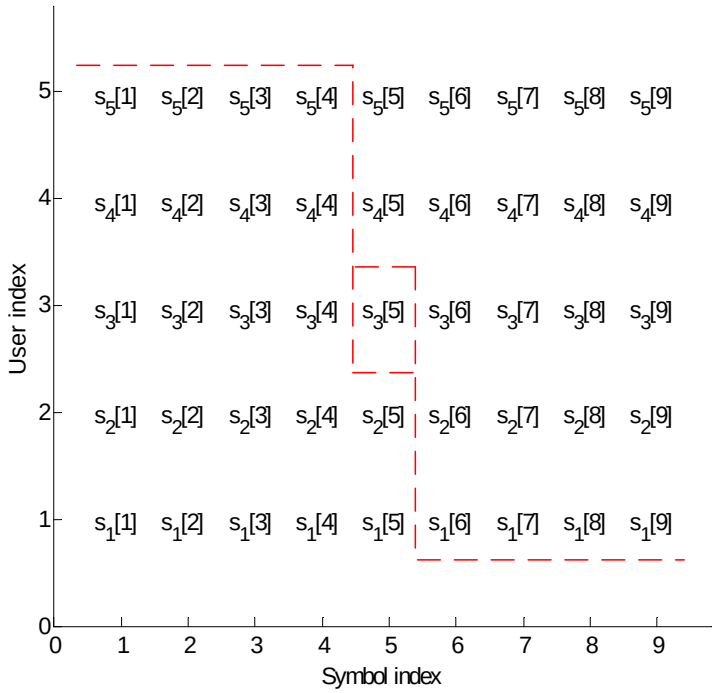

Figure 3.4: Illustration of the causality of interference caused by symbols of users.

by

$$b_{kj}[l] = \begin{cases} \alpha_k \mathbf{h}_{kl}^H \mathbf{g}_j, & l = L_D + 1, \ldots, 2L_D - 1, \forall j, \text{ or } l = L_D, j < k, \\ 0, & \text{otherwise.} \end{cases} \tag{3.23}$$

Substituting (3.23) into (3.22), we have

$$\begin{aligned} \text{MSE}_k = & \sum_{j=1}^{K} \sum_{l=1}^{L_D-1} |\alpha_k \mathbf{h}_{kl}^H \mathbf{g}_j|^2 P_V + \sum_{j>k} |\alpha_k \mathbf{h}_{kL_D}^H \mathbf{g}_j|^2 P_V \\ & + |\alpha_k \mathbf{h}_{kL_D}^H \mathbf{g}_k - 1|^2 P_V + |\alpha_k|^2 P_N. \end{aligned} \tag{3.24}$$

It can be seen that user k's optimal waveform $\mathbf{g}_k$ relies on other users' optimal waveforms. Therefore, unlike the single-user case, the closed form global optimal solution of the multi-user problem is difficult to find. Hence, we propose two iterative algorithms to search for locally optimal solutions. One approach is an alternating

optimization method and the other is a gradient method. The convergence of both iterative algorithms can be guaranteed by showing the monotonicity of the objective functions during the iterations.

3.3.1 Alternating Optimization Algorithm

The alternating optimization algorithm is to iteratively optimize over a restricted subset of all variables [15]. In this proposed algorithm, we iteratively update the waveforms $\{\mathbf{g}_k\}$ and the gains $\{\alpha_k\}$ to optimize the total MSE subject to a power constraint. It will be shown that fixing one set of variables, optimization over the other set of variables is a convex problem and the closed-form solution can be derived. The total MSE in each iteration is non-increasing and thus the alternating optimization algorithm is guaranteed to converge.

It is easy to optimize the gains $\{\alpha_k\}$ given a set of fixed waveforms $\{\mathbf{g}_k\}$ since the total MSE $\sum_{k=1}^{K} \mathrm{MSE}_k$ is a quadratic function of $\{\alpha_k\}$. We can consider the first order condition, i.e., the first order derivative of the total MSE with respect to α_k equals zero. We can have

$$\alpha_k = \left(\sum_{j \geq k} |\mathbf{h}_{kL_D}^H \mathbf{g}_j|^2 + \sum_{j=1}^{K} \sum_{l=1}^{L_D-1} |\mathbf{h}_{kl}^H \mathbf{g}_j|^2 + \frac{P_N}{P_X} \right)^{-1} \mathbf{g}_k^H \mathbf{h}_{kL_D}, \quad \forall k. \tag{3.25}$$

Next, we consider the optimization of the waveforms $\{\mathbf{g}_k\}$ subject to a power constraint, with a set of fixed gains $\{\alpha_k\}$. Directly taking the derivative of the Lagrangian with respect to $\{\mathbf{g}_k\}$ leads to an expression in terms of the Lagrange multiplier λ associated with the power constraint. Solving λ, however, is quite difficult and arouses the need for numerical search. Motivated by the technique in

(3.6)-(3.11) where the Lagrange multiplier can be explicitly obtained, we propose to keep the ratio between $\{\alpha_k\}$ fixed and optimize the corresponding $\{\mathbf{g}_k\}$ so that the Lagrange multiplier can be solved explicitly. That is, instead of fixing $\{\alpha_k\}$, we fix $\bar{\alpha}_k = \gamma^{-1}\alpha_k$, for all k, where $\gamma = \sqrt{\sum_k |\alpha_k|^2 / P_{\max}}$, which means $\sum_k |\bar{\alpha}_k|^2 = P_{\max}$, and γ is considered as a variable in the optimization problem. The Lagrangian of minimizing the total MSE subject to the power constraint, with variables γ and $\mathbf{g}_k, \forall k$, is given by

$$\mathcal{L}(\mathbf{g}_1, ..., \mathbf{g}_K, \gamma, \lambda) = \sum_{k=1}^{K} \mathrm{MSE}_k + \lambda \left(\sum_{k=1}^{K} \mathbf{g}_k^H \mathbf{g}_k - P_{\max} \right). \tag{3.26}$$

Taking the first order derivative of $\mathcal{L}$ with respect to $\mathbf{g}_k^*$, we have

$$\mathbf{g}_k = \gamma^{-1} \bar{\alpha}_k^* \left(\sum_{j \le k} |\bar{\alpha}_j|^2 \mathbf{h}_{jL_D} \mathbf{h}_{jL_D}^H + \sum_{j=1}^{K} \sum_{l=1}^{L_D - 1} |\bar{\alpha}_j|^2 \mathbf{h}_{jl} \mathbf{h}_{jl}^H + \frac{\lambda}{P_X} \mathbf{I} \right)^{-1} \mathbf{h}_{kL_D} \tag{3.27}$$

Taking the first order derivative of $\mathcal{L}$ with respect to γ, we have

$$\gamma = \left(\sum_{k=1}^{K} \bar{\alpha}_k^* \mathbf{g}_k^H \mathbf{h}_{kL_D} \right) \left(\sum_{k=1}^{K} \left(\sum_{j \le k} |\bar{\alpha}_j \mathbf{h}_{jL_D}^H \mathbf{g}_k|^2 + \sum_{j=1}^{K} \sum_{l=1}^{L_D - 1} |\bar{\alpha}_j \mathbf{h}_{jl}^H \mathbf{g}_k|^2 + \frac{P_N}{P_X} |\bar{\alpha}_k|^2 \right) \right)^{-1} \tag{3.28}$$

From (3.27), (3.28), and the power constraint $\sum_k \mathbf{g}_k^H \mathbf{g}_k = P_{\max}$, we can have $\lambda = P_N$. By substituting γ and $\lambda = P_N$ into (3.27), the closed form solution of $\mathbf{g}_k$ can be obtained.

The proposed alternating optimization algorithm, summarized in Table 3.1, is to fix one set of variables and optimize the other set of variables to decrease the total MSE until convergence or the maximum number of iterations is reached. When the waveforms $\{\mathbf{g}_k\}$ are fixed, updating the gains $\{\alpha_k\}$ can only reduce the total MSE or keep it unchanged. Similarly, when the normalized gains $\{\bar{\alpha}_k\}$ are fixed, updating

Table 3.1: Alternating Optimization Algorithm for Multi-user Downlink Waveform Design

(i) Initialize $\alpha_k = 1, \forall k$.

(ii) **Loop** :

1. *Calculate waveforms*: $\{\mathbf{g}_k\}$ and γ by (3.27) and (3.28).
2. *Calculate gains*: $\{\alpha_k\}$ by (3.25).

Until α_k, $\{\mathbf{g}_k\}$ and γ converge or the max. number of iterations is reached.

the waveforms $\{\mathbf{g}_k\}$ also makes the total MSE non-increasing. Thus, it can be easily seen that the proposed alternating optimization algorithm always converges since the total MSE is always non-increasing during the iterations and the total MSE is lower bounded by zero. Note that the converged solution may not be a global optimum but it is a local optimum where none of the two optimization steps can further improve the performance.

3.3.2 Gradient Algorithm

The gradient method, by iteratively updating the variables to the steepest direction that decreases the objective function, is able to locate the global minimum for convex functions, but only a local optimum for a wide class of non-convex functions [15]. We propose to remove the dependence of $\{\alpha_k\}$ by substitute (3.6) into the MSE in (3.24) so that the gradient method can focus on updating $\{\mathbf{g}_k\}$ only. Then the resulting total MSE as a function of $\{\mathbf{g}_k\}$ is given by

$$\sum_{k=1}^{K} \mathrm{MSE}_k = P_V \sum_{k=1}^{K} \left(1 - t_k^{-1} |\mathbf{g}_k^H \mathbf{h}_{kL_D}|^2\right), \tag{3.29}$$

where

$$t_k = \sum_{j \geq k} |\mathbf{h}_{kL_D}^H \mathbf{g}_j|^2 + \sum_{j=1}^{K} \sum_{l=1}^{L_D-1} |\mathbf{h}_{kl}^H \mathbf{g}_j|^2 + \frac{P_N}{P_V}. \tag{3.30}$$

It can be easily verified that the total MSE in (3.29) is non-convex in $\{\mathbf{g}_k\}$. The gradient of $\mathbf{g}_k$ can be obtained as

$$\Delta \mathbf{g}_k \triangleq \frac{\partial}{\partial \mathbf{g}_k^*} \left(\sum_k \text{MSE}_k \right) = P_V \left(-\mathbf{h}_{kL_D} \mathbf{h}_{kL_D}^H t_k^{-1} + \sum_{j=1}^{k} |\mathbf{g}_j^H \mathbf{h}_{jL_D}|^2 \mathbf{h}_{jL_D} \mathbf{h}_{jL_D}^H t_j^{-2} + \sum_{j=1}^{K} \sum_{l=1}^{L_D-1} |\mathbf{g}_j^H \mathbf{h}_{jL_D}|^2 \mathbf{h}_{jl} \mathbf{h}_{jl}^H t_j^{-2} \right) \mathbf{g}_k. \tag{3.31}$$

The gradient algorithm is summarized in Table 3.2, where the waveforms are iteratively updated by

$$\mathbf{g}_k^{(n+1)} = \text{proj}_{\mathcal{C}} \left[\mathbf{g}_k^{(n)} - \delta^{(n)} \frac{\Delta \mathbf{g}_k^{(n)}}{\|\Delta \mathbf{g}_k^{(n)}\|_2} \right]. \tag{3.32}$$

We choose the step size $\delta^{(n)}$ to be the harmonic sequence $\frac{1}{d}, d = 1, 2, \ldots$ for its good convergence behavior [15]. The projection operator $\text{proj}_{\mathcal{C}}$ is to project the updated waveforms into the constraint set $\sum_{k=1}^{K} \mathbf{g}_k^H \mathbf{g}_k = P_{\max}$ by normalization. In each iteration, the total MSE generated by the proposed gradient algorithm is non-increasing. By the same argument that the sequence of the total MSE is non-increasing and bounded below, the proposed gradient algorithm is guaranteed to converge to a local minimum, where the gradient is zero.

3.4 Numerical Simulation

In this section, we perform numerical simulation to study the performance of the proposed joint design. The Saleh-Valenzuela channel model for indoor environment is adopted to generate the instances of a multipath channel impulse response.

Table 3.2: Gradient Algorithm for Multi-user Downlink Waveform Design

(i) Initialize $\mathbf{g}_k = \mathbf{h}_{kL_D}, \forall k$.

(ii) **Loop**:

(a) *Calculate gradients*: $\{\Delta\mathbf{g}_k\}$ by (3.31).

(b) *Update waveforms*: $\{\mathbf{g}_k^{(n)}\}$ by (3.32).

(c) *Line search*:

If $\sum_k \mathrm{MSE}_k^{(n)} > \sum_k \mathrm{MSE}_k^{(n-1)}$

$d = d + 1$, $\delta^{(n)} = \frac{1}{d}$.

goto (b).

else

$n = n + 1$.

end if

Until $\{\mathbf{g}_k\}$ converge or the max. number of iterations is reached.

In Figure 3.5, we plot the equivalent channels, $(\mathbf{g} * \mathbf{h})$, i.e., the composite effect of the transmit waveform and the channel impulse response. Figure 3.5(a) shows the equivalent channel of using pure waveform design, and Figure 3.5(b) shows the equivalent channel of using joint waveform waveform design. Since the joint waveform design only suppresses the anti-causal interference and the causal part is pre-cancelled by the feedback filter, we can see that the causal interference is untamed and significantly larger than the pure waveform design in Figure 3.5(a). However, with the same degrees of freedom, the joint waveform design only needs to suppress about half of the interference compared to the pure waveform design, and it is able to achieve higher peak amplitude and better interference suppression for the anti-causal interference.

Figure 3.6 and 3.7 show the single-user BER performance for different waveform design schemes when $D = 1$ and $D = 3$, respectively. 'Basic TR' denotes the

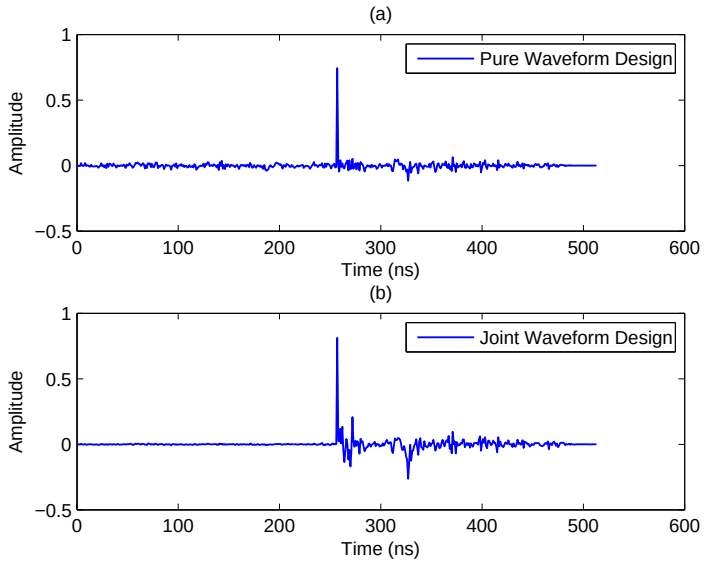

Figure 3.5: Equivalent channels for pure waveform design and joint waveform design.

traditional TR waveform, which is the time-reversed and conjugated version of the channel impulse response. It can be seen that the joint waveform design can achieve a remarkable performance gain at high SNR region for $D = 1$ compared to $D = 3$. This is because when D is smaller, i.e., the symbol rate is higher, and when the signal power is more dominant than the noise power, the interference is more severe and the joint design has a substantial advantage under such a scenario. The theoretical analysis of the BER performance for the proposed joint design with $D = 1$ is quite close to the simulated result. The theoretical BER of $D = 1$ is more accurate than $D = 3$ due to the fact that the analysis is greatly based on the assumption of a Gaussian distributed interference, and a smaller rate back-off factor results in more interfering multipaths, which makes the distribution of the ISI more similar to a Gaussian one.

A typical convergence behavior of the two proposed iterative algorithms is

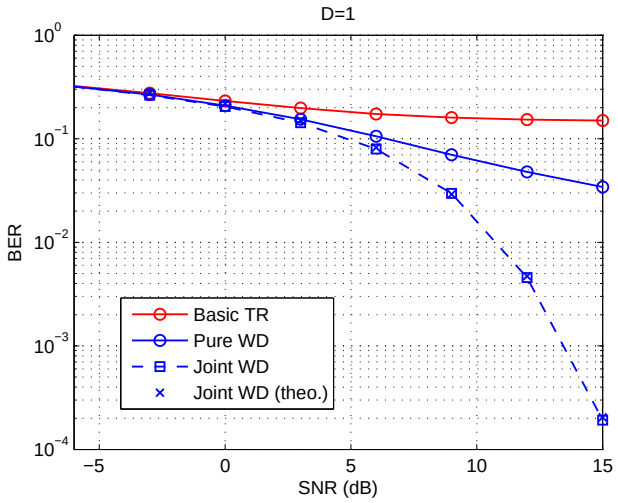

Figure 3.6: BER performance comparison for $D = 1$.

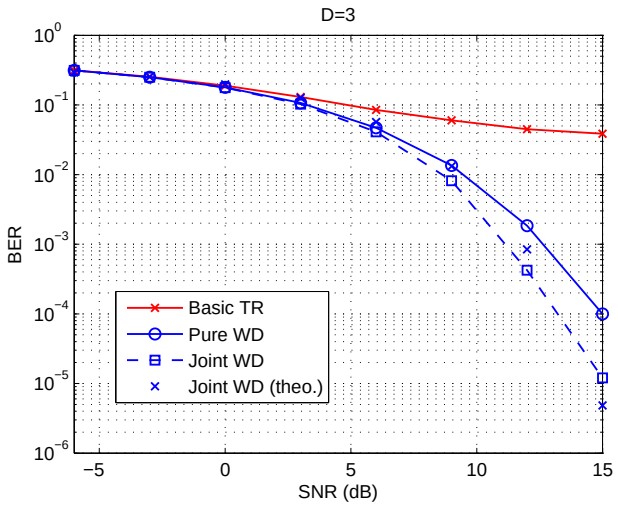

Figure 3.7: BER performance comparison for $D = 3$.

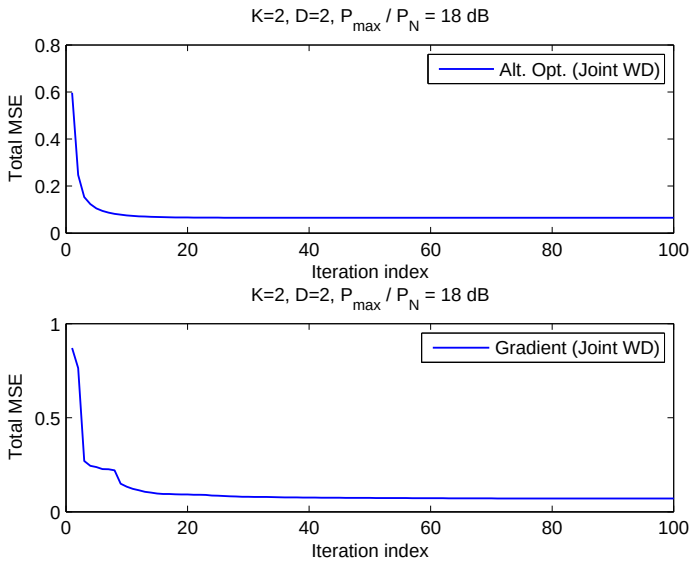

Figure 3.8: Convergence behavior of the two proposed iterative algorithms.

plotted in Figure 3.8 with $K = 2$, $D = 2$ and $P_{\max}/P_N = 18$ dB. The average number of convergence for the proposed alternating optimization algorithm is 10.34 at 0 dB and 26.88 at 18 dB. For the proposed gradient method, the average number of iterations is 7.49 at 0 dB and 48.51 at 18 dB. When $P_{\max}/P_N$ is low, the noise power dominates the interference power, and thus the waveform calculation is easier since a user's waveform should be close to the basic time-reversal waveform which is based its own channel and irrelevant to others'. On the other hand, when the noise power is low, the severe ISI and IUI greatly influence the performance, and a user's waveform has to take into account others' waveforms to avoid the interference. Therefore, high $P_{\max}/P_N$ region typically requires more iterations for the algorithms to converge.

For both the alternating optimization algorithm and the gradient algorithm, the ordering of users has to be determined first. As discussed in Section 3.3, finding

the optimal ordering requires an exhaustive search. Heuristic algorithms for finding a suboptimal user ordering, such as the ones in [68, 69], can be adopted. Let us consider the initial step in the alternating optimization algorithm, the α_k's are initialized to be the same, and by substituting the solutions of $\mathbf{g}_k$'s into the MSE in (3.24), the resulting total MSE is given by

$$\sum_{k=1}^{K} \mathrm{MSE}_k = \sum_{k=1}^{K} P_V \left(1 - \mathbf{h}_{\pi_k L_D} \mathbf{T}_{\pi_k}^{-1} \mathbf{h}_{\pi_k L_D}\right), \tag{3.33}$$

where

$$\mathbf{T}_{\pi_k} = \sum_{j \le k} \mathbf{h}_{\pi_j L_D} \mathbf{h}_{\pi_j L_D}^H + \sum_{j=1}^{K} \sum_{l=1}^{L_D} \mathbf{h}_{\pi_j l} \mathbf{h}_{\pi_j l}^H + \frac{P_N}{P_V} \mathbf{I}. \tag{3.34}$$

We consider a greedy algorithm exploiting the fact that $\mathbf{T}_{\pi_k}$ does not depend on the particular ordering of $\{\pi_j, j \le k\}$ for the first term in (3.34) and the second term is the sum of all users' causal ISI and does not rely on the overall ordering. Based on this, once $\{\pi_j, j > k\}$ is determined, MSE_k can be optimized by choosing π_k. We can sequentially choose $\pi_K, \ldots, \pi_1$, i.e., the greedy $\{\pi_k^{\mathrm{G}}\}$ can be determined by

$$\pi_k^{\mathrm{G}} = \arg \max_{\pi_k \notin \{\pi_j^{\mathrm{G}}, j > k\}} \mathbf{h}_{\pi_k L_D} \mathbf{T}_{\pi_k}^{-1} \mathbf{h}_{\pi_k L_D}, \qquad \text{for } k = K, K-1 \ldots, 1. \tag{3.35}$$

However, such a greedy approach is not globally optimal since first of all, the objective function in (3.33) is an approximation since we assume $\{\alpha_k\}$ the same, and secondly, even if the globally optimal $\{\pi_j, j > k\}$ can be found, the subsequent global optimization of π_k has to take into account all terms in (3.33) instead of only $\mathbf{h}_{\pi_k L_D} \mathbf{T}_{\pi_k}^{-1} \mathbf{h}_{\pi_k L_D}$, but such optimization is quite involved and does not permit a better solution other than the exhaustive search.

In Figure 3.9 and 3.10, we compare the total MSE and the average BER performance of the methods with $K = 2$ and $D = 2$. It can be seen that for the total MSE, the alternating optimization algorithm performs slightly better than the gradient method at the high power region while it performs a bit worse at the low power region. However, such a difference does not appear obvious in the average BER performance. The greedy ordering algorithm does not show any perceivable advantage since the current symbols only contribute a small portion to the total interference. For $K = 4$ and $D = 4$, the average BER and the total MSE are shown in Figure 3.11 and 3.12. We can observe a similar comparison of the two algorithms for the total MSE performance with a magnified difference. Specifically, for both the total MSE and the average BER performance at the high power region, the alternating optimization shows a noticeable advantage over the gradient algorithm. At the low power region, the total MSE performance of the gradient method is slightly superior than the alternating optimization algorithm, but such a difference is imperceptible in the average BER performance.

3.5 Conclusion

In this chapter, we proposed the joint waveform design and interference pre-cancellation for TR communication systems by exploiting the symbol information available at the transmitter. It was shown that the optimal joint design is to pre-cancel the causal interference by a feedback filter and to suppress the anti-causal interference using the waveform. For the multi-user scenario, the causality of both

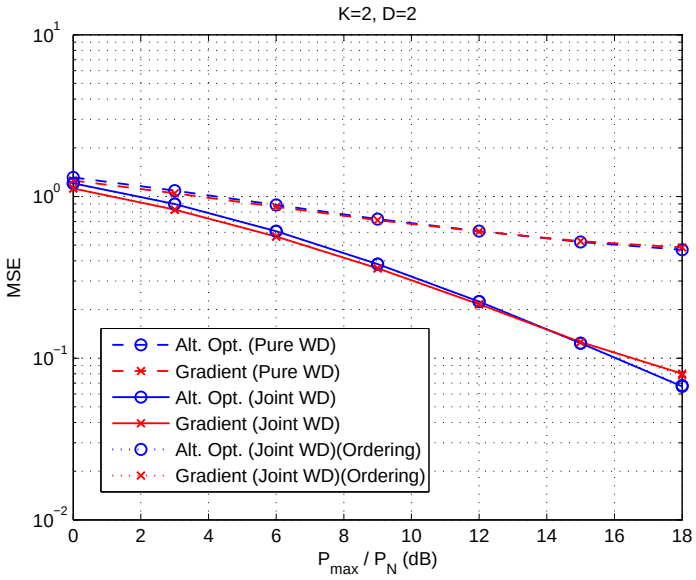

Figure 3.9: Total MSE performance comparison for $K = 2$ and $D = 2$.

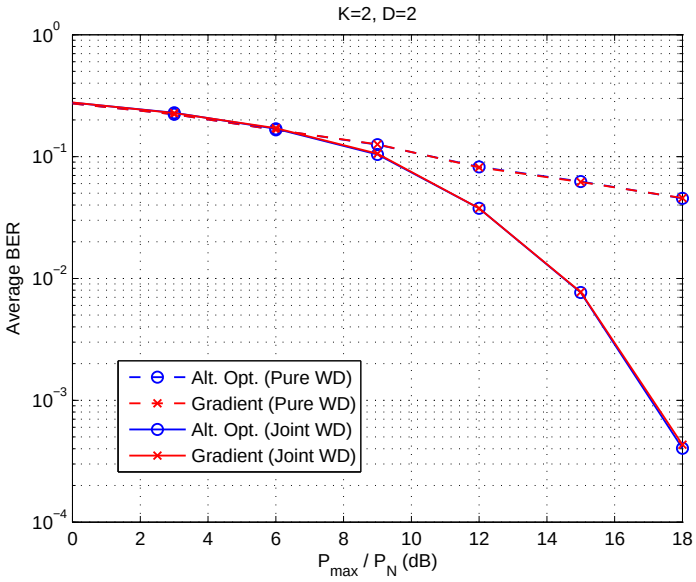

Figure 3.10: Average BER performance comparison for $K = 2$ and $D = 2$.

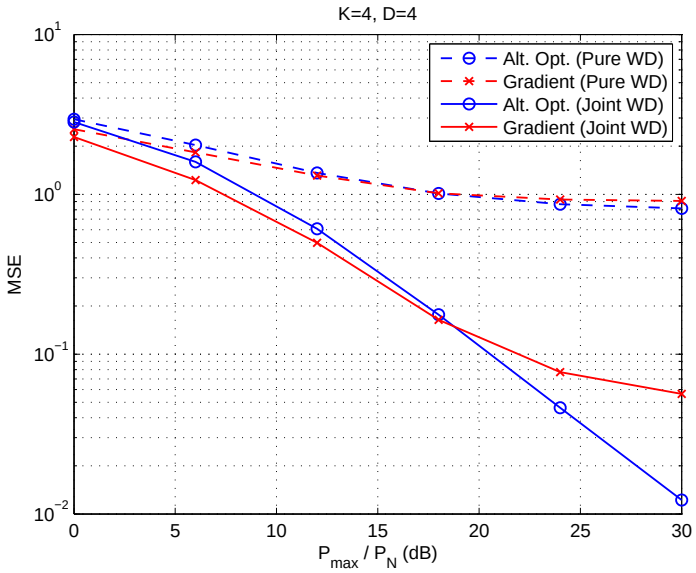

Figure 3.11: Total MSE performance comparison for $K = 4$ and $D = 4$.

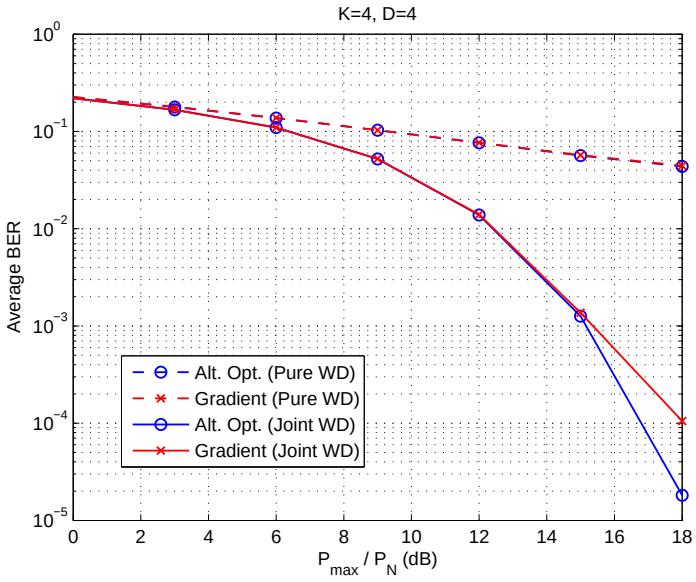

Figure 3.12: Average BER performance comparison for $K = 4$ and $D = 4$.

ISI and IUI determines its similar role in the joint design. The resulting multi-user waveform design is a non-convex optimization problem, for which we proposed two iterative algorithms, including an alternating optimization algorithm and a gradient method. Both algorithms can be guaranteed to converge to sub-optimal solutions. Simulation results were shown to validate the convergence of the proposed algorithms and demonstrate the effectiveness of the proposed joint design, especially in the high interference regime. As possible future extensions, applications of the proposed joint design to the multi-antenna scenarios can be attained by utilizing the idea of pre-cancelling the causal interference and suppressing the anti-causal interference.

Chapter 4

Wireless Access Network Selection Game with Negative Network Externality

Nowadays, wireless network services such as Femtocells [19] and Wi-Fi access points are widely deployed to provide Internet access in areas such as homes, offices, airports, hotels, etc. While there may be multiple available wireless networks, a user can only choose one to join. Figure 4.1 shows an example of the Wi-Fi network selection from a smart phone. Since the networks can be owned by different operators, the network selection problem, which used to be resolved in a centralized manner by admission control [3, 40], should be investigated in a distributed perspective by considering users' own interests. In the wireless access network selection problem, a myopic strategy can usually be adopted by choosing the one with the strongest signal. A consequence of this strategy is the congestion of users to communicate with certain network controllers such as access points (APs), switches, or routers. The concentration of users creates an unbalanced load in the network, which leads to an inefficient resource utilization for service providers and a poor quality-of-service (QoS) for users.

Efficient resource utilization is an important issue in modern wireless access networks due to limited available resources such as signal power, temporal and spa-

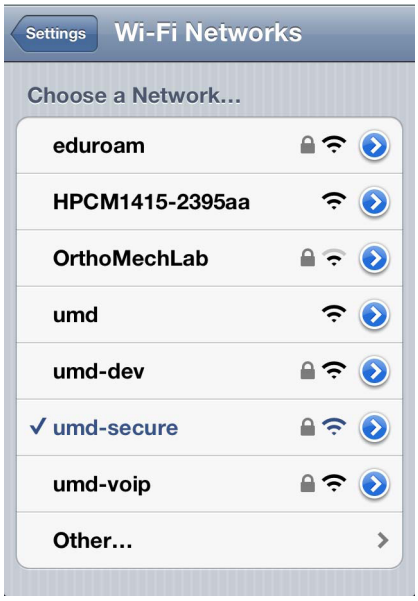

Figure 4.1: Wi-Fi network selection.

tial bandwidth. On one hand, the service provider attempts to maximize resource utilization such that the available resources can accommodate as many users as possible. On the other hand, due to the individual rationality and the selfish nature, a user aims to optimize his/her own utility. Therefore, a user's optimal strategy in such a resource-sharing scenario inevitably has to take into consideration the *negative network externality* [35, 83], i.e., the influence of other users' strategies on the user's own utility. Commonly referred in economics and business, the negative network externality is the effect that occurs when more users make the available resource less valuable. For example, the traffic congestion overloads the highway. Overwhelming customers degrade the quality-of-service in a restaurant. The negative network externality in these examples impairs the utilities of the users making the same decision.

In this chapter, we firstly focus on how a user should choose one of the available

wireless access networks considering the negative network externality. Wireless access network selection is an essential problem of resource utilization and has received great attention recently [6, 8, 18, 20, 21, 50, 58, 70, 74, 86, 92, 117]. In [8], centralized approaches are investigated to provide congestion relief by explicit channel switching and network-directed roaming. A distributed access point selection algorithm based on no regret learning is proposed in [21]. The authors show that the algorithm can guarantee convergence to an equilibrium. The arrival and departure of the users in network selection problems are also considered in [58] and [117]. Another class of network selection approaches is based on game theory. Game theory has been recognized as an ideal tool to study the interactions among users [39, 106]. It has been widely used in wireless communications and networking for many different problems [22, 46, 66, 104, 106] including power control [46], cooperation stimulation [22], and security enforcement [116]. In [70], Mittal et al. consider users changing locations as strategies to obtain more resources and analyze the corresponding Nash equilibria (NE). In [18], the network selection is modelled as a congestion game, where players make decisions simultaneously to optimize the interference and throughput. Also, the congestion in the network selection game is similar to that in the channel selection game, e.g., [97, 119, 120]. In [97], an atomic congestion game in which resources are allowed to be reused among non-interfering users is considered. In [119] and [120], the authors investigated game theoretic solutions to the distributed channel selection problem in opportunistic spectrum access systems. A comprehensive review and comparison of existing decision-theoretic solutions including Markov decision process, game theory and stochastic control can be found

in [118].

However, most of the existing works study the network selection problem under the scenario where users make decisions simultaneously. In this chapter, we consider the problem under a different scenario where users make decisions *sequentially* and their optimal decisions involve the prediction of subsequent users' decisions due to the negative network externality. Sequential decisions considering the negative network externality effect are studied in the Chinese restaurant game [54, 107, 108], in which the equilibrium of grouping under the scenario of a fixed total number of players is characterized. In this chapter, we formulate the wireless access network selection problem as a stochastic game with negative network externality, where users arrive at and depart from networks in a probabilistic manner. The problem of finding the optimal decision rule is shown to be a multi-dimensional Markov Decision Process (MDP). Different from the conventional MDP [79], the multi-dimensional MDP has multiple potential functions and thus the dynamic programming (DP) [11] cannot be directly applied. We propose a modified value iteration algorithm to find the equilibrium for the multi-dimensional MDP. The analysis of the proposed algorithm shows that the strategy profile generated by the algorithm has a threshold structure, which enables us to save the storage space of the strategy profile from $\mathcal{O}(N^2)$ to $\mathcal{O}(N \log N)$, where N^2 is the number of system states in the two-network scenario. Simulation results verify the analysis and demonstrate the efficiency and effectiveness of the proposed algorithm, i.e., while achieving the optimal strategy for the individual, the proposed algorithm attains similar performance of social welfare compared to the centralized method that maximizes the social welfare.

The second focus of this chapter is the truthful mechanism design [38, 62, 72, 73, 102] for the network selection game. Mechanism design is to devise pricing and allocation rules satisfying the incentive compatibility [62, 73]. In the network selection game, users makes decisions relying on the system states which consist of the information provided by the networks, possibly owned by different operators with different interests. Therefore, the reported state may be untruthful if it is profitable to make a deceitful claim. In this chapter, we investigate the mechanism design problem with incentive compatibility constraints, which enforce the networks to report truthfully, while optimizing the utility of users. The formulated problem is a mixed integer programming problem which in general lacks an efficient solution. Exploiting the optimality of substructures, we propose a dynamic programming algorithm that can efficiently and optimally solve the problem in the two-network scenario. For the multi-network scenario, the proposed algorithm can outperform the heuristic greedy approach in a polynomial-time complexity. Finally, simulation results are shown to validate the analysis and demonstrate the effectiveness of the proposed algorithms.

The novelty and technical contribution of this chapter are summarized as follows. We formulate the distributed wireless access network selection problem as a multi-dimensional MDP, which, to the best of our knowledge, is new and has not been studied before. We propose a modified value iteration algorithm to search for an equilibrium. We also analyze the proposed algorithm and show that the resulting strategy profile has a threshold structure. We further propose an efficient dynamic programming algorithm to design a truthful mechanism which enforces the networks

to truthfully reveal the state information.

The rest of the chapter is organized as follows. The system model and the formulation of the wireless access network selection game is described in Section 4.1. In Section 4.2, we propose a modified value iteration algorithm for the multi-dimensional MDP. The threshold structure of the strategy profile generated by the proposed algorithm is analyzed in Section 4.3. In Section 4.4, we describe the mechanism design problem for the network selection game and propose the dynamic programming algorithm. In Section 4.5, the performance of the proposed algorithms is evaluated using numerical simulation. Finally, Section 4.7 concludes the chapter.

4.1 System Model and Problem Formulation

In this section, we describe in detail the system model and the problem formulation of the wireless access network selection problem. To better illustrate the idea, we first introduce some necessary notations including the probabilistic model and then characterize the (approximate) equilibrium. Note that as will be seen, the model is quite general and hence its application is not restricted to the network selection problem but can also be deployed in other problems with negative network externality.

4.1.1 System Model

The system under consideration comprises K wireless access networks and each network has a capacity of N users, i.e., a network can simultaneously serve at most N

users. For the sake of notational conciseness, we consider that all the networks have the same capacity. The analysis can be easily extended to the system with networks of different capacity. We also assume that the networks have no buffer room for users, which means when a network is full, users cannot make request of connection to the network. Each user in network k obtains a utility $R_k(s_k)$ per unit time, where s_k is the current number of users in network k. The utility function is defined as the individual throughput, i.e., $R_k(s_k) = \log(1 + \frac{P_S/N_0}{(s_k-1)P_I/N_0+1}), \forall k$, which represents the achievable data rate under inter-user interference, where P_S/N_0 denotes the signal-to-noise power ratio, and P_I/N_0 is the interference-to-noise power ratio. The utility represents the quality-of-service (QoS) guaranteed by the network but restricted to the available resource such as the total transmission power and the bandwidth of radio frequency. The negative network externality is manifested in the decrease of the data rate as the number of users in the network increases due to a higher inter-user interference. Note that the utilities of users in the same network are assumed the same at each time slot since the network can provide the same QoS to each user by means of resource allocation, even though the instantaneous channel conditions of different users may be different. For example, centralized downlink power control algorithms [65, 129] can be applied by the network to attain a common signal to interference-plus-noise ratio (SINR) or to maximize the minimum SINR among the users.

The users with Poisson distributed arrival rate $\bar{\lambda}_0$ (users per second) have choices of connecting to one of the K networks. After a user makes his decision, he/she cannot switch to any of other networks and has to stay during a period of

time with exponential distribution of parameter $\bar{\mu}$, which is assumed the same for all networks for simplicity. The users with arrival rate $\bar{\lambda}_k$ can only choose network k, for $k = 1, \ldots, K$. These users can be envisioned as either the users with certain deterministic behavior, or the users who can only have access to one specific network due to the geographical distribution. Note that incorporating this type of users only makes the system model more general since we can simply set these rates as zero if there are no such users.*

The system state $\mathbf{s} = (s_1, \ldots, s_K)$ takes its value from the state space $\mathcal{S} = \{(s_1, \ldots, s_K) | s_k = 0, 1, ..., N, k = 1, \ldots, K\}$, and represents the state that s_k users are in network k, for $k = 1, \ldots, K$. We consider a discrete time Markov system where a time slot has duration T (seconds). Then the arrival and departure probabilities $\lambda_k = \bar{\lambda}_k T e^{-\bar{\lambda}_k T}$ and $\mu = \bar{\mu} T e^{-\bar{\mu} T}$ can be approximated as $\lambda_k \approx \bar{\lambda}_k T, k = 0, \ldots, K$ and $\mu \approx \bar{\mu} T$ when T is sufficiently small [67, 77, 109]. Let $\mathcal{F}(\mathbf{s}) = \{k | s_k = N, k = 1, \ldots, K\}$ be the index set of the full networks which are serving the maximum number of users and thus cannot accept any more. The complement set of $\mathcal{F}(\mathbf{s})$ is denoted by $\bar{\mathcal{F}}(\mathbf{s}) = \{k | s_k < N, k = 1, \ldots, K\}$, i.e., the index set of the non-full networks. The strategy space of network selection is restricted in $\bar{\mathcal{F}}(\mathbf{s})$ when $\mathbf{s}$ is a boundary state, i.e., when $\sigma_{\mathbf{s}} \in \bar{\mathcal{F}}(\mathbf{s})$. We assume that the connection request from users arriving at the full networks will be rejected and the

*More general types of users, such as users who can only connect to one of a subset of K networks, can be considered. Here for simplicity we only consider two types of users, i.e., users who have choices of connecting to any one of K networks, and users who can only choose one specific network.

traffic then goes to other non-full networks. To model such a traffic transition, we therefore assume that the traffic immediately flows to the non-full network. For the two-network case, at most only one non-full network has room for those users, so the traffic goes to that non-full network. For the multi-network case, multiple non-full networks can accommodate those users. In order to provide a well-defined Markov system and to simplify the notation, we assume that the traffic goes to a specific network, i.e., $\min \bar{\mathcal{F}}(\mathbf{s})$, the network with the minimum index. Notice that if $\bar{\mathcal{F}}(\mathbf{s}) = \phi$, i.e., all networks are full, no connection request can be accepted. The network selection strategy when the user observes state $\mathbf{s}$ is denoted as $\sigma_{\mathbf{s}}$, which takes value in $\bar{\mathcal{F}}(\mathbf{s})$. We define $\sigma_{\mathbf{s}} = j$ if network j is chosen. The indicator function $I_k(\sigma_{\mathbf{s}})$ is then defined as: if $\sigma_{\mathbf{s}} = j$, $I_j(\sigma_{\mathbf{s}}) = 1$; otherwise $I_j(\sigma_{\mathbf{s}}) = 0$. We have the state transition probability of an arrival event as

$$P_{\text{sys}}\left(\mathbf{s}+\mathbf{e}_j|\mathbf{s}\right) = \begin{cases} \sum_{i\in\mathcal{F}(\mathbf{s})}\lambda_i + \lambda_j + I_j(\sigma_{\mathbf{s}})\lambda_0, & \text{if } j = \min\bar{\mathcal{F}}(\mathbf{s}), \\ \lambda_j + I_j(\sigma_{\mathbf{s}})\lambda_0, & \text{if } j \in \bar{\mathcal{F}}(\mathbf{s})\backslash\left\{\min\bar{\mathcal{F}}(\mathbf{s})\right\}, \end{cases} \tag{4.1}$$

where $\mathbf{s}$ and $\mathbf{s}+\mathbf{e}_j$ denote the system states at the current time slot and the next time slot, and $\mathbf{e}_j$ is a standard basis vector whose j-th coordinate is 1 and other coordinates are 0. At system state $\mathbf{s}$, since the number of users in network j is s_j, the transition probability of a departure event is given by

$$P_{\text{sys}}\left(\mathbf{s}-\mathbf{e}_j|\mathbf{s}\right) = s_j\mu,\ j = 1,\ldots,K. \tag{4.2}$$

Furthermore, the probability that the system state remains the same is

$$P_{\text{sys}}(\mathbf{s}|\mathbf{s}) = \begin{cases} 1 - \sum_{j=0}^{K} \lambda_j - \sum_{j=1}^{K} s_j \mu, & \text{if } \bar{\mathcal{F}}(\mathbf{s}) \neq \phi, \\ 1 - \sum_{j=1}^{K} s_j \mu, & \text{if } \bar{\mathcal{F}}(\mathbf{s}) = \phi. \end{cases} \tag{4.3}$$

The duration of a time slot T should be chosen such that $\sum_{j=0}^{K} \lambda_j + KN\mu \leq 1$, i.e., $T \leq 1/(\sum_{j=0}^{K} \bar{\lambda}_j + KN\bar{\mu})$.

For instance, when $K = 2$, $0 \leq s_1 \leq N-1$, and $0 \leq s_2 \leq N-1$, the transition probability is given by

$$P_{\text{sys}}\{\mathbf{s}'|\mathbf{s} = (s_1, s_2)\} = \begin{cases} I_1(\sigma_{\mathbf{s}})\lambda_0 + \lambda_1, & \text{if } \mathbf{s}' = (s_1 + 1, s_2), \\ I_2(\sigma_{\mathbf{s}})\lambda_0 + \lambda_2, & \text{if } \mathbf{s}' = (s_1, s_2 + 1), \\ s_1\mu, & \text{if } \mathbf{s}' = (s_1 - 1, s_2), \\ s_2\mu, & \text{if } \mathbf{s}' = (s_1, s_2 - 1), \\ 1 - \lambda_0 - \lambda_1 - \lambda_2 - s_1\mu - s_2\mu, & \text{if } \mathbf{s}' = (s_1, s_2), \\ 0, & \text{otherwise.} \end{cases} \tag{4.4}$$

Similarly the corresponding transition probability for $s_1 = N$, $0 \leq s_2 \leq N-1$ or $0 \leq s_1 \leq N-1$, $s_2 = N$ can also be defined.

Figure 4.2 depicts the state transition diagram when $K = 2$. The dynamic of the two-network system can be described by a two-dimensional (2-D) Markov chain where the probability $P_{\text{sys}}(\mathbf{s}|\mathbf{s})$ is not shown in Figure 4.2 for conciseness.

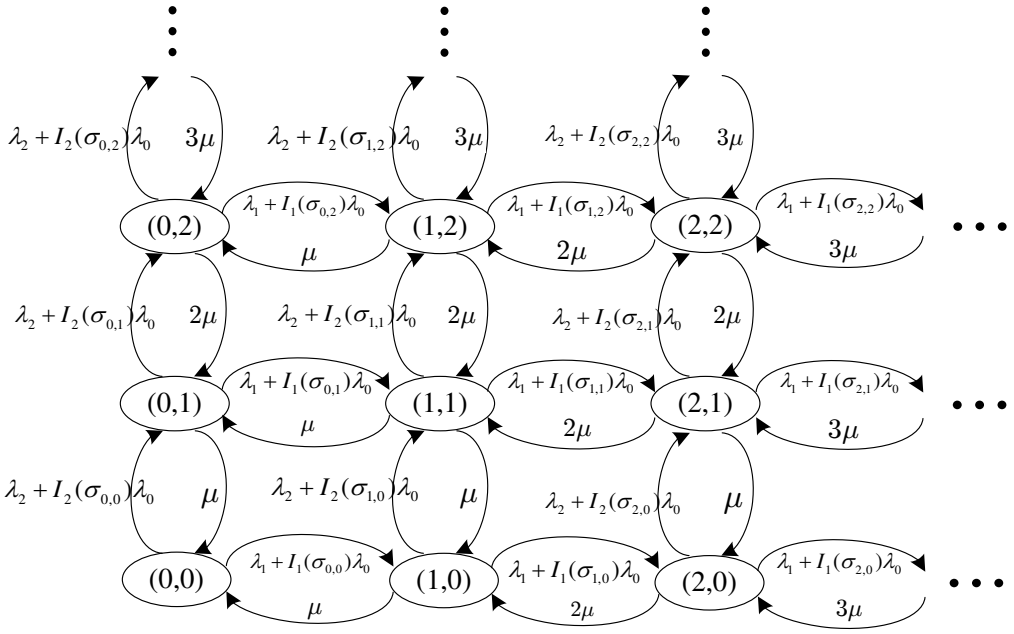

Figure 4.2: State diagram of the 2-D Markov chain.

4.1.2 Expected utility

The strategy profile $\boldsymbol{\sigma} = \{\sigma_{\mathbf{s}} | \forall \mathbf{s} \in \mathcal{S}\}$ is a mapping from the aggregate state space to the action space, i.e., $\boldsymbol{\sigma} : \{0, 1, ..., N\}^K \mapsto \{1, 2, \ldots, K\}$. Given a strategy profile $\boldsymbol{\sigma}$, we can obtain the system transition probability in (4.1) - (4.3). When a rational user arrives and observes system state $\mathbf{s}_0$, he/she makes the decision $\sigma_{\mathbf{s}_0} = \hat{k}$ which leads the user into the system state $\mathbf{s}_1 = \mathbf{s}_0 + \mathbf{e}_{\hat{k}}$. Then, the expected utility of the rational user is given by

$$V_{\hat{k}}(\mathbf{s}_1) = E\left[\sum_{t=1}^{\infty}(1-\mu)^{t-1} R_{\hat{k}}(\mathbf{s}_t) \middle| \mathbf{s}_1\right], \tag{4.5}$$

where $\mathbf{s}_t$ denotes the system state at time t. Since μ is the probability that the service is terminated in one time slot, then $(1-\mu)$ can be interpreted as the probability that the user stays in the network in one time slot. The value $(1-\mu)$ can also be regarded

as the discounting factor for the future utility as shown later in (4.6). The strategy $\sigma_{\mathbf{s}_0} = \hat{k}$ determines which network the user will enter and thus which expected utility function the user will obtain. Denoted by $V_{\hat{k}}(\mathbf{s}_1)$, the expected utility function is the expected value of the discounted sum of the immediate utilities $R_{\hat{k}}(\mathbf{s}_t)$ accumulated from the next time slot. Notice that $\mathbf{s}_1 = \mathbf{s}_0 + \mathbf{e}_{\hat{k}}$ is uniquely determined by the user's strategy $\sigma_{\mathbf{s}_0}$, but the subsequent states $\mathbf{s}_t$, for $t \geq 2$, are stochastic and dependent on the arrival of other users, including users from user-arrival stream k, $1 \leq k \leq K$, and other rational users.

From the Bellman equation [79], the expected utility in (4.5) can be shown to satisfy the following recursive expression.

$$V_k(\mathbf{s}) = R_k(s_k) + (1-\mu) \sum_{\mathbf{s}'} P_k\left(\mathbf{s}'|\mathbf{s}\right) V_k(\mathbf{s}'), \tag{4.6}$$

where

$$P_k\left(\mathbf{s}'|\mathbf{s}\right) = \begin{cases} \sum_{i \in \mathcal{F}(\mathbf{s})} \lambda_i + \lambda_j + I_j(\sigma_{\mathbf{s}})\lambda_0, & \text{if } j = \min \bar{\mathcal{F}}(\mathbf{s}), \\ \lambda_j + I_j(\sigma_{\mathbf{s}})\lambda_0, & \text{if } j \in \bar{\mathcal{F}}(\mathbf{s}) \backslash \left\{\min \bar{\mathcal{F}}(\mathbf{s})\right\}, \\ s_i\mu, & \text{if } \mathbf{s}' = \mathbf{s} - \mathbf{e}_i, \forall i \neq k, \\ (s_k - 1)\mu, & \text{if } \mathbf{s}' = \mathbf{s} - \mathbf{e}_k, \\ 1 - \sum_{j=0}^{K} \lambda_j - \sum_{j=1}^{K} s_j\mu + \mu, & \text{if } \mathbf{s}' = \mathbf{s}, \\ 0, & \text{otherwise.} \end{cases} \tag{4.7}$$

which is the transition probability given that the user still stays in network k. The probability of transition from $\mathbf{s}$ to $\mathbf{s} - \mathbf{e}_k$ is $(s_k - 1)\mu$ since $s_k - 1$ users may leave the network. The transition probability from $\mathbf{s}$ to other states is similar to the definition

of P_{sys} in (4.4).

4.1.3 Best Response of Rational Users

Due to the selfish nature, when observing the state $\mathbf{s}$, a rational user will choose the strategy $\sigma_{\mathbf{s}}$ to maximize his expected utility. Thus, the rational strategy $\sigma_{\mathbf{s}}$ has to satisfy

$$\sigma_{\mathbf{s}} = \arg\max_{k} V_k(\mathbf{s} + \mathbf{e}_k). \tag{4.8}$$

It can be seen that with the strategy profile in which the strategy of every state satisfies (4.8), no user can obtain a higher expected utility by unilateral deviation to any other strategy. Therefore, the strategy profile satisfying (4.6)-(4.8) is a Nash equilibrium of the stochastic game.

4.2 Modified Value Iteration Algorithm

The problem of finding the strategy profile satisfying (4.6)-(4.8) is not a conventional Markov Decision Process problem. In a conventional MDP problem [79], a single potential function is associated with each system state, and the optimal strategy can be obtained directly by optimizing the potential function. Such a problem can often be solved via the theory of dynamic programming (DP) [11]. However, in

our model, multiple potential functions are related in a vector form:

$$\begin{bmatrix} V_1(\mathbf{s}) \\ V_2(\mathbf{s}) \\ \vdots \\ V_K(\mathbf{s}) \end{bmatrix} = \begin{bmatrix} R_1(s_1) \\ R_2(s_2) \\ \vdots \\ R_K(s_K) \end{bmatrix} + (1-\mu) \begin{bmatrix} \mathbf{p}_1 & \mathbf{0} & \cdots & \mathbf{0} \\ \mathbf{0} & \mathbf{p}_2 & \cdots & \mathbf{0} \\ \vdots & & \ddots & \vdots \\ \mathbf{0} & \mathbf{0} & \cdots & \mathbf{p}_K \end{bmatrix}^T \begin{bmatrix} \mathbf{v}_1 \\ \mathbf{v}_2 \\ \vdots \\ \mathbf{v}_K \end{bmatrix}, \tag{4.9}$$

where $\mathbf{0}$ denotes an all-zero vector, $\mathbf{p}_k$ and $\mathbf{v}_k$ are vectors comprising $P_k(\mathbf{s}'|\mathbf{s})$ and $V_k(\mathbf{s}')$ as elements, $k = 1, \ldots, K$. The transpose operator is denoted by $(\cdot)^T$.

The strategy $\sigma_{\mathbf{s}}$ is determined by comparing $V_k(\mathbf{s} + \mathbf{e}_k)$ for all k as in (4.8). Thus, DP cannot be directly applied in such a problem. It is important to point out that a user makes a decision after he arrives and observes the system state $\mathbf{s}$. The strategy leads the user into some network k and results in an expected utility $V_k(\mathbf{s} + \mathbf{e}_k)$. In subsequent time slots, the user cannot change from the network he/she is staying to any other network. The expected utility is affected by others' strategies through the transition probabilities as given in (4.6).

We can see that given the expected utilities $\{V_k\}_{k=1}^K$, the rational strategy profile $\boldsymbol{\sigma}$ should satisfy (4.8). On the other hand, given a strategy profile $\boldsymbol{\sigma}$, the expected utilities $\{V_k\}_{k=1}^K$ can be found by (4.6), where the transition probability $P_k(\mathbf{s}'|\mathbf{s})$ is a function of the strategy $\sigma_{\mathbf{s}}$. To obtain the optimal strategy profile $\boldsymbol{\sigma}^*$ satisfying (4.6)-(4.8), we propose a modified value iteration algorithm to iteratively solve the problem. At the n-th iteration, the rational strategy profile is given by

$$\sigma_{\mathbf{s}}^{(n+1)} = \arg\max_k V_k^{(n)}(\mathbf{s} + \mathbf{e}_k), \forall \mathbf{s} \in \mathcal{S}. \tag{4.10}$$

The expected utility functions can be obtained by solving

$$V_k^{(n+1)}(\mathbf{s}) = R_k(s_k) + (1-\mu)\sum_{\mathbf{s}'\in\mathcal{S}} P_k^{(n+1)}\left(\mathbf{s}'|\mathbf{s}\right) V_k^{(n+1)}(\mathbf{s}'), \forall \mathbf{s}\in\mathcal{S}, \forall k\in\{1,\ldots,K\}, \tag{4.11}$$

where the transition probability $P_k^{(n+1)}(\mathbf{s}'|\mathbf{s})$ is updated using the corresponding updated strategies, i.e.,

$$P_k^{(n+1)}\left(\mathbf{s}'|\mathbf{s}\right) = \begin{cases} \sum_{i\in\mathcal{F}(\mathbf{s})}\lambda_i + \lambda_j + I_j(\sigma_{\mathbf{s}}^{(n+1)})\lambda_0, & \text{if } \mathbf{s}' = \mathbf{s}+\mathbf{e}_j, j = \min\bar{\mathcal{F}}(\mathbf{s}) \\ \lambda_j + I_j(\sigma_{\mathbf{s}}^{(n+1)})\lambda_0, & \text{if } \mathbf{s}' = \mathbf{s}+\mathbf{e}_j, j\in\bar{\mathcal{F}}(\mathbf{s})\backslash\left\{\min\bar{\mathcal{F}}(\mathbf{s})\right\} \\ s_j\mu, & \text{if } \mathbf{s}' = \mathbf{s}-\mathbf{e}_j, j\neq k \\ (s_k-1)\mu, & \text{if } \mathbf{s}' = \mathbf{s}-\mathbf{e}_k \\ 1-\sum_{j\in\bar{\mathcal{F}}_{\mathbf{s}}} P_k\left(\mathbf{s}+\mathbf{e}_j|\mathbf{s}\right) & \\ \quad -\sum_{j=1}^{K} P_k\left(\mathbf{s}-\mathbf{e}_j|\mathbf{s}\right), & \text{if } \mathbf{s}' = \mathbf{s}, \\ 0, & \text{otherwise,} \end{cases} \tag{4.12}$$

The solution to (4.11) can be obtained through several approaches, one of which is the value iteration algorithm [79]. The algorithm first initializes $V_k^{(n+1)}(\mathbf{s})$ as an arbitrary value such as zero and iteratively updates it using (4.11). The iteration function is a contraction mapping so the convergence to a unique fixed point is guaranteed. Another approach is to consider (4.11) as K sets of linear systems, where each set has N^2 unknown variables corresponding to $\{V_k^{(n+1)}(\mathbf{s}), \forall\mathbf{s}\}$ and N^2 equations. Such linear systems can be solved by linear programming or matrix inversion.

In the next section, we will theoretically show that for $K = 2$, the proposed

algorithm results in a threshold structure of the strategy profile at each iteration, and such a threshold structure is also observed for general $K > 2$. However, the strategy profile may not converge but oscillates near the threshold due to the hard decision rule in (4.8). The non-convergence occurs when the rational strategy of the state near the threshold oscillates between different choices each time when the expected utility is updated. When such a situation happens, the expected utilities corresponding to different strategies are very close to each other. Hence, to solve this problem, we relax the hard decision rule by allowing a small region of tolerance for switching among the strategies [82], which leads to the soft decision rule as follows.

$$\sigma_{\mathbf{s}}^{(n+1)} = \begin{cases} \sigma_{\mathbf{s}}^{(n)}, & \text{if } V_{\sigma_{\mathbf{s}}^{(n)}}^{(n)}(\mathbf{s}+\mathbf{e}_{\sigma_{\mathbf{s}}^{(n)}}) \geq \max_k V_k^{(n)}(\mathbf{s}+\mathbf{e}_k) - \epsilon, \\ \arg\max_k V_k^{(n)}(\mathbf{s}+\mathbf{e}_k), & \text{if } V_{\sigma_{\mathbf{s}}^{(n)}}^{(n)}(\mathbf{s}+\mathbf{e}_{\sigma_{\mathbf{s}}^{(n)}}) < \max_k V_k^{(n)}(\mathbf{s}+\mathbf{e}_k) - \epsilon, \end{cases} \tag{4.13}$$

where $\epsilon > 0$ is a small constant. Table 4.1 summarizes the proposed modified value iteration algorithm for the multi-dimensional MDP. Notice that the algorithm stops when an equilibrium is found or all the strategy profiles are searched. By definition, when the algorithm obtains a solution, the resulting strategy profile is an ϵ-approximate NE [39], in which the strategy at each state has an expected utility that is at most ϵ less than that of any other strategy. Note that there may be multiple ϵ-approximate NEs especially for a larger ϵ when a larger region of tolerance is allowed for switching among the strategies.

Table 4.1: Modified Value Iteration Algorithm

(i) Initialize: $V_k^{(0)}(\mathbf{s}) = 0$, $\forall k \in \{1, \ldots, K\}$, $\forall \mathbf{s} \in \mathcal{S}$. $T = \phi$.

(ii) **Loop** :

1. Update $\{\sigma_{\mathbf{s}}^{(n+1)}\}$ by (4.13).

   If $\{\boldsymbol{\sigma}_{\mathbf{s}}^{(n+1)}\} = \{\boldsymbol{\sigma}_{\mathbf{s}}^{(n)}\}$, **then** stop loop.

   else

   if $\{\boldsymbol{\sigma}_{\mathbf{s}}^{(n+1)}\} \in T$, **then** choose a $\{\boldsymbol{\sigma}_{\mathbf{s}}\} \in \bar{T}$, and let $\{\boldsymbol{\sigma}_{\mathbf{s}}^{(n+1)}\} = \{\boldsymbol{\sigma}_{\mathbf{s}}\}$.

   end if

   end if

   $T = T \cup \{\boldsymbol{\sigma}_{\mathbf{s}}^{(n+1)}\}$.

2. Update $\{P_k^{(n+1)}(\mathbf{s}'|\mathbf{s})\}$ by (4.12).

3. Solve $\{V_k^{(n+1)}(\mathbf{s})\}$ in (4.11) by value iteration or linear programming.

Until $\bar{T} = \phi$ or $\{\boldsymbol{\sigma}_{\mathbf{s}}^{(n+1)}\} = \{\boldsymbol{\sigma}_{\mathbf{s}}^{(n)}\}$.

4.3 Threshold Structure of Strategy Profile

In this section, we show that the strategy profile produced by the proposed modified value iteration algorithm in each iteration exhibits a threshold structure for two-network systems. With the assumption that $R_k(s_k)$, $k = 1, 2$, are non-increasing, the following lemma shows that $V_1(\mathbf{s})$ is non-decreasing and $V_2(\mathbf{s})$ is non-increasing along the line of $s_1 + s_2 = m$, $\forall m \in \{1, 2, ..., 2N\}$.

Lemma 2 *For $n \geq 0$,*

$$V_1^{(n)}(\mathbf{s}) \geq V_1^{(n)}(\mathbf{s} + \mathbf{e}_1 - \mathbf{e}_2), \tag{4.14}$$

$$V_2^{(n)}(\mathbf{s}) \leq V_2^{(n)}(\mathbf{s} + \mathbf{e}_1 - \mathbf{e}_2). \tag{4.15}$$

Proof: We use induction to show that (4.14) and (4.15) hold for all $n \geq 0$.

i) Since $V_1^{(0)}(\mathbf{s})$ and $V_2^{(0)}(\mathbf{s})$ are initialized as zeros, (4.14) and (4.15) hold for $n = 0$.

ii) We assume the induction hypothesis holds for some $n \geq 0$. Then it can be shown that (4.14) and (4.15) also hold for $(n+1)$ by analyzing the following difference. Let $\mathbf{s}' = \mathbf{s} + \mathbf{e}_1 - \mathbf{e}_2$. For $0 \leq s_1 \leq N-2$ and $1 \leq s_2 \leq N-1$,

$$\begin{aligned} V_1^{(n+1)}(\mathbf{s}) - V_1^{(n+1)}(\mathbf{s}') = R_1(s_1) - R_1(s_1+1) + (1-\mu)\Big[\lambda_1 \Big(V_1^{(n)}(\mathbf{s}+\mathbf{e}_1) - V_1^{(n)}(\mathbf{s}'+\mathbf{e}_1)\Big) \\ + \lambda_0 \Big(I_1(\sigma_{\mathbf{s}})V_1^{(n)}(\mathbf{s}+\mathbf{e}_1) - I_1(\sigma_{\mathbf{s}'})V_1^{(n)}(\mathbf{s}'+\mathbf{e}_1)\Big) \\ + \lambda_2 \Big(V_1^{(n)}(\mathbf{s}+\mathbf{e}_2) - V_1^{(n)}(\mathbf{s}'+\mathbf{e}_2)\Big) \\ + \lambda_0 \Big(I_2(\sigma_{\mathbf{s}})V_1^{(n)}(\mathbf{s}+\mathbf{e}_2) - I_2(\sigma_{\mathbf{s}'})V_1^{(n)}(\mathbf{s}'+\mathbf{e}_2)\Big) \\ + (s_1-1)\mu V_1^{(n)}(\mathbf{s}-\mathbf{e}_1) - s_1\mu V_1^{(n)}(\mathbf{s}'-\mathbf{e}_1) \\ + s_2\mu V_1^{(n)}(\mathbf{s}-\mathbf{e}_2) - (s_2-1)\mu V_1^{(n)}(\mathbf{s}'-\mathbf{e}_2) \\ + (1-\lambda_0-\lambda_1-\lambda_2-s_1\mu-s_2\mu)\Big(V_1^{(n)}(\mathbf{s}) - V_1^{(n)}(\mathbf{s}')\Big)\Big]. \end{aligned} \tag{4.16}$$

Due to the fact that the utility function $R_1(s_1)$ is non-increasing in s_1 and the induction hypothesis which guarantees the non-negativeness of many differences of terms in (4.16), by rearranging a few terms, it suffices to discuss the following cases.

Case 1: $\sigma_{\mathbf{s}}^{(n)} = \sigma_{\mathbf{s}'}^{(n)} = 1$. Then, $V_1^{(n)}(\mathbf{s}+\mathbf{e}_1) - V_1^{(n)}(\mathbf{s}'+\mathbf{e}_1) \geq 0$ by the induction hypothesis.

Case 2: $\sigma_{\mathbf{s}}^{(n)} = \sigma_{\mathbf{s}'}^{(n)} = 2$. Then, $V_1^{(n)}(\mathbf{s}+\mathbf{e}_2) - V_1^{(n)}(\mathbf{s}'+\mathbf{e}_2) \geq 0$ by the induction hypothesis.

Case 3: $\sigma_{\mathbf{s}}^{(n)} = 1$ and $\sigma_{\mathbf{s}'}^{(n)} = 2$. Then, $V_1^{(n)}(\mathbf{s}+\mathbf{e}_1) - V_1^{(n)}(\mathbf{s}'+\mathbf{e}_2) = 0$.

Case 4: $\sigma_{\mathbf{s}}^{(n)} = 2$ and $\sigma_{\mathbf{s}'}^{(n)} = 1$. Then, $V_1^{(n)}(\mathbf{s}+\mathbf{e}_2) - V_1^{(n)}(\mathbf{s}'+\mathbf{e}_1) \geq 0$ by the induction hypothesis.

Therefore, we have $V_1^{(n+1)}(\mathbf{s}) - V_1^{(n+1)}(\mathbf{s}') \geq 0$, for $0 \leq s_1 \leq N-2$ and $1 \leq s_2 \leq N-1$. Next, it can be easily checked that the inequality still holds for the case of $s_1 = N-1$, $1 \leq s_2 \leq N-1$ as well as the case of $0 \leq s_1 \leq N-1$, $s_2 = N$. Similarly, $V_2^{(n)}(\mathbf{s}) \leq V_2^{(n)}(\mathbf{s}')$ can also be established. □

The following lemma shows the difference of $V_1(\mathbf{s}+\mathbf{e}_1)$ and $V_2(\mathbf{s}+\mathbf{e}_2)$ is non-increasing along the line of $s_1 + s_2 = m$, $\forall m \in \{1, 2, ..., 2N\}$.

Lemma 3 $V_1^{(n)}(\mathbf{s}+\mathbf{e}_1) - V_2^{(n)}(\mathbf{s}+\mathbf{e}_2) \geq V_1^{(n)}(\mathbf{s}'+\mathbf{e}_1) - V_2^{(n)}(\mathbf{s}'+\mathbf{e}_2)$, *where* $\mathbf{s}' = \mathbf{s}+\mathbf{e}_1-\mathbf{e}_2$.

Proof: It can be easily shown using Lemma 2. □

Theorem 1 *The strategy profile generated by the modified value iteration algorithm has a threshold structure for* $K = 2$.

Proof: The soft decision rule in (4.13) for $K = 2$ can be rewritten as

$$\sigma_{\mathbf{s}}^{(n+1)} = \begin{cases} \sigma_{\mathbf{s}}^{(n)}, & \text{if } |V_1^{(n)}(\mathbf{s}+\mathbf{e}_1) - V_2^{(n)}(\mathbf{s}+\mathbf{e}_2)| \leq \epsilon, \\ 1, & \text{if } V_1^{(n)}(\mathbf{s}+\mathbf{e}_1) > V_2^{(n)}(\mathbf{s}+\mathbf{e}_2) + \epsilon, \\ 2, & \text{if } V_2^{(n)}(\mathbf{s}+\mathbf{e}_2) > V_1^{(n)}(\mathbf{s}+\mathbf{e}_1) + \epsilon. \end{cases} \tag{4.17}$$

If $\sigma_{\mathbf{s}}^{(n)} = 2$ and $\sigma_{\mathbf{s}}^{(n+1)} = 1$, i.e., the strategy of the current iteration is updated to be different from the one of the previous iteration, then we must have $V_1^{(n)}(\mathbf{s}+\mathbf{e}_1) > V_2^{(n)}(\mathbf{s}+\mathbf{e}_2) + \epsilon$. Lemma 3 implies that $V_1(\mathbf{s}'+\mathbf{e}_1) - V_2(\mathbf{s}'+\mathbf{e}_2)$ is non-increasing along the line of $s_1' + s_2' = s_1 + s_2$. Thus, we have

$$V_1(\mathbf{s}'+\mathbf{e}_1) - V_2(\mathbf{s}'+\mathbf{e}_2) \geq V_1(\mathbf{s}+\mathbf{e}_1) - V_2(\mathbf{s}+\mathbf{e}_2) > \epsilon > 0,$$
$$\text{for } \mathbf{s}' = \mathbf{s} - k\mathbf{e}_1 + k\mathbf{e}_2, k = 1, 2, \ldots, \min\{s_1, N - s_2\}. \tag{4.18}$$

Therefore, $\sigma_{\mathbf{s}'}^{(n+1)} = 1$ for $\mathbf{s}' = \mathbf{s} - k\mathbf{e}_1 + k\mathbf{e}_2, k = 1, 2, ..., \min\{s_1, N - s_2\}$. Similarly, if $\sigma_{\mathbf{s}}^{(n)} = 1$ and $\sigma_{\mathbf{s}}^{(n+1)} = 2$, then $\sigma_{\mathbf{s}''}^{(n+1)} = 2$, for $\mathbf{s}'' = \mathbf{s} + k\mathbf{e}_1 - k\mathbf{e}_2, k = 1, 2, ..., \min\{N - s_1, s_2\}$. With the above discussion, the strategies along the line of $s_1 + s_2 = m$, $\forall m \in \{1, 2, ..., 2N\}$ retain a threshold structure in each iteration. Since the initialization of the strategy profile exhibits a threshold structure trivially, the strategy profile obtained in each iteration of the algorithm has a threshold structure. □

In a two-network system, the number of system states is N^2 and thus N^2 strategies are needed to be stored without the threshold structure. The storage space of each strategy is 1 bits. Now with such threshold structure on each line $s_1 + s_2 = m$, $m = 1, 2, ..., 2N$, we can simply store the threshold point on each line. Each threshold point requires the storage space of $\log N$ bits. Therefore, The storage of the strategy profile can be reduced from $\mathcal{O}(N^2)$ to $\mathcal{O}(N \log N)$.

In this chapter, we only provide the analysis for the two-network systems. The analysis for systems with more than two networks is difficult due to the lack of the optimality in a single potential function as in the admission control problem [26, 59]. However, it is observed from the simulation results in Section 4.5 that the multi-network systems also possess the strategy profiles with threshold structures. The theoretic analysis of the threshold structure for the multi-network systems is important but out of the scope of this chapter, and will serve as one of our future work.

4.4 Truthful Mechanism Design

In the above discussion, we have implicitly assumed the networks truthfully report their states s_k, and therefore the user can observe the true system state $\mathbf{s}$, by which he/she can make a decision to maximize his/her utility. However, without appropriate incentives, the networks may not truthfully report their states. Instead, a network may untruthfully report some state s'_k different from the true state s_k if profitable. In this section, we consider to enforce truth-telling as a dominant strategy for the networks by incorporating pricing rules into the wireless access network selection game.

A mechanism consists of pricing rules $\{P_k(\mathbf{s})\}$ and allocation rules $\{a_k(\mathbf{s})\}$, where $P_k(\mathbf{s})$ is denoted as the unit price of the expected rate $V_k(\mathbf{s})$ provided by network k at state $\mathbf{s}$, and $a_k(\mathbf{s})$ is denoted as the allocation probability, which is either 1 or 0, i.e., whether or not the user enters network k. The utility of network k is given by

$$U_k(\mathbf{s}) = V_k(\mathbf{s}+\mathbf{e}_k)P_k(\mathbf{s}) - c_k(\mathbf{s}+\mathbf{e}_k)a_k(\mathbf{s}), \tag{4.19}$$

where $c_k(\mathbf{s}+\mathbf{e}_k)$ is the cost per user. With the states reported from the networks, these rules determine the user allocation and the price the user has to pay, both as functions of the reports from networks. For example, if network k reports his state as s'_k and others report $s_{-k} = \{s_j : j \neq k\}$, his utility becomes $V_k(\mathbf{s}+\mathbf{e}_k)P_k(s'_k, s_{-k}) - c_k(\mathbf{s}+\mathbf{e}_k)a_k(s'_k, s_{-k})$. Notice that $V_k(\mathbf{s}+\mathbf{e}_k)$ and $c_k(\mathbf{s}+\mathbf{e}_k)$ are functions of true states that do not depend on the reports. Thus, the truth-telling or the incentive

compatibility (IC) constraints are

$$V_k(s_k+1,s_{-k})P_k(s_k,s_{-k}) - c_k(s_k+1,s_{-k})a_k(s_k,s_{-k})$$
$$\geq V_k(s_k+1,s_{-k})P_k(s'_k,s_{-k}) - c_k(s_k+1,s_{-k})a_k(s'_k,s_{-k}), \forall s_k, s'_k, s_{-k}, \quad (4.20)$$

which means truth-telling is a dominant strategy for each network at each state. The mechanism also has to satisfy the individual rationality (IR) constraints, i.e.,

$$V_k(s_k+1,s_{-k})P_k(s_k,s_{-k}) - c_k(s_k+1,s_{-k})a_k(s_k,s_{-k}) \geq 0, \forall s_k, s_{-k}, \quad (4.21)$$

which guarantees all networks would attend the mechanism.

In the previous sections, we study the network selection game with the focus of the interdependence between the users. In this section, we study the interplay among the networks. To this end, we assume that users' strategies are chosen based on the *ex ante* optimality [39,62], i.e., the allocation rule is based on optimizing the expected objective over the state probability. The truthful mechanism design is to construct a set of pricing and allocation rules which optimize a specific objective while satisfying IC and IR constraints. For example, the mechanism design problem $\boldsymbol{\mathcal{P}}_p$ for minimizing the expected payment can be formulated as follows.

$$\boldsymbol{\mathcal{P}}_p: \quad \min_{\{P_k\},\{a_k\}} \quad \sum_{\mathbf{s}\in\mathcal{S}} \pi(\mathbf{s}) \sum_{k=1}^{K} P_k(\mathbf{s}) V_k(\mathbf{s}+\mathbf{e}_k) \quad (4.22)$$

$$\text{s.t.} \quad \text{(IC), (IR)}, \quad (4.23)$$

$$\sum_{k=1}^{K} a_k(\mathbf{s}) = 1, \forall \mathbf{s} \in \mathcal{S}, \quad (4.24)$$

$$a_k(\mathbf{s}) \in \{0,1\}, \forall \mathbf{s}, \forall k. \quad (4.25)$$

Other mechanism design objectives such as the utility maximization $\boldsymbol{\mathcal{P}}_u$ can be formulated by substituting (4.22) with users' expected utility function as follows.

$$\boldsymbol{\mathcal{P}}_u: \quad \max_{\{P_k\},\{a_k\}} \quad \sum_{\mathbf{s}\in\mathcal{S}} \pi(\mathbf{s}) \sum_{k=1}^{K} \left[\lambda a_k(\mathbf{s}) V_k(\mathbf{s}+\mathbf{e}_k) - P_k(\mathbf{s}) V_k(\mathbf{s}+\mathbf{e}_k)\right] \tag{4.26}$$

$$\text{s.t.} \quad (4.23), (4.24), (4.25).$$

The unit cost $c_k(\mathbf{s}+\mathbf{e}_k)/V_k(\mathbf{s}+\mathbf{e}_k)$ is denoted as $w_k(\mathbf{s})$. The (IC) constraints become

$$P_k(s_k, s_{-k}) - w_k(s_k, s_{-k}) a_k(s_k, s_{-k}) \geq P_k(s'_k, s_{-k}) - w_k(s_k, s_{-k}) a_k(s'_k, s_{-k}), \forall s_k, s'_k, s_{-k}. \tag{4.27}$$

In the following, we need a monotonicity assumption for the unit cost, i.e., $w_k(s_k, s_{-k})$ is non-decreasing in s_k, i.e., $w_k(s_k, s_{-k}) \geq w_k(s'_k, s_{-k})$, if $s_k \geq s'_k$. Since $V_k(s_k, s_{-k})$ is non-increasing in s_k, the assumption holds when $c_k(s_k, s_{-k})$ is non-decreasing in s_k. For example, if the per-user cost is a constant in each network, i.e., $c_k(s_k, s_{-k}) = C_k$, then the assumption holds. The monotonicity of $w_k(s_k, s_{-k})$ leads to the threshold structure of $a_k(s_k, s_{-k})$ as in the following lemma.

Lemma 4 *Under IC constraints, there exists a threshold value of s_k on the allocation rule $a_k(s_k, s_{-k})$, i.e., given s_{-k}, there exists $s_k^*(s_{-k}) \in \{-1, 0, 1, \ldots, N\}$, such that*

$$a_k(s_k, s_{-k}) = \begin{cases} 1, & s_k \leq s_k^*(s_{-k}) \\ 0, & s_k > s_k^*(s_{-k}). \end{cases} \tag{4.28}$$

Proof: From (4.27), we have

$$P_k(s_k, s_{-k}) - P_k(s'_k, s_{-k}) \geq w_k(s_k, s_{-k}) \left[a_k(s_k, s_{-k}) - a_k(s'_k, s_{-k})\right]. \tag{4.29}$$

Interchanging s_k and s'_k, we also have

$$P_k(s'_k, s_{-k}) - P_k(s_k, s_{-k}) \geq w_k(s'_k, s_{-k}) \left[a_k(s'_k, s_{-k}) - a_k(s_k, s_{-k})\right]. \tag{4.30}$$

Combining the above two inequality leads to

$$\left[w_k(s_k, s_{-k}) - w_k(s'_k, s_{-k})\right] \left[a_k(s_k, s_{-k}) - a_k(s'_k, s_{-k})\right] \leq 0. \tag{4.31}$$

Thus, since $w_k(s_k, s_{-k})$ is non-decreasing in s_k, the allocation rule $a_k(s_k, s_{-k})$ has to be non-increasing in s_k. With this monotonicity and the fact that $a_k(s_k, s_{-k})$ can only have value of 0 or 1 as in (4.25), we can conclude that there exists a threshold of $a_k(s_k, s_{-k})$ in s_k as described in (4.28). □

Corollary 1 *If $K = 2$, then $s_1^*(s_2)$ is non-decreasing in s_2, and $s_2^*(s_1)$ is non-decreasing in s_1.*

Proof: Suppose $\exists s_2$ such that $s_1^*(s_2 + 1) < s_1^*(s_2)$. By Lemma 4, we have $a_1(s_1, s_2+1) = 0$, for $s_1 > s_1^*(s_2+1)$, which implies $a_2(s_1, s_2+1) = 1$, for $s_1 > s_1^*(s_2+1)$, due to the constraint that $a_1(\mathbf{s}) + a_2(\mathbf{s}) = 1$, $\forall \mathbf{s}$. Therefore, $a_2(s_1^*(s_2), s_2+1) = 1$, which implies $a_2(s_1^*(s_2), s_2) = 1$ by Lemma 4, but we also have $a_1(s_1^*(s_2), s_1) = 1$, which leads to a contradiction. □

The following lemma shows that only adjacent IC constraints are necessary.

Lemma 5 *Non-adjacent IC constraints are redundant.*

Proof: Let us consider the two adjacent IC constraints as follows.

$$P_k(s_k, s_{-k}) - w_k(s_k, s_{-k})a_k(s_k, s_{-k}) \geq P_k(s_k - 1, s_{-k}) - w_k(s_k, s_{-k})a_k(s_k - 1, s_{-k}), \tag{4.32}$$

$$P_k(s_k - 1, s_{-k}) - w_k(s_k - 1, s_{-k})a_k(s_k - 1, s_{-k}) \geq P_k(s_k - 2, s_{-k}) - w_k(s_k - 1, s_{-k})a_k(s_k - 2, s_{-k}). \tag{4.33}$$

Adding (4.32) and (4.33), we have

$$\begin{aligned} & P_k(s_k, s_{-k}) - w_k(s_k, s_{-k})a_k(s_k, s_{-k}) \\ & \geq P_k(s_k - 2, s_{-k}) - w_k(s_k, s_{-k})a_k(s_k - 2, s_{-k}) \\ & \quad - w_k(s_k, s_{-k}) \left[a_k(s_k - 1, s_{-k}) - a_k(s_k - 2, s_{-k})\right] \\ & \quad + w_k(s_k - 1, s_{-k}) \left[a_k(s_k - 1, s_{-k}) - a_k(s_k - 2, s_{-k})\right] \\ & \geq P_k(s_k - 2, s_{-k}) - w_k(s_k, s_{-k})a_k(s_k - 2, s_{-k}). \end{aligned} \tag{4.34}$$

The last inequality is due to that $w_k(s_k, s_{-k})$ is increasing in s_k and $a_k(s_k, s_{-k})$ is decreasing in s_k. It shows that the non-adjacent IC constraints can be inferred from the adjacent ones. □

Using the adjacent IC constraints, we can obtain the bounds for the payments, i.e., given an allocation rule $\{a_k(\mathbf{s})\}$, the incentive compatible payment rule $\{P_k(\mathbf{s})\}$ satisfies

$$\begin{aligned} P_k(s_k, s_{-k}) + w_k(s_k, s_{-k}) \left[a_k(s_k - 1, s_{-k}) - a_k(s_k, s_{-k})\right] & \geq P_k(s_k - 1, s_{-k}) \\ & \geq P_k(s_k, s_{-k}) + w_k(s_k - 1, s_{-k}) \left[a_k(s_k - 1, s_{-k}) - a_k(s_k, s_{-k})\right] \end{aligned} \tag{4.35}$$

In the optimization problems $\boldsymbol{\mathcal{P}}_p$, we aim to minimize a linear combination of $P_k(s_k, s_{-k})$ with nonnegative coefficients. Clearly, the lower bound in (4.35) should be binding; otherwise, the objective function can always be better optimized by decreasing the non-binding $P_k(s_k, s_{-k})$. Hence, the payment rule can be expressed as

$$P_k(s_k, s_{-k}) = P_k(N, s_{-k}) + \sum_{r=s_k+1}^{N} w_k(r-1, s_{-k}) \left[a_k(r-1, s_{-k}) - a_k(r, s_{-k})\right]. \tag{4.36}$$

To minimize $P_k(s_k, s_{-k})$ while satisfying the IR constraint in (4.21), $P_k(N, s_{-k})$ should be set as 0. Substituting Lemma 4 into (4.36), we can conclude

$$P_k(s_k, s_{-k}) = \begin{cases} w_k(s_k^*, s_{-k}), & s_k \leq s_k^*, \\ 0, & s_k > s_k^*, \end{cases} \tag{4.37}$$

where s_k^* denotes $s_k^*(s_{-k})$ for notational simplicity.

From the IC and IR constraints, the pricing rule $\{P_k\}$ can be determined given the allocation rule $\{a_k\}$, which is specified by the thresholds $\{s_k^*\}$. Thus (4.37) simply means the pricing rule $\{P_k\}$ is also specified by the thresholds $\{s_k^*\}$. Using $\{s_k^*\}$ as optimization variables, the problem $\boldsymbol{\mathcal{P}}_p$ can be simplified as

$$\begin{aligned} \min_{\{s_k^*\}} \quad & \sum_{\mathbf{s}\in\mathcal{S}} \pi(\mathbf{s}) \sum_{k=1}^{K} P_k(\mathbf{s}) V_k(\mathbf{s}) \\ \text{s.t.} \quad & (4.24), (4.28), (4.37). \end{aligned} \tag{4.38}$$

With the simplification, however, the optimization problem is still difficult to be solved optimally since the optimization variables $\{s_k^*\}$ is discrete and the exhaustive search requires exponential-time complexity in N. Motivated by the optimal

substructures in the two-network case, a dynamic programming algorithm is proposed for the above problem. The optimal solution to the primary problem can be broken down into solving the optimal solutions to its subproblems. The dynamic programming technique essentially performs recursive divide-and-conquer to tackle each of these sub-problems. However, for the multi-network case, the proposed dynamic programming approach is suboptimal but the performance is satisfactory compared to the greedy method. Other traditional optimization algorithms such as branch-and-bound can be applied to optimally solve the mixed integer programming problem, but the computational complexity is prohibitively high (exponential in the number of states) since such an algorithm basically performs exhaustive tree search with certain pruning strategies. In general a mixed integer program does not have an efficient solution. In this chapter, we aim to propose an algorithm that is able to achieve satisfactory performance with reasonable complexity (polynomial in the number of states).

4.4.1 Proposed Algorithm

Since the number of states is N^K, the exhaustive search over all possible allocation rules requires complexity of $\mathcal{O}(K^{N^K})$. Such an exponential complexity is formidably high even for a moderate N. In this subsection, we propose a polynomial time algorithm based on dynamic programming to search for the thresholds $\{s_k^*\}$. Let $f_k^{\mathrm{DP}}(\{s_i : i \in \mathcal{I}\}|\{s_j : j \in \mathcal{J}\})$ denote the optimal value of a set of system states specified by $(\{s_i : i \in \mathcal{I}\}|\{s_j : j \in \mathcal{J}\})$, where the set $\mathcal{J}$ consists of coordinates

with coordinate j being fixed as s_j. The set $\mathcal{I}$ consists of the coordinates with ranges, where coordinate i ranges from 1 to s_i. The set $\mathcal{I}$ has k coordinates, i.e., the considered set of system states is k-dimensional. The optimal value function f_k^{DP} can be computed using lower-dimensional optimal value functions. The recursive calculation is described by the following equations. For $k = 2, \ldots, K$,

$$\begin{aligned} &f_k^{\mathrm{DP}}(\{s_i : i \in \mathcal{I}\}|\{s_j : j \in \mathcal{J}\}) \\ &= \min_{i \in \mathcal{I}} \left\{ f_k^{\mathrm{DP}}(s_i - 1, s_{-i}|\{s_j : j \in \mathcal{J}\}) + f_{k-1}^{\mathrm{DP}}\left(s_{-i}|\left\{s_j : j \in \mathcal{J} \cup \{i\}\right\}\right)\right\}, \end{aligned} \tag{4.39}$$

where $s_{-i} = \{s_l : l \neq i, l \in \mathcal{I}\}$.

$$a_{i^*}(s_{i^*}, s'_{-i^*}, s_j, s_{-j}) = 0, \forall s'_{-i^*} \preceq s_{-i^*}, \tag{4.40}$$

$$i^* = \arg\min_{i \in \mathcal{I}} \left\{ f_k^{\mathrm{DP}}(s_i - 1, s_{-i}|\{s_j : j \in \mathcal{J}\}) + f_{k-1}^{\mathrm{DP}}(s_{-i}|\{s_j : j \in \mathcal{J} \cup \{i\}\})\right\}, \tag{4.41}$$

where $s'_{-i^*} \preceq s_{-i^*}$ denotes $s'_{-i^*} \in \{s'_l : s'_l \leq s_l, l \neq i^*, l \in \mathcal{I}\}$. The boundary condition is

$$f_1^{\mathrm{DP}}(s_i|s_{-i}) = f_1^{\mathrm{DP}}(s_i - 1|s_{-i}) \frac{w_i(s_i, s_{-i})}{w_i(s_i - 1, s_{-i})} + \pi(s_i, s_{-i}) V_i(s_i + 1, s_{-i}) w_i(s_i, s_{-i}), \tag{4.42}$$

$$a_{-i^*}(s_{i^*}, s'_{-i^*}, s_j, s_{-j}) = 1, \forall s'_{-i^*} \leq s_{-i^*}, \tag{4.43}$$

where i^* is the minimizer in (4.41) when $k = 2$. Notice that (4.42) is equivalent to $f_1^{\mathrm{DP}}(s_i|s_{-i}) = \sum_{r=0}^{s_i} \pi(r, s_{-i}) V_i(r+1, s_{-i}) w_i(s_i, s_{-i})$, but the recursive form in (4.42) is more efficient in computation with the price of using more storage space. The proposed algorithm is to evaluate $f_K^{\mathrm{DP}}(N, \ldots, N)$ with $\mathcal{I} = \{1, \ldots, K\}$ and $\mathcal{J} = \phi$ by

using (4.39)-(4.43). The following proposition shows the optimality of the solution obtained by the proposed algorithm when $K = 2$.

Proposition 2 *For $K = 2$, the proposed algorithm optimally solves $\boldsymbol{\mathcal{P}}_p$ in $\mathcal{O}(N^2)$.*

Proof: For $K = 2$, (4.39)-(4.43) become

$$f_2^{\mathrm{DP}}(s_1, s_2) = \min\left\{ f_2^{\mathrm{DP}}(s_1 - 1, s_2) + f_1^{\mathrm{DP}}(s_2|s_1), f_2^{\mathrm{DP}}(s_1, s_2 - 1) + f_1^{\mathrm{DP}}(s_1|s_2) \right\}, \tag{4.44}$$

$$(a_1(s_1, s_2'), a_2(s_1, s_2')) = (0, 1), \forall s_2' \leq s_2, \quad \text{if } f_2^{\mathrm{DP}}(s_1 - 1, s_2) + f_1^{\mathrm{DP}}(s_2|s_1) > f_2^{\mathrm{DP}}(s_2 - 1, s_1) + f_1^{\mathrm{DP}}(s_1|s_2), \tag{4.45}$$

$$(a_1(s_1', s_2), a_2(s_1', s_2)) = (1, 0), \forall s_1' \leq s_1, \quad \text{if } f_2^{\mathrm{DP}}(s_1 - 1, s_2) + f_1^{\mathrm{DP}}(s_2|s_1) \leq f_2^{\mathrm{DP}}(s_2 - 1, s_1) + f_1^{\mathrm{DP}}(s_1|s_2). \tag{4.46}$$

The (4.45) means that when $f_2^{\mathrm{DP}}(s_1 - 1, s_2) + f_1^{\mathrm{DP}}(s_2|s_1)$ is larger than $f_2^{\mathrm{DP}}(s_2 - 1, s_1) + f_1^{\mathrm{DP}}(s_1|s_2)$, state (s_1, s_2) is allocated to network 1, and due to Lemma 4, the states $\{(s_1', s_2), \forall s_1' \leq s_1\}$ are also allocated to network 1. Similarly (4.46) is the case that state (s_1, s_2) is allocated to network 2.

To show the dynamic programming algorithm optimally solves the problem, we need to show the optimal substructures, i.e., the optimal solution to the problem contains the optimal solutions to the subproblems [27]. In evaluating $f_2^{\mathrm{DP}}(N, N)$, we consider the allocation of state (N, N), i.e., either $a_1(N, N) = 1$ or $a_2(N, N) = 1$.

Table 4.2: Dynamic Programming Algorithm for Mechanism Design

(i) Initialization: obtain $\{V_k^{(0)}(\mathbf{s})\}$ and $\{\pi^{(0)}(\mathbf{s})\}$ using Table 4.1.

(ii) **Loop**:

1. With initial $\mathcal{I} = \{1, \ldots, K\}$, $\mathcal{J} = \phi$, evaluate $f_K^{(n)}(N, \ldots, N)$ using (4.39)-(4.43) to obtain $\{a_k^{(n+1)}(\mathbf{s})\}$ and $\{P_k^{(n+1)}(\mathbf{s})\}$.
2. Calculate $\{V_k^{(n+1)}(\mathbf{s})\}$ and $\{\pi^{(n+1)}(\mathbf{s})\}$.

Until $\{a_k^{(n+1)}(\mathbf{s})\}$ and $\{P_k^{(n+1)}(\mathbf{s})\}$ converge.

If $a_1(N, N) = 1$, then from Lemma 4, we have $s_1^*(N) = N$ and thus $a_1(s_1, N) = 1$, $0 \leq s_1 \leq N$. Also in this case, $a_2(N, N) = 0$, and $s_2^*(N) \leq N - 1$. Moreover, from Corollary 1, we know $s_1^*(s_2) \leq N$, for $s_2 \leq N - 1$, and $s_2^*(s_1) \leq N - 1$, for $s_1 \leq N$. Hence, the allocation of the states $\{(s_1, s_2) : 0 \leq s_1 \leq N, 0 \leq s_2 \leq N - 1\}$ is independent of the allocation of the states $\{(s_1, N) : 0 \leq s_1 \leq N\}$, which means the evaluation of $f_2^{\mathrm{DP}}(N, N-1)$ is independent of $f_1^{\mathrm{DP}}(s_1 = N | s_2 = N)$. Therefore, if $a_1(N, N) = 1$, then $f_2^{\mathrm{DP}}(N, N) = f_2^{\mathrm{DP}}(N, N-1) + f_1^{\mathrm{DP}}(s_1 = N | s_2 = N)$. Similarly, if $a_2(N, N) = 1$, then $f_2^{\mathrm{DP}}(N, N) = f_2^{\mathrm{DP}}(N-1, N) + f_1^{\mathrm{DP}}(s_2 = N | s_1 = N)$. For each state (s_1, s_2), recursively applying the same argument, we have $f_2^{\mathrm{DP}}(s_1, s_2)$ is optimal. Hence, $f_2^{\mathrm{DP}}(N, N)$ is optimal. For the computational complexity, since the number of states is N^2, there are N^2 different $f_2^{\mathrm{DP}}(s_1, s_2)$, $f_1^{\mathrm{DP}}(s_1|s_2)$ and $f_1^{\mathrm{DP}}(s_2|s_1)$ to calculate, and each calculation takes $\mathcal{O}(1)$ using (4.44)-(4.46). Therefore, the complexity of evaluating $f_2^{\mathrm{DP}}(N, N)$ is $\mathcal{O}(N^2)$. □

For $K \geq 3$, the solution obtained by the proposed algorithm may be sub-optimal since monotonicity of allocation thresholds in Corollary 1 only holds when

$K = 2$. However, it will be shown in Section 4.5 that the proposed algorithm still outperforms the heuristic greedy method. For a general K, the computational complexity of the proposed algorithm can be shown to be $\mathcal{O}(N^K)$, which is polynomial in N.

Given the expected rate $\{V_k(\mathbf{s})\}$ and the stationary probability $\{\pi(\mathbf{s})\}$, the proposed dynamic programming can efficiently find solutions of the allocation rule $\{a_k(\mathbf{s})\}$ and the pricing rule $\{P_k(\mathbf{s})\}$ to the problem $\boldsymbol{\mathcal{P}}_p$. However, $\{V_k(\mathbf{s})\}$ and $\{\pi(\mathbf{s})\}$ depend on $\{a_k(\mathbf{s})\}$ since the state transition probability depends on $\{a_k(\mathbf{s})\}$. Therefore, we propose to iteratively update $\{V_k(\mathbf{s})\}$, $\{\pi(\mathbf{s})\}$, and $\{a_k(\mathbf{s})\}$. The proposed mechanism design algorithm for the network selection game is summarized in Table 4.2. In the numerical simulation, we observed that the iterative algorithm exhibits very fast convergence. The typical number of iterations to converge is between 5 to 8.

The proposed algorithm can be easily modified to solve $\boldsymbol{\mathcal{P}}_u$ by replacing the min in (4.39) and (4.41) with the max, and changing the boundary condition in (4.42) to be $f_1(s_i|s_{-i}) = \sum_{r=0}^{s_i} \pi(r, s_{-i}) V_k(r, s_{-i})(\lambda - w(s_i, s_{-i}))$.

4.5 Numerical Simulation

In this section, we use numerical simulation to verify the analysis and evaluate the performance of the proposed modified value iteration algorithm as the rational strategy. The proposed method is compared with the following schemes. We first define the social welfare given a strategy profile $\boldsymbol{\sigma}$ as $SW^{\boldsymbol{\sigma}} = \sum_{\mathbf{s}\in\mathcal{S}} \pi^{\boldsymbol{\sigma}}(\mathbf{s}) \sum_{k=1}^{K} s_k R_k(s_k)$,

where $\pi^{\boldsymbol{\sigma}}(\mathbf{s})$ is the stationary probability at system state $\mathbf{s}$. The centralized method is to exhaustively search through all the possible strategy profiles and choose the one that achieves the largest social welfare, i.e., $\boldsymbol{\sigma}^{\text{cent}} = \arg\max_{\boldsymbol{\sigma}} SW^{\boldsymbol{\sigma}}$. Thus, the centralized method requires a computational complexity of $\mathcal{O}(K^{|\mathcal{S}|})$, which is exponentially increasing in the number of system states and is impossible to be used in practice. The myopic strategy is obtained by choosing the largest immediate utility after making the decision, i.e., $\sigma_{\mathbf{s}}^{\text{myop}} = \arg\max_{k\in\{1,\ldots,K\}} R_k(s_k+1)$. In current cellular systems, the cell selection is done by choosing the base-station with the highest detected SNR. Such an approach is similar to the myopic strategy since it only concerns about the immediate utility. Finally, the random strategy is to randomly make the decision with equal probability, i.e., $Pr\left\{\sigma_{\mathbf{s}}^{\text{rand}} = k\right\} = \frac{1}{|\bar{\mathcal{F}}(\mathbf{s})|}, \forall k \in \bar{\mathcal{F}}(\mathbf{s})$, where $|\cdot|$ denotes the cardinality of a set. In the following simulation, the performance of the random strategy is obtained by averaging the performance of 1000 instances for each set of parameters.

The algorithm analysis in Section 4.3 shows that there exists a threshold structure of the strategies along each line of $s_1 + s_2 = m$, $\forall m \in \{1, 2, ..., 2N\}$. We verify the analysis by numerical simulation in Figure 4.3, which illustrates the strategy profile computed by the proposed algorithm in a two-network system where $P_s/N_0 = 50$, $P_I/N_0 = 10$, $T = 0.08$ (sec), $\bar{\lambda}_0 = 0.5$ (users/sec), $\bar{\lambda}_1 = 0.125$ (users/sec), $\bar{\lambda}_2 = 2.5$ (users/sec), $\bar{\mu} = 1.25$ (users/sec), $\epsilon = 0.05$ and $N = 8$. The x-axis (y-axis) denotes s_1 (s_2), i.e., the number of users in network 1 (network 2). The number marked at the coordinate $\mathbf{s} = (s_1, s_2)$ denotes the computed strategy $\sigma_{\mathbf{s}}$, which is either 1 or 2 in this scenario. This figure shows the strategy profile converges in 30 iterations.

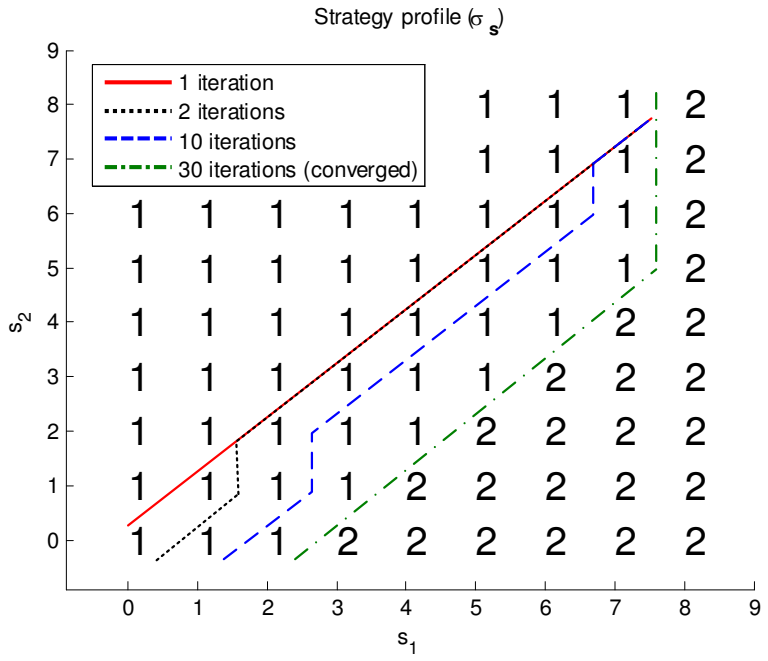

Figure 4.3: The threshold structure of the strategy profile during iterations of the proposed algorithm.

The green (dot-dash) line is drawn in between different strategies to emphasize the threshold. The threshold lines of certain iterations (1, 2, and 10) are also shown in the figure to illustrate the evolution of the strategy profile during the iterations of the proposed algorithm. It is observed that at each iteration, the threshold structure of the strategies always exists along the diagonal lines as the analysis in Section 4.3. In the rest of simulations, instead of specifying the arrival rates and the time slot duration, we consider the parameters as transition probabilities since the relative values of these probabilities directly influence the resulting performance. Figure 4.4 shows the converged strategy profile of a three-network system, where $P_s/N_0 = 50$, $P_I/N_0 = 10$, $\lambda_0 = 0.1$, $\lambda_1 = 0.1$, $\lambda_2 = 0.2$, $\lambda_3 = 0.3$, $\mu = 0.1$, $\epsilon = 0.05$ and $N = 5$. It is observed that the strategy profile also has a threshold structure.

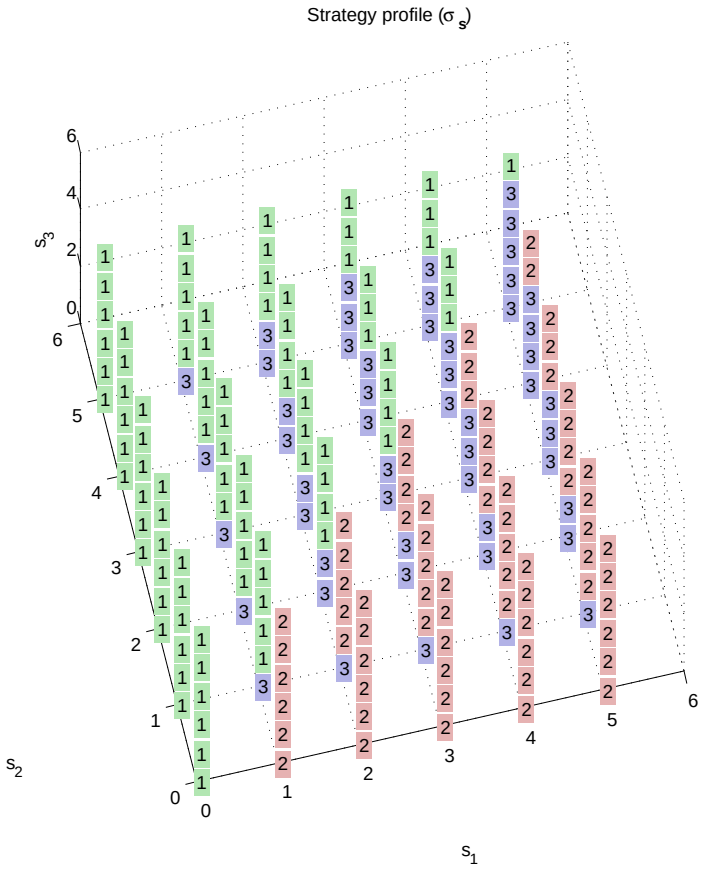

Figure 4.4: The threshold structure of the strategy profile for a three-network system.

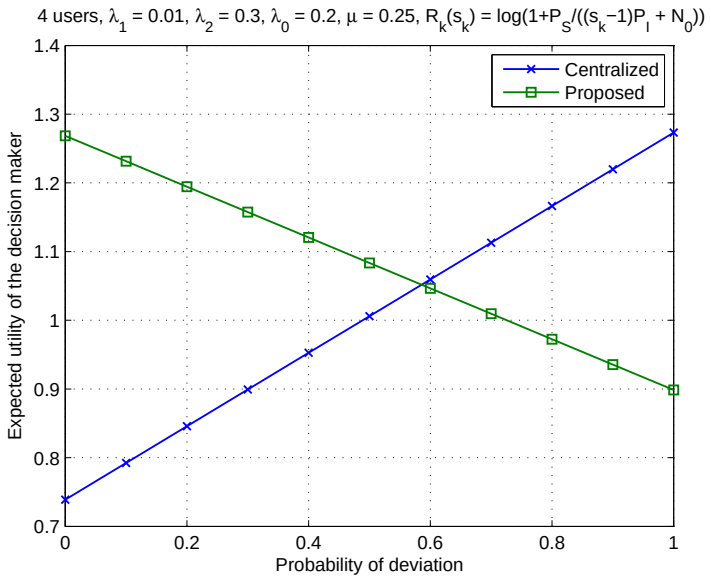

Figure 4.5: Comparison of the proposed method and the centralized method for the decision maker's expected utility versus probability of deviation.

Figure 4.5 validates the individual rationality of the proposed method in a two-network system, where the parameters are set to be $P_s/N_0 = 50$, $P_I/N_0 = 10$, $\lambda_0 = 0.2$, $\lambda_1 = 0.01$, $\lambda_2 = 0.3$, $\mu = 0.25$, $\epsilon = 0.05$, and $N = 4$. The decision maker's expected utility, defined as $E[V_{\sigma_{\mathbf{s}}}(\mathbf{s} + \mathbf{e}_{\sigma_{\mathbf{s}}})]$, is evaluated versus the probability of deviation p_d. For computational tractability of the centralized method, the number of users N is set to be 4. Note that the time slot duration is chosen to ensure that $\lambda_0 + \lambda_1 + \lambda_2 + 2N\mu \leq 1$ but the relative values of these probabilities are retained. The user at state $\mathbf{s}$ deviates from the given strategy $\sigma_{\mathbf{s}}$ with probability p_d. The decision maker's expected utility can only be impaired if he deviates from the strategy profile generated by the proposed method. However, by deviating from the centralized strategy that maximizes the social welfare, the user can possibly obtain higher expected utility (about 70% performance improvement in Figure 4.5).

Clearly, the individual rationality is not satisfied for the centralized strategy.

Figure 4.6(a) and 4.6(b) show the comparison of the decision maker's expected utility with different strategy profiles in a two-network system where $P_s/N_0 = 50$, $P_I/N_0 = 10$, $\lambda_1 = 0.01$, $\mu = 0.15$, $\epsilon = 0.5$, and $N = 4$. We use the myopic strategy as the baseline by normalizing the performance of other methods with that of the myopic strategy. In Figure 4.6(a), $\lambda_0 = 0.2$ and λ_2 is varied from 0.05 to 0.75. In Figure 4.7(b), $\lambda_2 = 0.3$ and λ_0 is varied from 0.05 to 0.75. It can be seen that the proposed method performs the best among all the schemes since the decision maker optimizes his expected utility by choosing network to his best advantage. The myopic strategy always has performance 1 due to the normalization. The random strategy is worse than the myopic method which exploits the information of the immediate utility. The centralized method performs the worst because it maximizes the social welfare and results in sacrificing the decision maker's expected utility.

In Figure 4.7(a) and 4.7(b), we compare the social welfare performance of the strategy profiles generated by different approaches in a two-network system where the parameters are $P_s/N_0 = 50$, $P_I/N_0 = 10$, $\lambda_0 = 0.2$, $\mu = 0.25$, $\epsilon = 0.05$ and $N = 4$. In Figure 4.7(a), $\lambda_1 = 0.01$ and λ_2 is varied from 0.05 to 0.75. In Figure 4.7(b), $\lambda_2 = 0.3$ and λ_0 is varied from 0.05 to 0.75. The performance of each method is normalized by the myopic one. It can be seen that the proposed method performs similar to that of the centralized method which maximizes the social welfare. Figure 4.8 shows the impact of ϵ on the number of iterations for the strategy profile to converge using the proposed modified value iteration algorithm. It can be seen that when ϵ increases, it requires smaller number of iterations to converge since the region

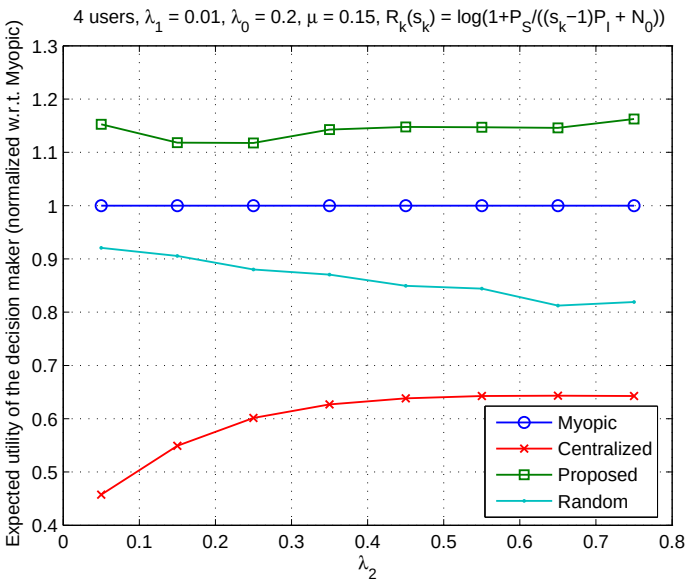

(a) The decision maker's expected utility versus λ_2.

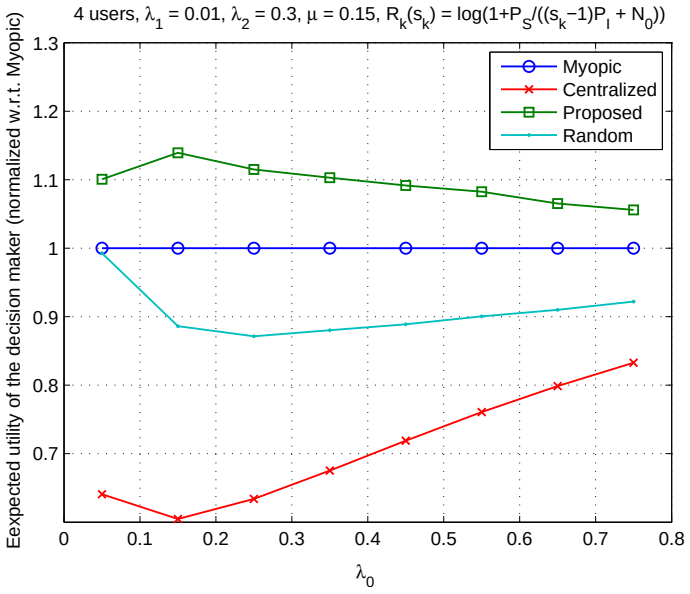

(b) The decision maker's expected utility versus λ_0.

Figure 4.6: Comparison of different strategies for the decision maker's expected utility.

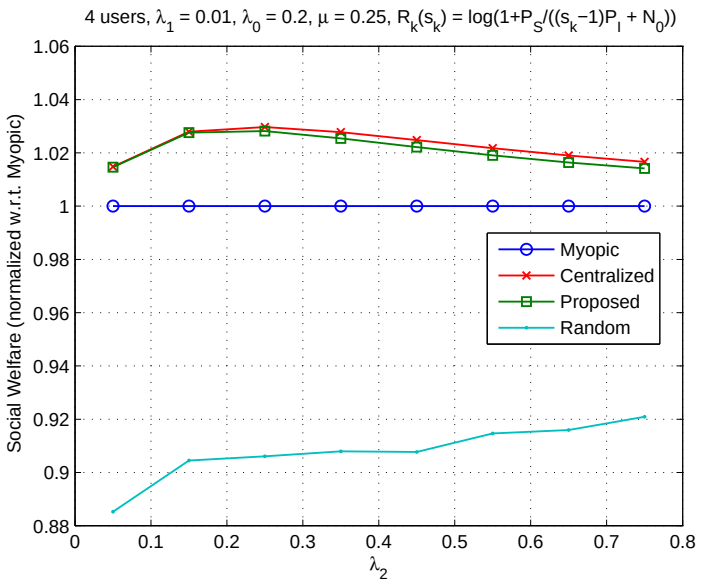

(a) The social welfare versus λ_2.

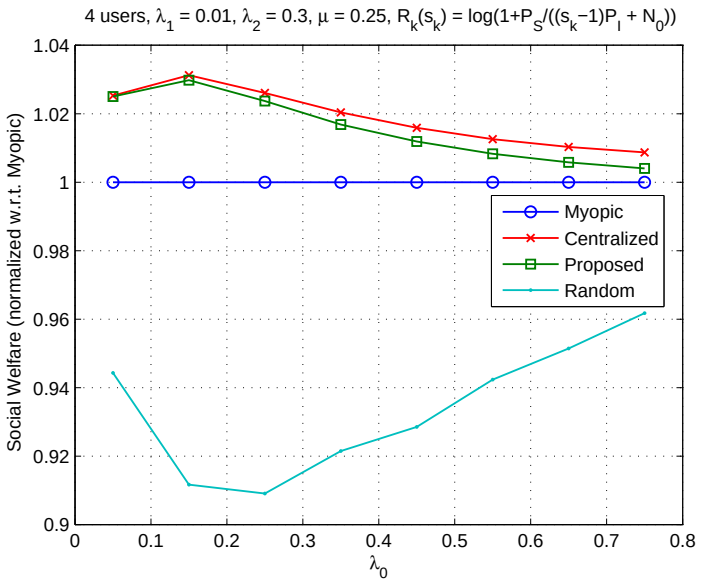

(b) The social welfare versus λ_0.

Figure 4.7: Comparison of different strategies for the social welfare.

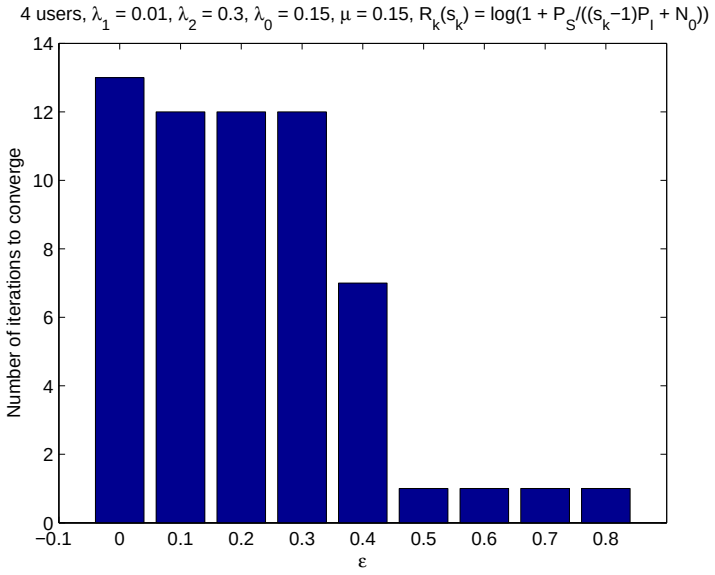

Figure 4.8: The impact of ϵ on the number of iterations for the strategy profile to converge.

of tolerance for switching among the strategy profile is larger, and possibly more ϵ-approximate NEs are available.

Figure 4.9 and 4.10 show the performance comparison for different mechanism designs when $K = 2$ and $K = 3$, respectively. The exhaustive search is to search over all possible allocation rules and find out the one with the optimal objective value. The greedy algorithm is characterized by the following recursive formula.

$$f_k^{\mathrm{G}}(\{s_i, i \in \mathcal{I}\}|\{s_j, j \in \mathcal{J}\}) = \min_{i \in \mathcal{I}} \left\{ f_{k-1}^{\mathrm{G}}(s_{-i}|\{s_j, j \in \mathcal{J} \cup \{i\}\}) \right\}, \tag{4.47}$$

$$a_{i^*}(s_{i^*}, s'_{-i^*}, s_j, s_{-j}) = 0, \forall s'_{-i^*} \preceq s_{-i^*}, \tag{4.48}$$

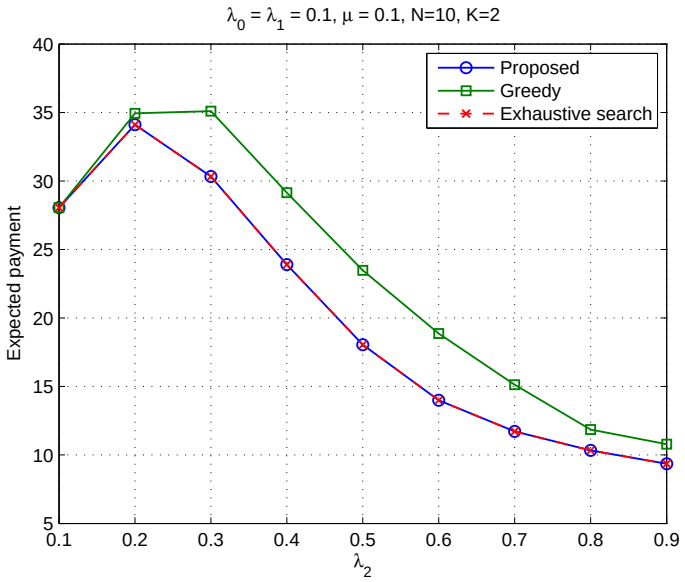

Figure 4.9: Comparison of different mechanism designs for the expected payment versus λ_2 when $K = 2$.

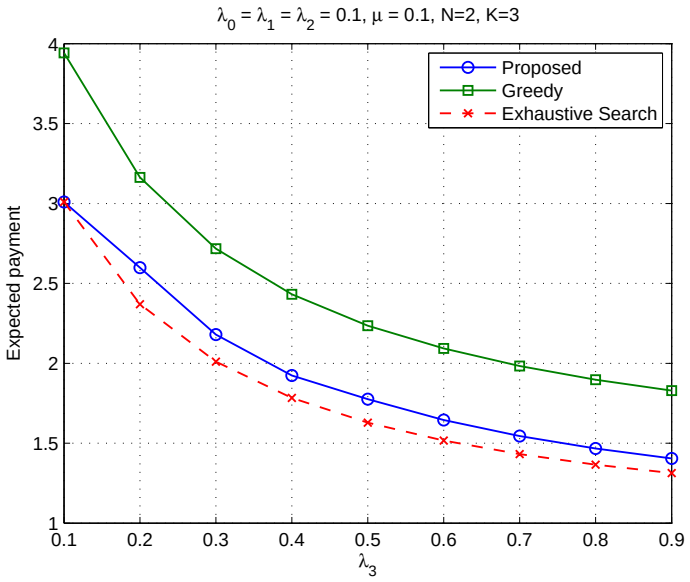

Figure 4.10: Comparison of different mechanism designs for the expected payment versus λ_3 when $K = 3$.

where $i^* = \arg\min_{i\in\mathcal{I}} \left\{ f^{\mathrm{G}}_{k-1}(s_{-i}|s_j, j \in \mathcal{J}\cup\{i\}) \right\}$. The boundary condition is

$$f^{\mathrm{G}}_1(s_i|s_{-i}) = f^{\mathrm{G}}_1(s_i-1|s_{-i})\frac{w_i(s_i,s_{-i})}{w_i(s_i-1,s_{-i})} + \pi(s_i,s_{-i})V_i(s_i+1,s_{-i})w_i(s_i,s_{-i}), \tag{4.49}$$

$$a_{-i^*}(s_{i^*}, s'_{-i^*}, s_j, s_{-j}) = 1, \forall s'_{-i^*} \leq s_{-i^*}, \tag{4.50}$$

where i^* is the minimizor in (4.48) when $K = 2$. The greedy algorithm is to evaluate $f^{\mathrm{G}}_K(N,\ldots,N)$ with $\mathcal{I} = \{1,\ldots,K\}$ and $\mathcal{J} = \phi$ by using (4.47)-(4.50). With a similar analysis, the computational complexity of the greedy algorithm can be shown to be $\mathcal{O}(N^K)$. Compared with the proposed DP algorithm, the greedy method is a heuristic approach which makes a local optimal decision according to lower dimensional results. We can see more clearly by considering the case $K = 2$, i.e.,

$$f^{\mathrm{G}}_2(s_1,s_2) = \min\left\{ f^{\mathrm{G}}_1(s_2|s_1), f^{\mathrm{G}}_1(s_1|s_2) \right\}, \tag{4.51}$$

$$(a_1(s_1,s'_2), a_2(s_1,s'_2)) = (0,1), \forall s'_2 \leq s_2, \text{ if } f^{\mathrm{G}}_1(s_2|s_1) > f^{\mathrm{G}}_1(s_1|s_2), \tag{4.52}$$

$$(a_1(s'_1,s_2), a_2(s'_1,s_2)) = (1,0), \forall s'_1 \leq s_1, \text{ if } f^{\mathrm{G}}_1(s_2|s_1) \leq f^{\mathrm{G}}_1(s_1|s_2). \tag{4.53}$$

For example, when evaluating $f^{\mathrm{G}}_2(N,N)$, if $f^{\mathrm{G}}_1(s_2 = N|s_1 = N)$ is larger than $f^{\mathrm{G}}_1(s_1 = N|s_2 = N)$, then state (N,N) is allocated to network 1. Due to Lemma 4, the states $\{(s_1,N), \forall s_1 \leq N\}$ are all allocated to network 1. Since the unallocated states so far are $\{(s_1,s_2), 0 \leq s_1 \leq N, 0 \leq s_2 \leq N-1\}$, we can then evaluate $f^{\mathrm{G}}_2(N,N-1)$, and so on. In Figure 4.9, we can see that the proposed DP algorithm can achieve the same performance as the exhaustive search when $K = 2$, but requires only a polynomial time complexity. The greedy algorithm has a worse performance

since it makes a local optimal decision to determine the thresholds of allocation rules. In Figure 4.10, different mechanism design approaches are compared for $K = 3$. It can be seen that the proposed DP algorithm still outperforms the greedy method. As discussed in Section 4.4, for a general K the proposed DP algorithm may not achieve the global optimum. However, with much lower complexity compared to the exhaustive search, the proposed algorithm can achieve reasonably good results and thus can serve as an approximate approach.

4.6 Discussion

Although we focus on the wireless access network selection problem in this chapter, we should notice that the model described in chapter is very general and can be applied into many other problems with negative network externality. A closely related scenario is the cell selection problem in cellular networks [5, 41, 84]. When a mobile station desires to inform the cellular system whether it is on the air, it registers to a base station which corresponds to a cellular cell. In most current cellular systems, the cell selection process is simply accomplished by a local signal-to-noise ratio (SNR)-based strategy, which is to detect the SNR of each cell and choose the cell with the largest SNR [5]. However, such a simple strategy does not take into account the strategies of others and the negative network externality. The QoS experienced by a mobile station will be degraded if the limited resources are shared with a large number of users. The utilization of system resources will also be degraded since such a strategy results in cellular cells with unbalanced load.

It can be seen that the cell selection problem has the same structure with the wireless access network selection problem. Mobile stations sequentially choose one cellular cell (corresponding to a base station) to register based on the obtained information about each available cell. The utility of a mobile station is determined by the expected throughput during the period it stays in the cell. Furthermore, the instantaneous throughput of a mobile station in a certain cell is affected by the crowdedness of the cell due to the limited bandwidth and the delay caused by the scheduling overhead. Thus, a rational mobile station should choose a cellular cell in consideration of other mobile stations' decisions to avoid the crowdedness.

4.7 Conclusion

In this chapter, we have studied the wireless access network selection problem as a stochastic game with negative network externality, where a user decides which network to connect to by considering subsequent users' decisions. The problem is shown to be a multi-dimensional MDP. We propose a modified value iteration algorithm to obtain the optimal strategy profile for each selfish user. The analysis of the proposed algorithm shows that the resulting strategy profile exhibits a threshold structure along each diagonal line. Such a threshold structure can be used to save the storage space of the strategy profile from $\mathcal{O}(N^2)$ to $\mathcal{O}(N \log N)$ in the two-network scenario. Simulation results are shown to validate the analysis and demonstrate that rational users will not deviate from the strategy profile obtained by the proposed algorithm. For the expected utility of the decision maker, the proposed method is

superior to other approaches. Moreover, its social welfare performance is shown to be similar to that of the centralized strategy which maximizes the social welfare.

We further investigated truth-telling enforcing mechanism design in the wireless access network selection problem. The mechanism design captures the incentive compatibility and individual rationality constraints while optimizing the utility of users. The formulated problem as a mixed integer program in general does not have an efficient solution. By exploiting the optimal substructures, a dynamic programming algorithm is proposed to optimally solve the mixed integer programming problem in the two-network scenario. For the multi-network scenario, the proposed algorithm can outperform the heuristic greedy approach in a polynomial-time complexity. Finally, simulation results substantiate the optimality in the two-network case and also demonstrate the effectiveness of the proposed algorithm in the multi-network scenario.

Chapter 5

Wireless Network Association Game with Data-Driven Statistical Modelling

In the previous chapter, the wireless network selection problem is investigated without considering the strategy of switching to another network, i.e., a user has to stay in a network until departure once he/she associates with the network. In addition, the proposed model in Chapter 4 is not justified based on the real-life data set analysis.

To tackle the wireless network association problem in a practical viewpoint, the model formulation has to take into account empirical study of user behavior, which is not possible without real-life data. The pattern and the statistical properties of user behavior can be extracted from massive amount of wireless LAN traces of APs available in various environments such as university campus, shopping malls, restaurants, coffee shops, airports, etc.

Recently, the wireless network association problem has attracted significant attention in the literature [6, 7, 9, 18, 20, 21, 28, 48, 50, 70, 74, 89, 90, 92, 110, 123]. The tutorial in [110] provides a comprehensive survey on many existing methods in the literature, in which utility functions and different attributes such as bandwidth, delay, packet loss, etc., are summarized and compared. One category of network asso-

ciation is based on centralized methods to optimize the system performance metrics such as sum rate, minimum rate, or proportional fairness [28, 48, 89, 123]. In [92], an analytic hierarchy process is applied to decide the relative weights of evaluative criteria set according to user preferences and service applications. In [74], Niyato et al. study a network-selection algorithm based on population evolution, which requires a centralized controller, and an algorithm based on reinforcement-learning, where a user can learn and adapt the decision on network selection to reach evolutionary equilibrium without any interaction with other users. In [123], the cell association and resource allocation are considered jointly, and a distributed algorithm via dual decomposition is proposed to solve a logarithmic utility maximization problem. Another category of network association methods is characterized by game theory, which models strategic interactions among users using formalized incentive structures [39, 106]. In wireless communications and networking, game theory has been widely studied in many applications [45, 53, 66, 104, 106, 115, 125, 126] including non-cooperative power control [45], cooperation stimulation [125,126], and spectrum allocation [53, 115]. In [7], Aryafar et al. investigate the dynamics of network selection games in heterogeneous wireless networks and the convergence properties of these games. In [18], the network selection is modelled as a congestion game, where players make decisions simultaneously to optimize the interference and throughput. The network association problem in [6] is formulated as a non-cooperative game in which users selfishly minimize an association cost accounting for the path length and the path interference to reach the gateway.

While most of the existing works study the scenario that users make simulta-

neous decisions, in this chapter, we consider the network association problem under the scenario where users make *sequential* decisions, and to obtain a better long term utility, users have to consider the negative network externality, i.e., the decisions of subsequent users, to determine his/her best response strategy. Sequential decisions considering the negative network externality effect are investigated in the Chinese Restaurant Game (CRG) [54, 107, 108], which studies the optimal decision and social learning with negative network externality but with a fixed number of users. In [54, 121], the dynamic CRG is proposed to allow users arriving and leaving stochastically.

In this chapter, we further extend the dynamic CRG in [121] to incorporate the behavior of switching to another network. We also extract statistical properties of users' behaviors in wireless networks by analyzing a data set of wireless LAN traces collected from Dartmouth campus networks in a span of 4 months. It is validated that the user arrival event is approximately Poisson distributed. The probability distribution functions of the number of user arrivals are plotted in Figure 5.1, where different curves represent the number of user arrivals in different durations. It can be seen that the behavior of these probability distribution curves is very similar to the Poisson distribution with different mean values. Furthermore, the waiting time to departure, i.e., the duration of a session, and the waiting time to switch to another network appear to be exponential distributions.

With the statistical properties extracted from the wireless LAN traces, we are able to construct a stochastic model for the wireless access network system. Next, we show that the problem of finding the best response strategy profile of network asso-

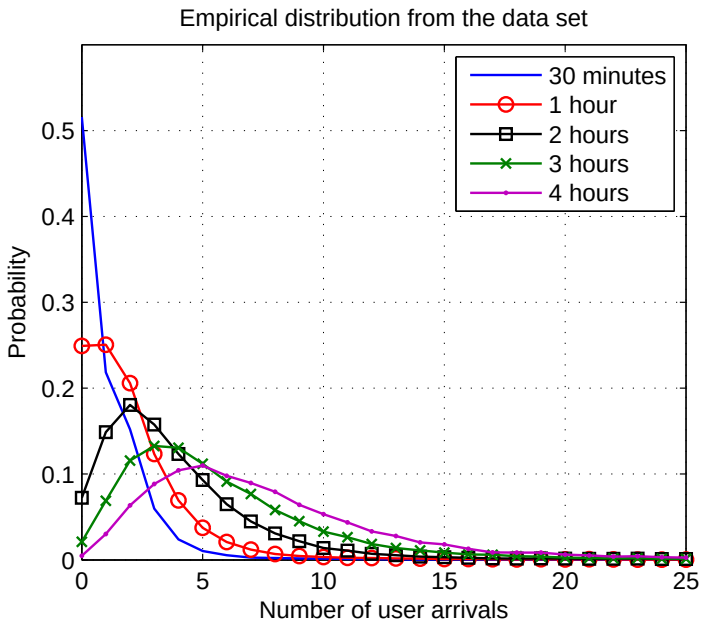

Figure 5.1: The empirical probability distribution of the number of user arrivals in different durations measured from the data set.

ciation when arriving and the best response strategy of switching during a session is a multi-dimensional Markov decision process (M-MDP). A modified value iteration algorithm is proposed to obtain a solution of an ϵ-approximate Nash equilibrium. It is observed that the strategy profile obtained by the proposed algorithm has a threshold structure, which allows a much smaller required space to store the strategy profile. Simulation results demonstrate the efficiency and effectiveness of the proposed algorithm, i.e., while achieving the best response strategy for the individual, the proposed algorithm attains similar performance of social welfare compared to the maximum social welfare strategy.

The rest of the chapter is organized as follows. In Section 5.1, the system model of the wireless network system is introduced. Section 5.2 describes the formulation of

the wireless access network association game, the expression of the expected utility, and the M-MDP. The analysis of the data set is contained in Section 5.3, in which we evaluate the probability distribution of user inter-arrival time, session time, and the waiting time to switch to another network. In Section 5.4, data-driven simulation results are shown to demonstrate the performance of the proposed value iteration algorithm. Finally, the conclusion is drawn in Section 5.5.

5.1 System Model

In this section, we describe the system model of the wireless access network association game. With the statistical model of the user arrival being a Poisson process and the user departure following an exponential distribution, we can formulate the wireless access network system as follows. The system consists of K networks, and network k acts as a server of a finite capacity N_k, i.e., the network is able to simultaneously serve at most N_k users. For simplicity, it is assumed there is no buffer or waiting room when a network is fully occupied by users. For simplicity, we only consider two types of users. The users of type I arrive with arrival rate $\bar{\lambda}_0$ and these users are able to choose among K networks. With arrival rate $\bar{\lambda}_k$, the users of type II can only choose network k, for $k = 1, \ldots, K$. Although it is feasible to consider all possible types of users who who can choose a subset of networks, the description would be too tedious and thus unnecessary. The user departure rate is denoted as $\bar{\mu}_0$ uniformly for all networks. We also define uniformly for all networks the network-switching rate $\bar{\mu}_1$, which means the rate that a user switches to another

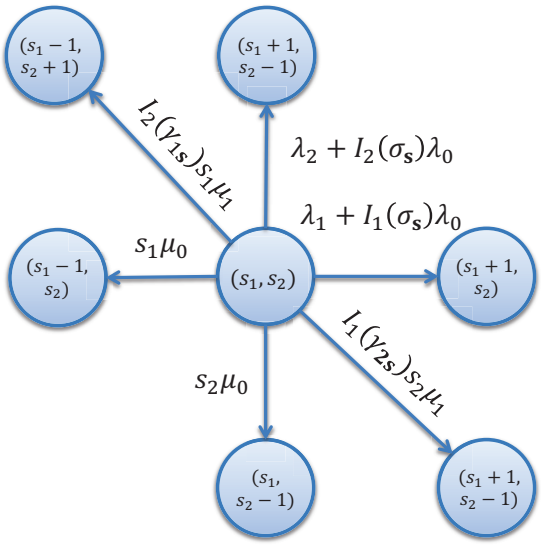

Figure 5.2: State transition diagram of the wireless access network association system.

network from his current network.

We consider a discrete time Markov system, where the system state $\mathbf{s} = (s_1, \ldots, s_K)$ takes its value from the state space $\mathcal{S} = \{(s_1, \ldots, s_K) | s_k = 0, 1, ..., N, k = 1, \ldots, K\}$, and s_k represents the number of users in network k, for $k = 1, \ldots, K$. The duration of a time unit is T (seconds). The arrival probability of type I users, denoted as λ_0, can be approximated as $1 - e^{-\bar{\lambda}_0 T} \approx \bar{\lambda}_0 T$. Similarly, the arrival probability of type II users is $\lambda_k = \bar{\lambda}_k T$, the departure probability of a user is $\mu_0 = \bar{\mu}_0 T$, and the network-switching probability is $\mu_1 = \bar{\mu}_1 T$.

The arriving user's strategy profile $\boldsymbol{\sigma} = \{\sigma_{\mathbf{s}} | \forall \mathbf{s} \in \mathcal{S}\}$ is a mapping from the aggregate state space to the action space, i.e., $\boldsymbol{\sigma} : \{0, 1, ..., N\}^K \mapsto \{1, \ldots, K\}$. The switching user's strategy profile $\boldsymbol{\gamma} = \{\gamma_{k,\mathbf{s}} | \forall \mathbf{s} \in \mathcal{S}, \forall k\}$ is a mapping from the Cartesian product set $\{1, \ldots, K\} \times \mathcal{S}$ to the action space, i.e., $\boldsymbol{\gamma} : \{1, \ldots, K\} \times$

$\{0, 1, ..., N\}^K \mapsto \{1, \ldots, K\}$. The system transition probability of an arrival event is given by

$$P_{\text{sys}}(\mathbf{s} + \mathbf{e}_j|\mathbf{s}) = \lambda_j + I_j(\sigma_{\mathbf{s}})\lambda_0,\ j = 1, \ldots, K, \tag{5.1}$$

where $\sigma_{\mathbf{s}}$ denotes the strategy at state $\mathbf{s}$ and $\sigma_{\mathbf{s}} = j$ means the strategy is to enter network j. The indicator function $I_j(\sigma_{\mathbf{s}})$ is defined as to be $I_j(\sigma_{\mathbf{s}}) = 1$ if $\sigma_{\mathbf{s}} = j$; otherwise, $I_j(\sigma_{\mathbf{s}}) = 0$. At state $\mathbf{s}$, since there are s_j users in network k and each user has an independent departure probability, the probability that one user leaves network j is $s_j\mu_0$. Thus, the system transition probability of a departure event is given by

$$P_{\text{sys}}(\mathbf{s} - \mathbf{e}_j|\mathbf{s}) = s_j\mu_0,\ j = 1, \ldots, K. \tag{5.2}$$

The network-switching strategy for state $\mathbf{s}$ and network k is denoted by $\gamma_{k,\mathbf{s}}$, and $\gamma_{k,\mathbf{s}} = j$ means the strategy is to switch from network k to network j. The system transition probability of a network-switching event is then given by

$$P_{\text{sys}}(\mathbf{s} - \mathbf{e}_k + \mathbf{e}_j|\mathbf{s}) = I_j(\gamma_{k,\mathbf{s}})s_k\mu_1,\ j, k = 1, \ldots, K. \tag{5.3}$$

Lastly, the system transition probability of a staying event is given by

$$P_{\text{sys}}(\mathbf{s}|\mathbf{s}) = 1 - \sum_{j=0}^{K} \lambda_j - \sum_{j=1}^{K} s_j(\mu_0 + \mu_1). \tag{5.4}$$

Note that the duration T of a time slot should be chosen such that $\sum_{j=0}^{K} \lambda_j + \sum_{j=1}^{K} N_j(\mu_0 + \mu_1) \leq 1$, i.e.,

$$T \leq \left(\sum_{j=0}^{K} \bar{\lambda}_j + \sum_{j=1}^{K} N_j(\bar{\mu}_0 + \bar{\mu}_1) \right)^{-1}. \tag{5.5}$$

In one time slot, the utility obtained by a user in network k is defined by the function $R(s_k)$, which is a non-increasing function in s_k due to the negative network externality, i.e., the negative effect to the users in a network caused by the increasing number of users. For example, in a code division multiple access (CDMA) system where the available frequency spectrum is used at the same time by all users, $R(s_k)$ can be defined as the achievable data rate function, $\log\left(1+\frac{\mathsf{SNR}_k}{(s_k-1)\mathsf{INR}_k+1}\right)$, where SNR_k is the signal-to-noise power ratio, and INR_k is the interference-to-noise power ratio in network k. The increase of the number of users causes inter-user interference (IUI) to each user in the network. Such IUI results in a lower signal-to-interference-plus-noise power ratio (SINR) and thus a lower achievable data rate for each user in the network. In other scenarios where the available resource is allocated in an orthogonal way, e.g., time division multiple access (TDMA) for time resource allocation, frequency division multiple access (FDMA) for frequency resource allocation, or power control for total transmit power allocation. In these scenarios, the utility $R(s_k)$ can be defined by a simple fraction $\frac{C_k}{s_k}$, where C_k denotes the total amount of the entire available resource and $\frac{C_k}{s_k}$ is the amount of resource obtained by one user in the network.

5.2 Wireless Access Network Association Game

In this section, the wireless access network association game is formulated by first defining the utility function and deriving the expected utility function using the Bellman equation, based on which, the best response strategy is given. The net-

work association problem is then shown to be a multi-dimensional Markov decision process, for which a modified value iteration algorithm is proposed.

5.2.1 Expected Utility

The expected utility of a user arriving and choosing network k to enter when the system state is $\mathbf{s}$ is denoted by $V_k(\mathbf{s})$, which can be expressed by definition as follows.

$$V_k(\mathbf{s}) = E\left[\sum_{t=0}^{\infty}(1-\mu_0)^t R_{k_t}(\mathbf{s}_t)\right], \tag{5.6}$$

where k_t denotes the network the user stays in at time slot t, with the initial condition $k_0 = k$. Since μ is the probability that the user leaves the current network in one time slot, then $(1-\mu)$ is the probability that the user stays in the network in one time slot. Thus, the value $(1-\mu)$ can be regarded as the discounting factor for the future utility as time increases.

The expression in (5.6) can be simplified into a set of Bellman equations [79], i.e.,

$$V_k(\mathbf{s}) = R_k(\mathbf{s}) + (1-\mu_0)\sum_{k',\mathbf{s}'} P(k',\mathbf{s}'|k,\mathbf{s})V_{k'}(\mathbf{s}'), k = 1,\ldots,K, \tag{5.7}$$

where the transition probability $P(k',\mathbf{s}'|k,\mathbf{s})$ denotes the probability that in the current time slot, a user is in network k and the system state is at $\mathbf{s}$, and in the next time slot, the system state becomes $\mathbf{s}'$ and the user switches to network k' if $k' \neq k$, or the user keeps staying in the same network if $k' = k$. Considering different events as in the system transition probability, the conditional transition probability

is given by

$$P\left(k', \mathbf{s}' | k, \mathbf{s}\right) =$$

$$\begin{cases} \lambda_j + I_j(\sigma_{\mathbf{s}})\lambda_0, & \text{if } k' = k, \mathbf{s}' = \mathbf{s} + \mathbf{e}_j, \forall j, \\ s_j\mu_0, & \text{if } k' = k, \mathbf{s}' = \mathbf{s} - \mathbf{e}_j, \forall j \neq k, \\ (s_k - 1)\mu_0, & \text{if } k' = k, \mathbf{s}' = \mathbf{s} - \mathbf{e}_k, \\ I_j(\gamma_{k,\mathbf{s}})(s_k - 1)\mu_1, & \text{if } k' = k, \mathbf{s}' = \mathbf{s} - \mathbf{e}_k + \mathbf{e}_j, \forall j \neq k, \\ I_j(\gamma_{k,\mathbf{s}})\mu_1, & \text{if } k' = j, \mathbf{s}' = \mathbf{s} - \mathbf{e}_k + \mathbf{e}_j, \forall j \neq k, \\ 1 - \sum_{j=0}^{K} \lambda_j - \sum_{j=1}^{K} s_j(\mu_0 + \mu_1) + \mu_0, & \text{if } k' = k, \mathbf{s}' = \mathbf{s}, \\ 0, & \text{otherwise.} \end{cases} \tag{5.8}$$

Notice that there are slight differences in the departure probability and the switching probability between the system transition probability (5.2), (5.3) and the conditional transition probability (5.8).

5.2.2 Best Response Strategy

In the wireless access network association game, users adopt the best response strategy to maximize his own expected utility due to the selfish nature. A user makes a decision after he arrives and observes the system state $\mathbf{s}$. The strategy leads the user into certain network k and results in an expected utility $V_k(\mathbf{s} + \mathbf{e}_k)$. In subsequent time slots, the user may change from network k to another network based on $\gamma_{k,\mathbf{s}}$. When observing the state $\mathbf{s}$, the best response arriving strategy $\sigma_{\mathbf{s}}$

has to satisfy

$$\sigma_{\mathbf{s}} = \arg\max_{j} V_j(\mathbf{s}+\mathbf{e}_j), \forall \mathbf{s} \in \mathcal{S}. \tag{5.9}$$

Similarly, when observing the state $\mathbf{s}$, a switching user will choose the best response strategy $\gamma_{k,\mathbf{s}}$, which has to satisfy

$$\gamma_{k,\mathbf{s}} = \arg\max_{j} V_j(\mathbf{s}-\mathbf{e}_k+\mathbf{e}_j), \forall \mathbf{s} \in \mathcal{S}, \forall k. \tag{5.10}$$

It can be seen that with the arriving user's strategy profile satisfying (5.9) and the switching user's strategy profile (5.10), no user can obtain a higher expected utility by unilateral deviation to any other strategy. Therefore, the strategy profile satisfying (5.7)-(5.10) is a Nash equilibrium of the stochastic game.

From (5.9) and (5.10), it can be observed that

$$\gamma_{k,\mathbf{s}} = \sigma_{\mathbf{s}-\mathbf{e}_k}, \forall \mathbf{s} \in \mathcal{S}, \forall k. \tag{5.11}$$

Thus, the best response switching strategy in network k at state $\mathbf{s}$ can be interpreted as as the best response arriving strategy at state $\mathbf{s}-\mathbf{e}_k$, i.e., the state without the switching user in network k. In other words, the switching behavior can be equivalently considered as leaving the current network and arriving as an arriving user. From this perspective, the two best response strategy profiles are exactly the same, and the switching user's strategy $\gamma_{k,\mathbf{s}}$ in (5.8) can be replaced by $\sigma_{\mathbf{s}-\mathbf{e}_k}$.

5.2.3 Modified Value Iteration Algorithm

The problem of solving the strategy profile satisfying (5.7)-(5.10) is a Multi-dimensional Markov Decision Process (M-MDP) problem, in which multiple po-

tential functions are associated with each system state. For a conventional MDP problem [79], there is only one single potential function, by directly optimizing which using the theory of dynamic programming (DP) [11], the optimal strategy can be found with a low complexity. In an M-MDP, the dependency of the multiple potential functions can be expressed in a vector form:

$$\begin{bmatrix} V_1(\mathbf{s}) \\ V_2(\mathbf{s}) \\ \vdots \\ V_K(\mathbf{s}) \end{bmatrix} = \begin{bmatrix} R_1(s_1) \\ R_2(s_2) \\ \vdots \\ R_K(s_K) \end{bmatrix} + (1-\mu) \begin{bmatrix} \mathbf{p}_1^T \\ \mathbf{p}_2^T \\ \vdots \\ \mathbf{p}_K^T \end{bmatrix} \begin{bmatrix} \mathbf{v}_1 \\ \mathbf{v}_2 \\ \vdots \\ \mathbf{v}_K \end{bmatrix}, \tag{5.12}$$

where $\mathbf{p}_k$ and $\mathbf{v}_k$ denote vectors comprising $P(k', \mathbf{s}'|k, \mathbf{s})$ and $V_k(\mathbf{s}')$ as elements, $k = 1, \ldots, K$. The transpose operator is denoted by $(\cdot)^T$. DP cannot be directly applied in solving such a problem since the arriving strategy $\sigma_{\mathbf{s}}$ and the switching strategy $\gamma_{k,\mathbf{s}}$ are determined by comparing $V_k(\mathbf{s}+\mathbf{e}_k)$ for all k as in (5.9) and (5.10) instead of optimizing a single potential function. Note that different from the vector form given in [54,121], the probability matrix in (5.12) is more general since it allows non-block-diagonal terms due to the switching behavior, while the probability matrix in [54, 121] only has block-diagonal terms.

As described in Section 5.2.2, the best response strategy profile $\boldsymbol{\sigma}$ has to satisfy (5.9) given the expected utilities $\{V_k\}_{k=1}^K$. Given a strategy profile $\boldsymbol{\sigma}$, the expected utilities $\{V_k\}_{k=1}^K$ can be obtained using (5.7) or (5.12), where the conditional transition probability $P(k', \mathbf{s}'|k, \mathbf{s})$ is a function of the arriving strategy $\sigma_{\mathbf{s}}$ and the switching strategy $\sigma_{\mathbf{s}-\mathbf{e}_k}$. The expected utility of a user is influenced by other users' strategies through the transition probabilities as can be seen in the vector

form (5.12). To find the best response strategy profile $\boldsymbol{\sigma}$ satisfying (5.7)-(5.10), we propose a modified value iteration algorithm to solve the problem by iteratively update the strategy profile and the expected utilities, i.e., at the n-th iteration, given the expected utilities, the strategy profile is updated as

$$\sigma_{\mathbf{s}}^{(n+1)} = \arg\max_{k} V_k^{(n)}(\mathbf{s}+\mathbf{e}_k), \forall \mathbf{s} \in \mathcal{S}. \tag{5.13}$$

The expected utility functions can be obtained by solving

$$V_k^{(n+1)}(\mathbf{s}) = R_k(s_k) + (1-\mu)\sum_{k',\mathbf{s}'} P^{(n+1)}\left(k',\mathbf{s}'|k,\mathbf{s}\right) V_{k'}^{(n+1)}(\mathbf{s}'),$$
$$\forall \mathbf{s} \in \mathcal{S}, \forall k \in \{1,\ldots,K\}, \tag{5.14}$$

where the transition probability $P_k^{(n+1)}(\mathbf{s}'|\mathbf{s})$ is updated using the strategies obtained from (5.13), i.e.,

$$P^{(n+1)}\left(k',\mathbf{s}'|k,\mathbf{s}\right) =$$
$$\begin{cases} \lambda_j + I_j(\sigma_{\mathbf{s}}^{(n+1)})\lambda_0, & \text{if } k'=k, \mathbf{s}'=\mathbf{s}+\mathbf{e}_j, \forall j, \\ s_j\mu_0, & \text{if } k'=k, \mathbf{s}'=\mathbf{s}-\mathbf{e}_j, \forall j \neq k, \\ (s_k-1)\mu_0, & \text{if } k'=k, \mathbf{s}'=\mathbf{s}-\mathbf{e}_k, \\ I_j(\sigma_{\mathbf{s}-\mathbf{e}_k}^{(n+1)})(s_k-1)\mu_1, & \text{if } k'=k, \mathbf{s}'=\mathbf{s}-\mathbf{e}_k+\mathbf{e}_j, \forall j \neq k, \\ I_j(\sigma_{\mathbf{s}-\mathbf{e}_k}^{(n+1)})\mu_1, & \text{if } k'=j, \mathbf{s}'=\mathbf{s}-\mathbf{e}_k+\mathbf{e}_j, \forall j \neq k, \\ 1-\sum_{j=0}^{K}\lambda_j - \sum_{j=1}^{K} s_j(\mu_0+\mu_1)+\mu_0, & \text{if } k'=k, \mathbf{s}'=\mathbf{s}, \\ 0, & \text{otherwise.} \end{cases} \tag{5.15}$$

In (5.14), the problem of the expected utilities involves a set of linear system, which consists of KN^2 unknown variables corresponding to $\{V_k^{(n+1)}(\mathbf{s}), \forall \mathbf{s}, \forall k\}$ and KN^2 equations, which can be solved by either matrix inversion or linear programming. Another approach is the value iteration algorithm [79], which first initializes $V_k^{(n+1)}(\mathbf{s})$ as an arbitrary value such as zero and iteratively updates itself using (5.14). Since the iteration function is a contraction mapping, it is guaranteed to converge to a unique fixed point. However, the convergence may be slow if the system space is large since it takes longer for the effect of a strategy to propagate through the whole system.

The proposed algorithm iteratively updates the strategy profile $\boldsymbol{\sigma}$ and the expected utilities $V_k(\mathbf{s})$ until converged. When the proposed algorithm converges, it is observed that there exists a threshold structure of the strategy profile. In [121], a theoretical proof of the threshold structure is given for the special case of $K = 2$ and $\mu_1 = 0$, i.e., in a two-network scenario with no switching strategy allowed. Although it is difficult to theoretically prove the threshold structure for the general cases, in Section 5.4, by numerical simulations we have always observed a threshold structure of the strategy profile for all cases.

However, the strategy profile may not converge but oscillates due to the hard decision rule in (5.13). The non-convergence occurs when the strategy of a state near a threshold of strategy change oscillates between different choices each time when the expected utility is updated. When such a situation happens, the expected utilities corresponding to different strategies are very close to each other. Hence, to tackle the problem, we relax the hard decision rule by allowing a small region of

tolerance for switching among the strategies [82], which leads to the soft decision rule as follows.

$$\sigma_{\mathbf{s}}^{(n+1)} = \begin{cases} \sigma_{\mathbf{s}}^{(n)}, & \text{if } V_{\sigma_{\mathbf{s}}^{(n)}}^{(n)}(\mathbf{s}+\mathbf{e}_{\sigma_{\mathbf{s}}^{(n)}}) \geq \max_k V_k^{(n)}(\mathbf{s}+\mathbf{e}_k) - \epsilon, \\ \arg\max_k V_k^{(n)}(\mathbf{s}+\mathbf{e}_k), & \text{if } V_{\sigma_{\mathbf{s}}^{(n)}}^{(n)}(\mathbf{s}+\mathbf{e}_{\sigma_{\mathbf{s}}^{(n)}}) < \max_k V_k^{(n)}(\mathbf{s}+\mathbf{e}_k) - \epsilon, \end{cases} \tag{5.16}$$

where $\epsilon > 0$ is a small constant. Table 5.1 summarizes the proposed modified value iteration algorithm for the M-MDP. Notice that the algorithm stops when an equilibrium is found or all the strategy profiles are searched. By definition, when the algorithm obtains a solution, the resulting strategy profile is an ϵ-approximate NE [39], in which the strategy at each state has an expected utility that is at most ϵ less than that of any other strategy. Note that there may be multiple ϵ-approximate NEs especially for a larger ϵ when a larger region of tolerance is allowed for switching among the strategies.

We note that it is possible the multiple Bellman equations for an M-MDP can be modelled as a single Bellman equation by defining an equivalent model, where the states is denoted as $(\mathbf{s}, j)$, for $j = 0, 1, \ldots, K$ and $\mathbf{s} \in \mathcal{S}$. In this model, when a user arrives at state $\mathbf{s}_1$ in the original M-MDP model, equivalently, she arrives at state $(\mathbf{s}_1, 0)$ in the MDP. The user then decides to enter network k with the largest expected utility of transiting to state $(\mathbf{s}_1, k)$, among all networks $k = 1, \ldots, K$. The subsequent state transitions only involve transitions among $(\mathbf{s}, k)$, $\forall \mathbf{s} \in \mathcal{S}$. Such a reduction from multi-dimensional Bellman equations to a single-dimensional Bellman equation, however, does not mean that M-MDP can be reduced into a

Table 5.1: Modified Value Iteration Algorithm

(i) Initialize: $V_k^{(0)}(\mathbf{s}) = 0$, $\forall k \in \{1, \ldots, K\}$, $\forall \mathbf{s} \in \mathcal{S}$. $T = \phi$.

(ii) **Loop** :

1. Update $\{\sigma_{\mathbf{s}}^{(n+1)}\}$ by (5.16).

   If $\{\boldsymbol{\sigma}_{\mathbf{s}}^{(n+1)}\} = \{\boldsymbol{\sigma}_{\mathbf{s}}^{(n)}\}$, **then** stop loop.

   else if $\{\boldsymbol{\sigma}_{\mathbf{s}}^{(n+1)}\} \in T$, **then**

   choose a $\{\boldsymbol{\sigma}_{\mathbf{s}}\} \in \bar{T}$, and let $\{\boldsymbol{\sigma}_{\mathbf{s}}^{(n+1)}\} = \{\boldsymbol{\sigma}_{\mathbf{s}}\}$.

   end if

   $T = T \cup \{\boldsymbol{\sigma}_{\mathbf{s}}^{(n+1)}\}$.

2. Update $\{P^{(n+1)}(k', \mathbf{s}'|k, \mathbf{s})\}$ by (5.15).

3. Solve $\{V_k^{(n+1)}(\mathbf{s})\}$ in (5.14) by value iteration or linear programming.

Until $\bar{T} = \phi$ or $\{\boldsymbol{\sigma}_{\mathbf{s}}^{(n+1)}\} = \{\boldsymbol{\sigma}_{\mathbf{s}}^{(n)}\}$.

conventional MDP, in which the strategy of a certain state only affects the transitions to its adjacent states instead of those of nonadjacent states. In this equivalent model, since the strategies are made by states $(\mathbf{s}, 0)$, $\forall \mathbf{s}$, the transition probability of a state $(\mathbf{s}, k)$, $k \neq 0$, does not only depend on the state itself, but also is determined by other states. Although the equivalent model has only one Bellman equation, such a dependency does not simplify but complicate the problem.

5.2.4 Mechanism Design

In the previous section, we provided an algorithm, from the perspective of users, to search for the best response strategy profile given the system parameters, including the immediate utility function $R_k(s_k)$, the user arrival rate λ_k, the user departure rate μ_0, and the network-switching rate μ_1. On the other hand, for a network system operator, it is desirable to design some of the system parameters

such that the resulting best response strategy profile is preferred to the overall network system. In the literature of game theory, such a scenario is called mechanism design, in which the system operator constructs an environment or a system setting by taking into account users' rationality and incentives to achieve the system's objective.

In the system model described in Section 5.1, the arrival rate, departure rate, and network-switching rate are not controllable by the system operator. However, the immediate utility function is possible to be managed by means of resource allocation. In the following, we provide an example to demonstrate how to design a mechanism such that the resulting strategy profile is as desired.

Consider a network system with orthogonal resource allocation such as TDMA or FDMA, the utility can be modelled as a linear function $R_k(s_k) = \frac{C_k}{s_k}$, where C_k denotes the available resource in network k, and each of the s_k users in network k can obtain $\frac{C_k}{s_k}$ per unit time. Given the strategy profile $\boldsymbol{\sigma} = \{\sigma_{\mathbf{s}}, \forall \mathbf{s}\}$, the problem of designing C_k, i.e., managing appropriate resource to different networks, can be formulated as the following feasibility problem with variables $C_1, \ldots, C_K$ and $V_k(\mathbf{s})$, $\forall k$, $\forall \mathbf{s}$.

$$\boldsymbol{\mathcal{P}}_{\text{MD}}: \quad \text{Find} \qquad (C_1, \ldots, C_K) \tag{5.17}$$

$$\text{s.t.} \qquad V_k(\mathbf{s}) = R_k(s_k) + (1-\mu_0) \sum_{k', \mathbf{s}'} P(k', \mathbf{s}' | k, \mathbf{s}) V_{k'}(\mathbf{s}'), \forall k, \forall \mathbf{s}, \tag{5.18}$$

$$V_{\sigma_{\mathbf{s}}}(\mathbf{s} + \mathbf{e}_{\sigma_{\mathbf{s}}}) \geq \max_k V_k(\mathbf{s} + \mathbf{e}_k) - \epsilon, \forall \mathbf{s}. \tag{5.19}$$

Note that given the strategy profile, the conditional probability $P(k', \mathbf{s}' | k, \mathbf{s})$ is a constant in the above feasibility problem. Therefore, the constraints of the feasibility

problem $\boldsymbol{\mathcal{P}}_{\mathrm{MD}}$ comprise $K\Pi_{k=1}^{K}N_k$ equalities and $\Pi_{k=1}^{K}N_k$ inequalities linear in the variables, and thus the problem is a linear programming problem, which can be solved in polynomial time using an interior-point algorithm.

For nonlinear utility functions such as $R_k(s_k) = \log\left(1 + \frac{\mathsf{SNR}_k}{(s_k-1)\mathsf{INR}_k+1}\right)$, it is possible to similarly formulate the feasibility problem with variables SNR_k and INR_k instead of C_k in (5.17). However, the resulting feasibility problem has non-convex constraints and hence it is difficult to solve. Optimization techniques such as convex approximation or global search may be applied but it is beyond the scope of this chapter.

5.3 Data Set Analysis

Previous work on WLAN trace analysis [1,10,12,23,47,76,88,101,111] focus on different aspects, such as uplink/downlink traffic modelling, user mobility patterns, and geographic distribution of users. In [76], the arrival processes of users can be modelled as being generated by time-varying Poisson processes through a nonlinear transformation. It is not clear whether such a transformation preserves the Poisson distribution. In [23], the user occupancy distribution of an AP is shown to be a Poisson distribution. However, a Poisson user occupancy distribution which does not imply the user arrival process is Poisson.

In this chapter, we are interested in the statistical modelling for the events related to the association between users and APs. Specifically, we aim to validate the probability distribution of the user arrival, the waiting time to departure, the

waiting time to switch network. We adopt actual wireless network data drawn from CRAWDAD [61], a well known publicly available archive of wireless data resource for the research community, and analyze the probability distribution of user inter-arrivals, session time, and the switching frequency. In the following, we first introduce the basic information of the data set, our methodology, and the results of the analysis.

5.3.1 Data Set Description

The data set we use is the CRAWDAD Dartmouth campus WLAN trace [47, 60, 61], which includes syslog (system message log), SNMP (Simple Network Management Protocol polls), and tcpdump (TCP/IP packet analysis) during Fall term 2003 and Winter term 2004 in Dartmouth College. Both syslog and SNMP traces recorded the user association information with a timestamp, the user's MAC address, and the AP's name. However, we observe that sometimes a user's association record in the syslog traces is repeated for several times in a short period, and very often a user leaves without showing the record of a disassociation. As also noted in [47], most disassociation messages do not show a successful disassociate, but report an error that it attempts to disassociate with a wrong AP. Thus, it is rather difficult to uncover the true information of users' behavior by analyzing the syslog traces.

On the contrary, The SNMP traces, which collected the Simple Network Management Protocol (SNMP) polling every AP every 5 minutes, are more reliable for

our purpose since each poll contains the instantaneous information of which user is currently connected to the AP. Although the 5 minutes period may be coarse at first sight, from our statistical analysis below, we find it sufficient for estimating the relevant parameters of the M-MDP system model. The traces were recorded by a central server using the Simple Network Management Protocol to poll each of the 560 APs in 6 different types of buildings (Academic, Administrative, Residential, Social, Library, and Athletic) on campus from November 1st, 2003 to February 28th, 2004. The SNMP query collected the AP-related information including the number of inbound and outbound bytes, packets and errors, and the users currently or recently associated with a given AP, and the user-related information including MAC and IP addresses, signal strength and quality, the number of inbound and outbound bytes, packets and errors.

5.3.2 Statistical Analysis

We plot the number of user arrivals during the 4-month period in the lower part of Figure 5.3, in which we can see that there are two holes with zero arrivals when the SNMP poller was disabled due to maintenance. One is during the Christmas holidays and the other is in late February. Most of the time, the number of arrivals shows a regular periodicity as expected. Relatively fewer users arrive during weekends and holidays. The upper part of Figure 5.3 shows the average number of arrivals per hour in a weekday and a weekend day. Also as expected, the user arrivals occur more in the afternoon on weekdays than on weekends. Based on the above observation,

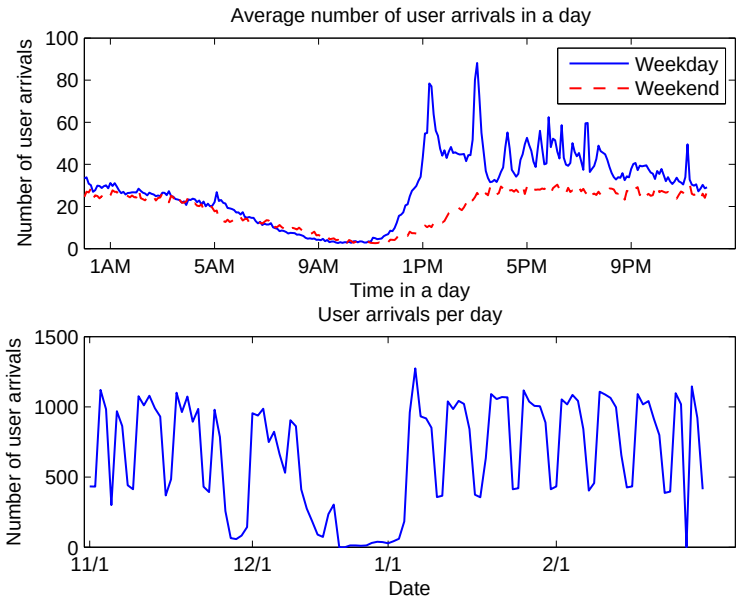

Figure 5.3: The upper part shows the average number of user arrivals per hour in a weekday and in a weekend day; the lower part shows the number of user arrivals per day during the 4-month period.

in the following analysis, we only consider the abundant traces on weekdays to have richer and consistent data. Only traces between 9AM and 5PM are extracted so that the typical behavior during the daytime can be captured.

An intuitive definition of a user arrival is the event that the user associated with an AP is not associated in the previous time slot. However, such a definition does not take into account of the scenario that there may be a time slot when the user is not recorded by any AP but the user is switching from an AP to another AP. Therefore, we define a user arrival by the event that a user is associated with an AP in a type of network and the user is not associated with any AP in the network in the past 2 time slots. Similarly, a user departure is defined by the event that a

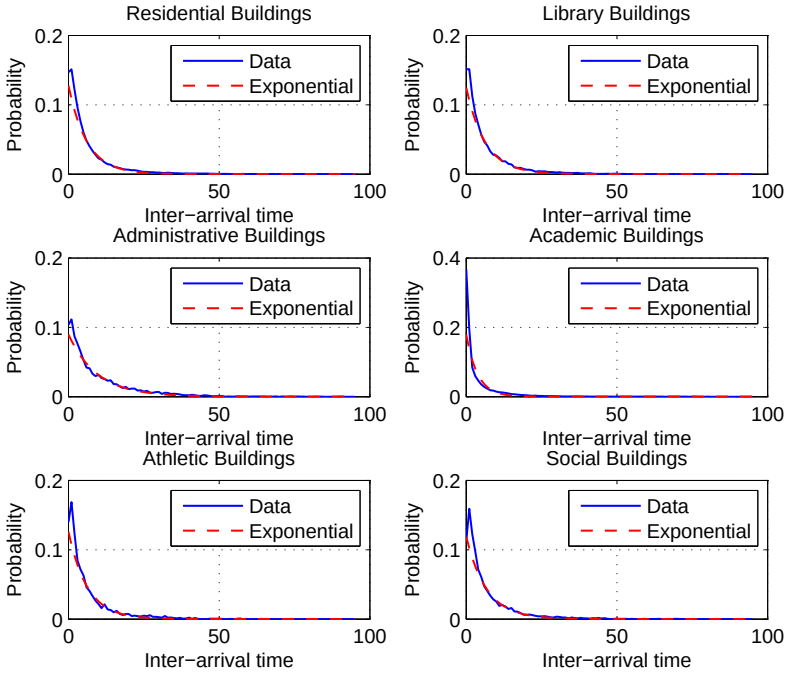

Figure 5.4: The probability density function of the inter-arrival time versus the exponential distribution with the same mean value.

user associated with an AP in a type of network becomes not associated with any AP in the network in the next 2 time slots. If a user is associated with multiple APs in one time slot, a switching event is defined to occur with a duration of 0. A switching event also occurs if the associated AP of a user has changed after k time slots to another AP before a departure event occurs. A session is then defined by the time between a user arrival and a departure with only switching events allowed in between.

Figure 5.4 shows the empirical probability density function (pdf) of the inter-arrival duration versus the theoretical exponential distribution with the same mean as the data set. It can be observed that the exponential distribution can provide a

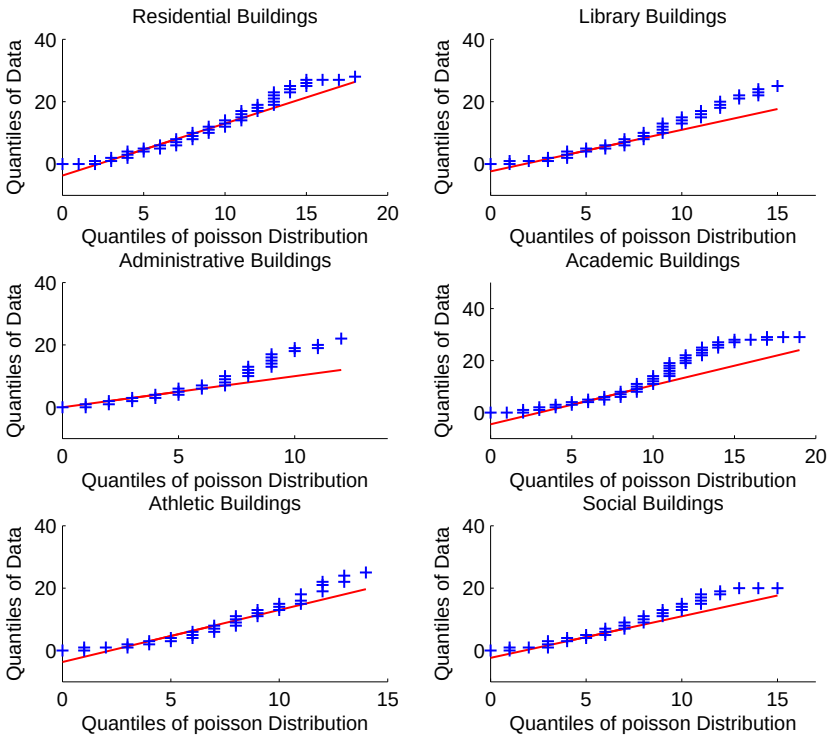

Figure 5.5: The quantile-quantile plot of the probability mass function of the number of user arrivals in 3 hours versus the Poisson distribution with the same mean value.

very good approximation to the empirical pdf for all 6 types of buildings. Compared to the theoretical exponential distribution, The empirical pdf tends to decrease faster in the middle range of the inter-arrival time, but when the inter-arrival time becomes larger, the tail of the empirical pdf stays longer. Such an tendency is especially prominent for Academic Buildings. We speculate that this may be due to the regular pattern of the activities on campus, where the durations of classes and break time are usually fixed. Hence, such a pattern may cause the user arrival event not as random than expected. Except this minor discrepancy, from Figure 5.4, the exponential distribution is still a satisfactory approximation.

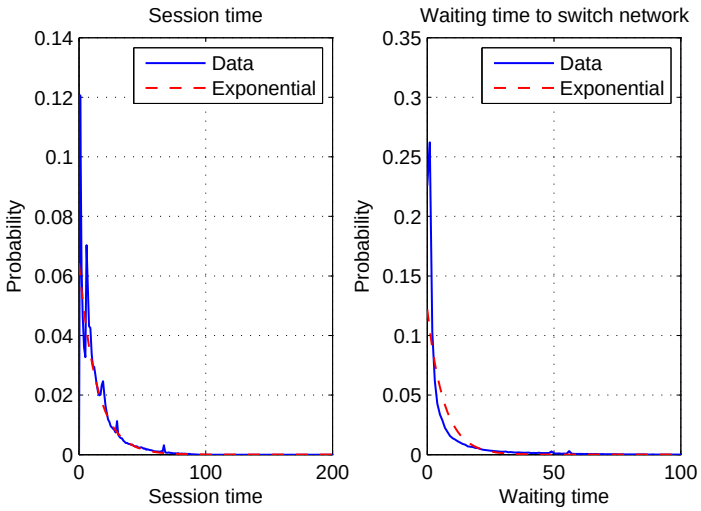

Figure 5.6: The probability density functions of a session time and the waiting time to switch to another network.

In Figure 5.5, we plot the quantile-quantile plot [113] of the empirical probability mass function (pmf) of the number of user arrivals in 3 hours versus the theoretical Poisson distribution with the same mean value of the data set. The quantile-quantile (Q-Q) plot is a graphical method for comparing two probability distributions. If the two distribution are similar or linearly related, the points will approximately lie on a straight line. If the two distributions are exactly identical, the points on the Q-Q plot should lie on the line $x = y$. In the Q-Q plots, the first and third quartiles are connected and extrapolated as a line to illustrate the degree of similarity of the empirical pmf to the Poisson distribution. From the figure, we can see that the empirical pmf has a high similarity to a Poisson distribution.

Figure 5.6 shows the pdfs of a session time and the waiting time to switch to another network. In each plot, we also compare the empirical curve with the exponential distribution with the same mean value. We can see that for the session

time distribution, there are a few peaks which may indicate some fixed patterns of activities on campus. As discussed above, there may be a relatively high probability that the session time is equal to the duration of a class or break time between classes, e.g., 50 or 15 minutes. Except those peaks, the general trend of a session time still approximately follows an exponential distribution with the same mean value. For the waiting time to switch network, the pdf decreases faster in the middle range and it has a longer tail when the time increases compared to an exponential distribution.

From the analysis of these statistical properties, we can model the realistic user arrivals as a Poisson distribution, and thus the inter-arrival time as an exponential distribution; the session time and the waiting time to switch network can be modelled as exponential distributions. Therefore, we have the Markov state model as described in Section 5.1, in which a state in the wireless network system can be represented by the numbers of users in different networks without knowing the history of user arrivals due to the Markovian property. The departure probability μ_0 for a user can be approximated by the inverse of the mean session time, i.e., $\bar{\mu}_0 T$; the switching probability μ_1 can also be approximated by the inverse of the mean waiting time to switch network, i.e., $\bar{\mu}_1 T$.

Table 5.2 summarizes the empirical average values of the parameters for the M-MDP model, including the mean inter-arrival time $\bar{\lambda}^{-1}$, mean session time $\bar{\mu}_0^{-1}$, and the mean switching time $\bar{\mu}_1^{-1}$, for different types of campus networks and the overall, that is, the average of all types of networks. Note that a unit time slot is 5 minutes. Thus, we may interpret the 'overall' row as: on average, every 26 minutes there is a user arrival event; each arrival stays for a session of 70 minutes in the

Table 5.2: Averaged empirical parameters for different types of campus networks.

Types	$\bar{\lambda}^{-1}$	$\bar{\mu}_0^{-1}$	$\bar{\mu}_1^{-1}$
Residential	6.1460	12.7200	7.4541
Library	6.3522	12.2097	8.2054
Administrative	9.5474	14.0074	8.4835
Academic	3.7513	13.4151	6.3910
Athletic	6.2693	16.6079	6.3641
Social	6.7630	12.2915	6.4784
Overall	5.1096	13.9891	6.5283

network before departure; during a session, every 33 minutes the user switches to another AP.

5.4 Data-Driven Simulation

In this section, a data-driven numerical simulation is conducted for the wireless access association game described in Section 5.2. Based on the data set analysis in section 5.3, we adopt most of the system parameters such as users' arrival, departure, and switching rates from Table 5.2. In the following simulation, the parameters are chosen as $K = 2$, $\bar{\mu}_0^{-1} = 13.9891$, $\bar{\mu}_1^{-1} = 6.5283$, $\bar{\lambda}_0^{-1} = 6.763$, $\bar{\lambda}_1^{-1} = 67.3669$, $\bar{\lambda}_2^{-1} = 5.1096$, , $T = 1$, $N = 4$, $\epsilon = 0.05$. Note that we choose $\bar{\lambda}_1^{-1}$ to be much larger than $\bar{\lambda}_2^{-1}$, since in such a scenario, the proposed best response strategy has more significant gain over other methods. The utility function $R_k(s_k)$ is defined to be the achievable data rate $\log\left(1 + \frac{\mathsf{SNR}_k}{(s_k-1)\mathsf{INR}_k+1}\right)$, where $\mathsf{SNR}_k = 50$, $k = 1, 2$, and $\mathsf{INR}_k = 10$, $k = 1, 2$. In the following, we will compare the proposed best response

strategy with other possible strategies including the random strategy, the myopic strategy, and the centralized strategy. The random strategy is to randomly (with uniform probability) select a network among all networks. The greedy strategy is to choose the network with the best immediate utility instead of the long term expected utility, i.e., $\sigma_{\mathbf{s}}^{\text{myopic}} = \arg\max_k R_k(s_k)$. The maximum social welfare strategy is the social welfare optimizer, i.e., the strategy profile that results in the globally maximum system throughput $\sum_{\mathbf{s}} \sum_k s_k R_k(s_k)$, which is the maximum amount of total achievable data rate from the entire network system. In the simulation, the maximum social welfare strategy profile is found by exhaustive searching all possible strategy profiles. Since the complexity is very high ($\mathcal{O}(K^{N^K})$) even for $K = 2$, we only simulate small N to demonstrate the comparison between different strategies.

In Figure 5.7, we verify the individual rationality by examining the relation between the deviation probability and the individual expected utility. It can be seen that if a user deviates from the proposed best response strategy profile, he/she can only obtain a worse individual expected utility; while for the maximum social welfare strategy profile, a user may be able to earn a better payoff by unilateral deviation to another strategy, since the objective of the maximum social welfare strategy is to optimize the social welfare without consideration of the individual rationality.

We compare the individual expected utility for different strategies in Figures 5.8. Using the greedy method as the baseline, the performance of each strategy is normalized with the corresponding value of the greedy method. Since each user optimizes his/her own expected utility, the proposed best response strategy as expected

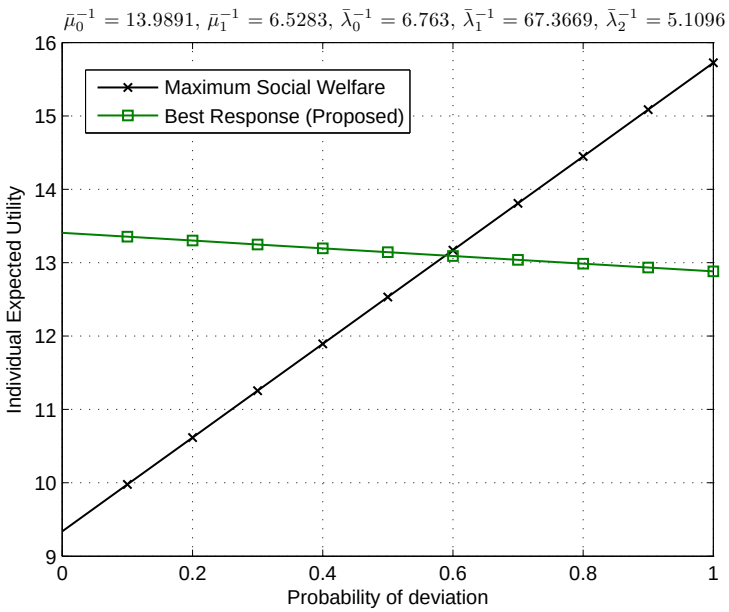

Figure 5.7: The individual expected utility versus probability of deviation with the proposed best response strategy and the maximum social welfare strategy.

performs the best among all other strategies in terms of the individual expected utility. When $\bar{\lambda}_0$ is higher, i.e., more users who are able to choose among the networks, the maximum social welfare strategy provides worse individual expected utility due to the crowdedness of users and thus the conflict between maximizing the social welfare and the individual performance. Without taking into account any information, the random strategy is inferior to all others.

In Figure 5.9, the social welfare performance (the system thoughput, i.e., the sum of the expected utility of each user) of different strategies is compared. Since the maximum social welfare strategy is the global maximizer among all the strategy profiles, it attains the best performance with certainty. We can see that the proposed best response strategy is able to achieve a similar performance to the maximum social

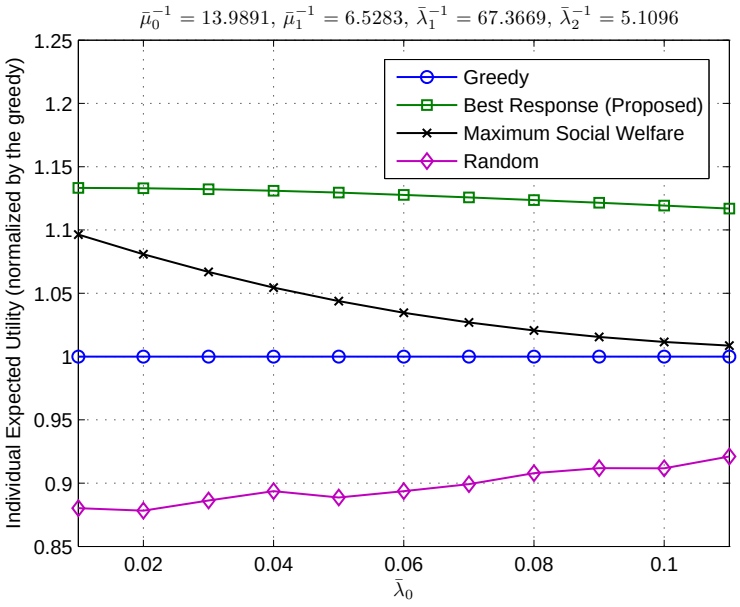

Figure 5.8: Individual expected utility comparison in a 2-network system with different strategies including the greedy method, the proposed best response strategy, the centralized maximum social welfare strategy, and the random strategy.

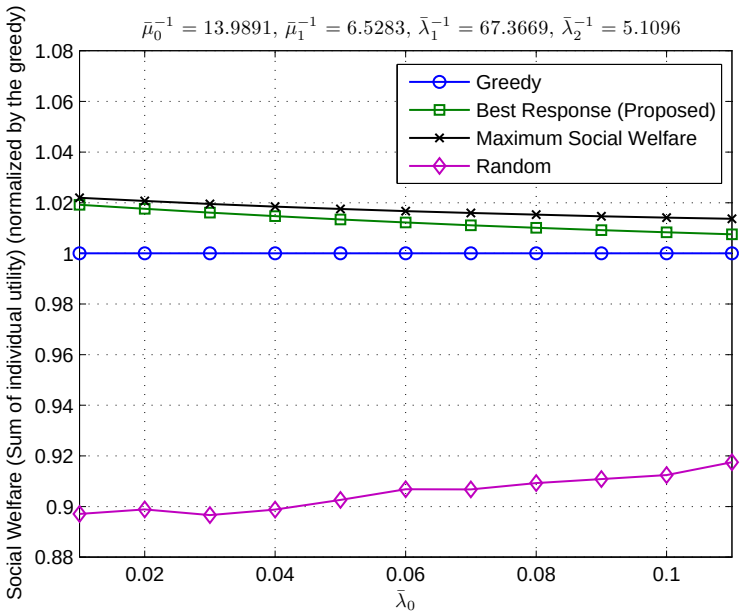

Figure 5.9: Social welfare (sum expected utility) comparison in a 2-network system with different strategies including the greedy method, the proposed best response strategy, the centralized maximum social welfare strategy, and the random strategy.

welfare strategy when $\bar{\lambda}_0$ is small, i.e., when the system is less crowded. When $\bar{\lambda}_0$ is higher, the performance becomes a bit worse but it is still better than the greedy strategy and the random strategy. It is interesting that although the proposed best response aims to optimize each user's own expected utility by considering other users' strategies, it has a similar social welfare performance to the global optimum.

Figure 5.10 shows the feasible region of (C_1, C_2) in the mechanism design

problem in (5.17), where the strategy profile $\{\sigma_{\mathbf{s}}\}$ is given as

$$\boldsymbol{\sigma} = \begin{bmatrix} 1 & 1 & 1 & 1 & 1 \\ 2 & 1 & 1 & 1 & 1 \\ 2 & 2 & 2 & 1 & 1 \\ 2 & 2 & 2 & 2 & 1 \\ 2 & 2 & 2 & 2 & 2 \end{bmatrix}, \tag{5.20}$$

where $[\boldsymbol{\sigma}]_{i,j} = \sigma_{(i,j)}$ denotes the strategy at state $\mathbf{s} = (i, j)$. Since the constraints are all linear in C_1 and C_2, the resulting feasible region is a 2-dimensional polytope, i.e., a convex region with piece-wise linear boundaries. The system operator can then manage the available resource to design C_1 and C_2 such that the desired strategy profile is a best response for the users. Note that the feasible set may not always be non-empty. Thus, the mechanism design for the wireless network association may be used to check the existence of the best response strategy profile.

5.5 Conclusion

In this chapter, we first used the four months trace of 560 APs at Dartmouth College to validate the statistical characteristics of the user arrival process being Poisson, the session time, and the waiting time to switch network being exponential. Based on these observations, we constructed a Markov system model to investigate the relation between users' strategies and their expected utilities. It has been shown that finding best response strategy, i.e., the approximate Nash equilibrium, requires solving a multi-dimensional Markov decison process. We proposed a modified value

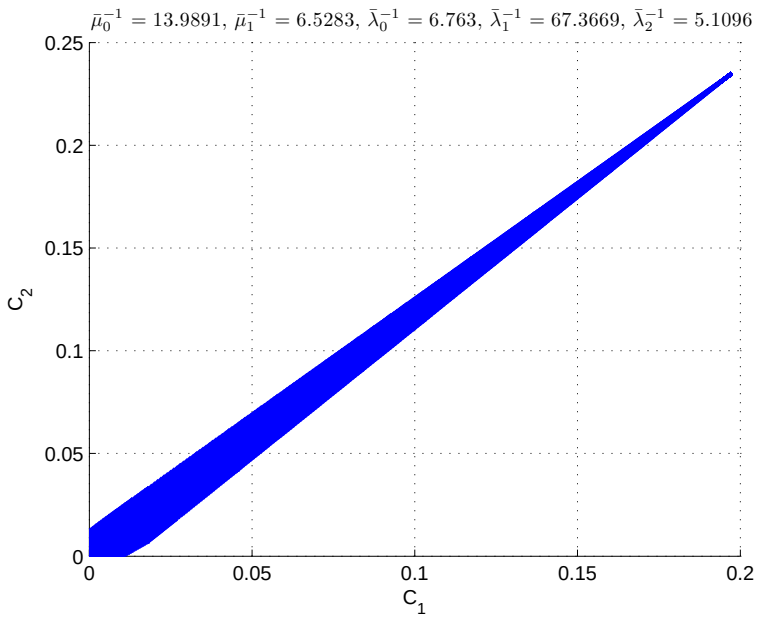

Figure 5.10: The feasible region of (C_1, C_2) in the mechanism design problem $\boldsymbol{\mathcal{P}}_{\text{MD}}$ in (5.17).

iteration algorithm to iteratively search for the solution. Data-driven simulations were conducted to verify the individual rationality, i.e., unilateral deviation from the best response strategy only leads to a decrease of the individual expected utility. Compared with other strategies, the proposed best response strategy can achieve better individual expected utility while also has a similar performance in the social welfare (the sum of the individual expected utilities) to the maximum social welfare strategy.

Chapter 6

Conclusions and Future Work

6.1 Conclusions

In the first part of this dissertation, we proposed advanced waveform design for multi-user time-reversal communication systems to tackle the interference problem from the base-station's perspective. We tackled the sum achievable rate optimization problem, and the joint waveform design problem with interference precancellation. In the second part of this dissertation, we investigated the wireless network selection problem from a user's perspective. i.e., how the strategy profile of users to associate with a wireless network affecting each individual's long term expected utility. More specifically, we addressed the following problems in this dissertation.

In Chapter 2, we explored the weighted sum rate optimization problem by transmit waveform design for the MIMO time-reversal multiuser downlink communication systems. We proposed a new power allocation scheme called Iterative SINR Waterfilling which, instead of directly allocating the power, the SINRs are first allocated to maximize the weighted sum rate. With the allocated target SINRs, the corresponding power allocation can be easily determined. For multiple data streams, Iterative Power Waterfilling is further proposed. Iterative algorithms al-

ternately optimize the transmit waveform and the power allocation for each user. Both of the proposed sum rate optimization algorithms significantly outperform other traditional approaches such as zero-forcing and time-reversal waveforms. We also demonstrated that Iterative SINR Waterfilling outperforms Iterative Power Waterfilling in the scenario of high interference, e.g., large number of users or high SNR region. With the optimal single-user waveform, Iterative SINR Waterfilling is shown to achieve near-optimal performance for multi-user scenario by comparing with exhaustively-searched global optimum.

In Chapter 3, we proposed the joint waveform design and interference pre-cancellation for TR communication systems by exploiting the symbol information available at the transmitter. It was shown that the optimal joint design is to pre-cancel the causal interference by a feedback filter and to suppress the anti-causal interference using the waveform. For the multi-user scenario, the causality of both ISI and IUI determines its similar role in the joint design. The resulting multi-user waveform design is a non-convex optimization problem, for which we proposed two iterative algorithms, including an alternating optimization algorithm and a gradient method. Both algorithms can be guaranteed to converge to sub-optimal solutions. Simulation results were shown to validate the convergence of the proposed algorithms and demonstrate the effectiveness of the proposed joint design, especially in the high interference regime.

In Chapter 4, we studied the wireless access network selection problem as a stochastic game with negative network externality, where a user decides which network to connect to by considering subsequent users' decisions. The problem

is shown to be a multi-dimensional MDP. We propose a modified value iteration algorithm to obtain the optimal strategy profile for each selfish user. The analysis of the proposed algorithm shows that the resulting strategy profile exhibits a threshold structure along each diagonal line. Such a threshold structure can be used to save the storage space of the strategy profile from $\mathcal{O}(N^2)$ to $\mathcal{O}(N \log N)$ in the two-network scenario. Further, we investigated truth-telling enforcing mechanism design in the wireless access network selection problem. The mechanism design captures the incentive compatibility and individual rationality constraints while optimizing the utility of users. By exploiting the optimal substructures, a dynamic programming algorithm is proposed to optimally solve the formulated problem in the two-network scenario. For the multi-network scenario, the proposed algorithm can outperform the heuristic greedy approach in a polynomial-time complexity. Finally, simulation results substantiate the optimality in the two-network case and also demonstrate the effectiveness of the proposed algorithm in the multi-network scenario.

Lastly, in Chapter 5, we first analyzed the four months trace of 560 APs at Dartmouth College to validate the statistical characteristics of the user arrival process being Poisson, the session time, and the waiting time to switch network being exponential. Based on these observations, we constructed a Markov system model to investigate the relation between users' strategies and their expected utilities. It has been shown that finding best response strategy, requires solving a multi-dimensional Markov decison process. We proposed a modified value iteration algorithm to iteratively search for the solution. Data-driven simulations were conducted to verify the individual rationality, i.e., unilateral deviation from the best response strategy only

leads to a decrease of the individual expected utility. Compared with other strategies, the proposed best response strategy can achieve better individual expected utility while also has a similar performance in the social welfare (the sum of the individual expected utilities) to the maximum social welfare strategy.

6.2 Future Work

To meet the exponentially increasing demand of wireless data, there are numerous challenges need to be addressed, and the development in surmounting these challenges will not only lead to fruitful research, but also benefit enhancing human life. In this dissertation, the waveform design problem and the network selection problem can be further studied in many perspectives as follows.

First, we have made several assumptions for the waveform design problem to better elucidate the proposed ideas of solving the problems. In practice, many possible impairments such as timing synchronization error, channel estimation error, carrier/sampling frequency offset, DC offset, and IQ imbalance, can weaken the assumptions and degrade the performance. Therefore, it is important to study the waveform design problem with consideration of these impairments. For example, the channel knowledge at the transmitter cannot be perfect due to all the impairments occurring when estimating the channel impulse response. To tackle the channel estimation error, the robust waveform design optimization problem can be formulated and a low complexity algorithm should be sought by approximating and exploiting the similar structure of the non-robust waveform design problem.

In the joint waveform design with interference pre-cancellation, the proposed joint waveform design for the multi-antenna scenarios can be attained by utilizing the idea of pre-cancelling the causal multi-antenna interference and suppressing the anti-causal multi-antenna interference. The channel information in the interference pre-cancellation is more critical since the interference compensation in a wrong direction can lead to a catastrophic interference construction. Thus, the robust joint waveform design with interference pre-cancellation can also be investigated.

For the network selection problem, we proved the threshold structure of the best response strategy profile in the two-network scenario with switching probability being 0. From the simulation, the threshold structure is always observed. Thus, it still remains to prove the existence of such a structure in more general scenarios. Moreover, in this dissertation, we have analyzed real-world data and conducted data-driven simulation to validate the proposed best response strategy for the wireless access network selection game. However, it is of interest to know how the proposed method performs in real-life practice. It may be possible to conduct such experiments using programmed wireless devices to verify the effectiveness of the proposed best response strategy by measuring the expected throughput of different strategies.

Bibliography

[1] M. Afanasyev, Tsuwei Chen, G.M. Voelker, and A.C. Snoeren. Usage patterns in an urban WiFi network. *IEEE/ACM Transactions on Networking*, 18(5):1359–1372, 2010.

[2] Z. Ahmadian, M.B. Shenouda, and L. Lampe. Design of pre-rake DS-UWB downlink with pre-equalization. *IEEE Transactions on Communications*, 60(2):400–410, february 2012.

[3] M.H. Ahmed. Call admission control in wireless networks: a comprehensive survey. *IEEE Commun. Surveys Tutorials*, 7(1):49–68, 2005.

[4] M.-S. Alouini and A. Goldsmith. Area spectral efficiency of cellular mobile radio systems. *IEEE Transactions on Vehicular Technology*, 48(4):1047–1066, 1999.

[5] D. Amzallag, R. Bar-Yehuda, D. Raz, and G. Scalosub. Cell selection in 4G cellular networks. In *Proc. of IEEE INFOCOM*, pages 700–708, Apr 2008.

[6] A. Argento, M. Cesana, N. Gatti, and I. Malanchini. A game theoretical study of access point association in wireless mesh networks. *Computer Commun.*, 35(5):541–553, 2012.

[7] Ehsan Aryafar, Alireza Keshavarz-Haddad, Michael Wang, and Mung Chiang. RAT selection games in HetNets. In *Proceedings of IEEE Infocom*, April 2013.

[8] A. Balachandran, P. Bahl, and G.M. Voelker. Hot-spot congestion relief in public-area wireless networks. In *Proc. of IEEE 4th Workshop on Mobile Comput. Syst. and Appl.*, pages 70–80, 2002.

[9] A. Balachandran, P. Bahl, and G.M. Voelker. Hot-spot congestion relief in public-area wireless networks. In *Proc. of IEEE 4th Workshop on Mobile Comput. Syst. and Appl.*, pages 70–80, 2002.

[10] Anand Balachandran, Geoffrey M. Voelker, Paramvir Bahl, and P. Venkat Rangan. Characterizing user behavior and network performance in a public wireless LAN. *ACM SIGMETRICS Perform. Eval. Rev.*, 30(1):195–205, June 2002.

[11] D. Bertsekas. *Dynamic Programming and Optimal Control*. Athena Scientific, 3 edition, 2007.

[12] David P. Blinn, Tristan Henderson, and David Kotz. Analysis of a Wi-Fi hotspot network. In *Workshop on Wireless Traffic Measurements and Modeling*, 2005.

[13] H Boche and M. Schubert. A general duality theory for uplink and downlink beamforming. In *Proc. VTC'02*, pages 87–91, 2002.

[14] Holger Boche and Marcin Wiczanowski. Stability-optimal transmission policy for the multiple antenna multiple access channel in the geometric view. *Signal Processing*, 86(8):1815–1833, 2006.

[15] Stephen Boyd and Lieven Vandenberghe. *Convex optimization*. Cambridge university press, 2004.

[16] M. Brandt-Pearce. Transmitter-based multiuser interference rejection for the downlink of a wireless CDMA system in a multipath environment. *IEEE J. Select. Areas Commun.*, 18(3):407–417, Mar 2000.

[17] D.W.H. Cai, T.Q.S. Quek, and C.W. Tan. Coordinated max-min sir optimization in multicell downlink - duality and algorithm. In *2011 IEEE International Conference on Communications (ICC)*, june 2011.

[18] Matteo Cesana, Nicola Gatti, and Ilaria Malanchini. Game theoretic analysis of wireless access network selection: models, inefficiency bounds, and algorithms. In *Proc. of the 3rd Intl. Conf. on Performance Evaluation Methodologies and Tools*, pages 6:1–6:10, 2008.

[19] V. Chandrasekhar, J. Andrews, and A. Gatherer. Femtocell networks: a survey. *IEEE Commun. Mag.*, 46(9):59–67, Sept. 2008.

[20] Dimitris Charilas, Ourania Markaki, Dimitris Nikitopoulos, and Michael Theologou. Packet-switched network selection with the highest QoS in 4G networks. *Computer Networks*, 52(1):248–258, 2008.

[21] Lin Chen. A distributed access point selection algorithm based on no-regret learning for wireless access networks. In *Proc. of IEEE VTC 2010-Spring*, pages 1–5, May 2010.

[22] Yan Chen and K. J. R. Liu. Indirect reciprocity game modelling for cooperation stimulation in cognitive networks. *IEEE Trans. Commun.*, 59(1):159–168, January 2011.

[23] Yung-Chih Chen, J. Kurose, and D. Towsley. A mixed queueing network model of mobility in a campus wireless network. In *IEEE INFOCOM*, pages 2656–2660, 2012.

[24] M. Chiang, Chee Wei Tan, D.P. Palomar, D. O'Neill, and D. Julian. Power control by geometric programming. *IEEE Transactions on Wireless Communications*, 6(7):2640–2651, July 2007.

[25] Søren Skovgaard Christensen, Rajiv Agarwal, Elisabeth de Carvalho, and John M. Cioffi. Weighted sum-rate maximization using weighted MMSE for MIMO-BC beamforming design. *IEEE Trans. Wireless Commun.*, 7(12):4792–4799, December 2008.

[26] Eren Cil, E. Ormeci, and Fikri Karaesmen. Effects of system parameters on the optimal policy structure in a class of queueing control problems. *Queueing Systems*, 61:273–304, 2009.

[27] Thomas Cormen, Charles Leiserson, Ron Rivest, and Cliff Stein. *Introduction to Algorithms*. MIT Press/McGraw-Hill, third edition, 2009.

[28] S. Corroy, L. Falconetti, and R. Mathar. Cell association in small heterogeneous networks: Downlink sum rate and min rate maximization. In *IEEE Wireless Communications and Networking Conference (WCNC)*, pages 888–892, 2012.

[29] M. H M Costa. Writing on dirty paper. *IEEE Trans. Inform. Theory*, 29(3):439–441, 1983.

[30] A.A. D'Amico and M. Morelli. Joint Tx-Rx MMSE design for MIMO multicarrier systems with tomlinson-harashima precoding. *IEEE Trans. Wireless Commun.*, 7(8):3118–3127, 2008.

[31] Robert C Daniels and Robert W Heath. Improving on time-reversal with MISO precoding. In *the Proceedings of the Eighth International Symposium on Wireless Personal Communications Conference*, Aalborg, Denmark, 2005.

[32] F. Dietrich, R. Hunger, M. Joham, and W. Utschick. Linear precoding over time-varying channels in TDD systems. In *Proc. ICASSP'03*, volume 5, pages 117–120, 2003.

[33] M. Emami, M. Vu, J. Hansen, A.J. Paulraj, and G. Papanicolaou. Matched filtering with rate back-off for low complexity communications in very large delay spread channels. In *the 38th Asilomar Conference on Signals, Systems and Computers*, pages 218–222, 2004.

[34] K. Eriksson, Shuying Shi, N. Vucic, M. Schubert, and E.G. Larsson. Globally optimal resource allocation for achieving maximum weighted sum rate. In *IEEE Global Telecommunications Conference (GLOBECOM 2010)*, Dec. 2010.

[35] G. Fagiolo. Endogenous neighborhood formation in a local coordination model with negative network externalities. *Journal of Economic Dynamics and Control*, 29(1-2):297–319, 2005.

[36] Mathias Fink. Time reversal of ultrasonic fields. I. basic principles. *IEEE Trans. Ultrason., Ferroelect., Freq. Contr.*, 39(5):555–566, 1992.

[37] G David Forney Jr. Trellis shaping. *IEEE Trans. Inform. Theory*, 38(2):281–300, 1992.

[38] Eric J. Friedman and David C. Parkes. Pricing WiFi at starbucks: issues in online mechanism design. In *Proc. of ACM conf. on Electronic commerce (EC)*, pages 240–241, New York, NY, USA, 2003.

[39] D. Fudenberg and J. Tirole. *Game Theory*. MIT Press, Cambridge, MA, 1991.

[40] Deyun Gao, Jianfei Cai, and King Ngi Ngan. Admission control in ieee 802.11e wireless lans. *IEEE Network*, 19(4):6–13, 2005.

[41] Lin Gao, Xinbing Wang, Gaofei Sun, and Youyun Xu. A game approach for cell selection and resource allocation in heterogeneous wireless networks. In *Proc. of IEEE SECON*, pages 530–538, June 2011.

[42] Dongning Guo, S. Shamai, and S. Verdu. Mutual information and minimum mean-square error in Gaussian channels. *IEEE Trans. Inform. Theory*, 51(4):1261–1282, 2005.

[43] Christian Guthy, Wolfgang Utschick, Raphael Hunger, and Michael Joham. Efficient weighted sum rate maximization with linear precoding. *IEEE Trans. Signal Processing*, 58(4):2284–2297, 2010.

[44] Feng Han, Yu-Han Yang, Beibei Wang, Yongle Wu, and K. J. Ray Liu. Time-reversal division multiple access over multi-path channels. *IEEE Trans. Commun.*, 60(7):1953–1965, 2012.

[45] Zhu Han, Zhu Ji, and K. J. R. Liu. Non-cooperative resource competition game by virtual referee in multi-cell OFDMA networks. *IEEE J. Select. Areas Commun.*, 25(6):1079–1090, 2007.

[46] Zhu Han and K. J. R. Liu. Noncooperative power-control game and throughput game over wireless networks. *IEEE Trans. Commun.*, 53(10):1625–1629, October 2005.

[47] Tristan Henderson, David Kotz, and Ilya Abyzov. The changing usage of a mature campus-wide wireless network. In *ACM MobiCom*, pages 187–201, 2004.

[48] Mingyi Hong and A. Garcia. Mechanism design for base station association and resource allocation in downlink ofdma network. *IEEE J. Select. Areas Commun.*, 30(11):2238–2250, 2012.

[49] R. A. Horn and C. R. Johnson. *Matrix Analysis*. Cambridge University Press, 1990.

[50] J. Hou and D. C. O'Brien. Vertical handover-decision-making algorithm using fuzzy logic for the integrated Radio-and-OW system. *IEEE Trans. Wireless Commun.*, 5(1):176–185, November 2006.

[51] J. Hoydis, M. Kobayashi, and M. Debbah. Green small-cell networks. *IEEE Vehicular Technology Magazine*, 6(1):37–43, 2011.

[52] R. Hunger and M. Joham. A general rate duality of the MIMO multiple access channel and the MIMO broadcast channel. In *IEEE Global Telecommunications Conference, 2008.*, pages 1 –5, Dec 2008.

[53] Zhu Ji and K. J. R. Liu. Multi-stage pricing game for collusion-resistant dynamic spectrum allocation. *IEEE J. Select. Areas Commun.*, 26(1):182–191, 2008.

[54] C. Jiang, Y. Chen, Y.-H. Yang, C.-Y.Wang, and K. J. Ray Liu. Dynamic chinese restaurant game in cognitive radio networks. In *Proc. of IEEE INFOCOM*, 2013.

[55] Yuanwei Jin, Jose M.F. Moura, and Nicholas O'Donoughue. Adaptive time reversal beamforming in dense multipath communication networks. In *Proc. 42nd Asilomar Conference on Signals, Systems and Computers*, pages 2027–2031, October 2008.

[56] H.H. Kha, H.D. Tuan, and H.H. Nguyen. Fast global optimal power allocation in wireless networks by local d.c. programming. *IEEE Transactions on Wireless Communications*, 11(2):510–515, Feb. 2012.

[57] M. Kobayashi and G. Caire. A practical approach for weighted rate sum maximization in mimo-ofdm broadcast channels. In *Conference Record of the 41st Asilomar Conference on Signals, Systems and Computers (ACSSC), 2007*, pages 1591–1595, nov. 2007.

[58] J. Konorski. Multihomed wireless terminals: Mac configuration and network selection games. In *Proc. of Intl. Conf. on Information Networking (ICOIN),*, pages 224–229, Jan. 2011.

[59] Ger Koole. Monotonicity in markov reward and decision chains: Theory and applications. *Found. Trends. Stoch. Sys.*, pages 1–76, 2007.

[60] David Kotz and Kobby Essien. Analysis of a campus-wide wireless network. *Wirel. Netw.*, 11(1-2):115–133, January 2005.

[61] David Kotz, Tristan Henderson, Ilya Abyzov, and Jihwang Yeo. CRAWDAD data set dartmouth/campus (v. 2009-09-09). Downloaded from http://crawdad.cs.dartmouth.edu/dartmouth/campus, September 2009.

[62] V. Krishna. *Auction Theory*. Academic Press/Elsevier, 2009.

[63] P. Kyritsi, G. Papanicolaou, P. Eggers, and A. Oprea. Time reversal techniques for wireless communications. In *IEEE Vehicular Technology Conference*, volume 1, pages 47–51, 2004.

[64] P. Kyritsi, P. Stoica, G. Papanicolaou, P. Eggers, and A. Oprea. Time reversal and zero-forcing equalization for fixed wireless access channels. In *the 39th Asilomar Conf. on Signals, Syst. and Comput.*, pages 1297–1301, 2005.

[65] Tsern-Huei Lee, Jen-Cheng Lin, and Yu.T. Su. Downlink power control algorithms for cellular radio systems. *IEEE Trans. Veh. Technol.*, 44(1):89–94, 1995.

[66] K. J. R. Liu and B. Wang. *Cognitive Radio Networking and Security: A Game Theoretical View*. Cambridge University Press, 2010.

[67] M. Lopez-Benitez and F. Casadevall. Discrete-time spectrum occupancy model based on markov chain and duty cycle models. In *Proc. of IEEE DySPAN*, pages 90–99, 2011.

[68] A. Mezghani, R. Hunger, M. Joham, and W. Utschick. Iterative THP transceiver optimization for multi-user MIMO systems based on weighted sum-mse minimization. In *Proc. 7th IEEE Workshop on Signal Processing Advances in Wireless Communications (SPAWC)*, Dec. 2006.

[69] Amine Mezghani, Rafik Ghiat, and Josef A. Nossek. Transmit processing with low resolution D/A-converters. In *Proc. 16th IEEE International Conference on Electronics, Circuits, and Systems (ICECS)*, pages 683–686, Dec. 2009.

[70] Kimaya Mittal, Elizabeth M. Belding, and Subhash Suri. A game-theoretic analysis of wireless access point selection by mobile users. *Computer Commun.*, 31(10):2049–2062, 2008.

[71] M Miyakawa and H Harashima. A method of code conversion for a digital communication channel with intersymbol interference. *Trans. Inst. Electron. Commun. Eng. Japan*, 52:272–273, 1969.

[72] Roger B. Myerson. Optimal auction design. *Mathematics of Operations Research*, 6(1):58–73, 1981.

[73] N. Nisan, T. Roughgarden, E. Tardos, and V.V. Vazirani. *Algorithmic Game Theory*. Cambridge University Press, 2007.

[74] D. Niyato and E. Hossain. Dynamics of network selection in heterogeneous wireless networks: An evolutionary game approach. *IEEE Trans. Veh. Technol.*, 58(4):2008–2017, May 2009.

[75] C. Oestges, A.D. Kim, G. Papanicolaou, and A.J. Paulraj. Characterization of space-time focusing in time-reversed random fields. *IEEE Trans. Antennas Propagat.*, 53(1):283–293, 2005.

[76] Maria Papadopouli, Haipeng Shen, and Manolis Spanakis. Modeling client arrivals at access points in wireless campus-wide networks. In *14th IEEE Workshop on Local and Metropolitan Area Networks*, pages 18–21, 2005.

[77] E. Parzen. *Stochastic Processes*. Holden-Day, San Francisco, CA, 1962.

[78] J.G. Proakis and M. Salehi. *Digital communications*. New York: McGraw-Hill, fifth edition, 2008.

[79] M. L. Puterman. *Markov Decision Processes: Discrete Stochastic Dynamic Programming*. John Wiley & Sons, 1994.

[80] F. Rashid-Farrokhi, K. J. R. Liu, and L. Tassiulas. Transmit beamforming and power control for cellular wireless systems. *IEEE J. Select. Areas Commun.*, 16(8):1437–1450, October 1998.

[81] F. Rashid-Farrokhi, L. Tassiulas, and K. J. R. Liu. Joint optimal power control and beamforming in wireless networks using antenna arrays. *IEEE Trans. Commun.*, 46(10):1313–1324, October 1998.

[82] J. Razavilar, K. J. R. Liu, and S.I. Marcus. Jointly optimized bit-rate/delay control policy for wireless packet networks with fading channels. *IEEE Trans. Commun.*, 50(3):484–494, Mar 2002.

[83] William H. Sandholm. Negative externalities and evolutionary implementation. *The Review of Economic Studies*, 72(3):885–915, Jul. 2005.

[84] Aimin Sang, Xiaodong Wang, Mohammad Madihian, and Richard Gitlin. Coordinated load balancing, handoff/cell-site selection, and scheduling in multi-cell packet data systems. *Wireless Networks*, 14:103–120, 2008.

[85] L. Sanguinetti and M. Morelli. Non-linear pre-coding for multiple-antenna multi-user downlink transmissions with different QoS requirements. *IEEE Trans. Wireless Commun.*, 6(3):852–856, 2007.

[86] M. Satyanarayanan. Pervasive computing: vision and challenges. *IEEE Personal Commun.*, 8(4):10–17, Aug 2001.

[87] M. Schubert and H. Boche. Solution of the multiuser downlink beamforming problem with individual SINR constraints. *IEEE Trans. Veh. Technol.*, 53(1):18–28, Jan. 2004.

[88] D. Schwab and R. Bunt. Characterising the use of a campus wireless network. In *IEEE INFOCOM*, volume 2, pages 862–870, 2004.

[89] Kaiming Shen and Wei Yu. Downlink cell association optimization for heteregeneous networks via dual coordinate descent. In *Proc. of IEEE International Conference on Acoustics, Speech and Signal Processing (ICASSP)*, 2013.

[90] Wei Shen and Qing-An Zeng. Cost-function-based network selection strategy in integrated wireless and mobile networks. *IEEE Transactions on Vehicular Technology*, 57(6):3778–3788, 2008.

[91] Shuying Shi, Martin Schubert, and Holger Boche. Rate optimization for multiuser MIMO systems with linear processing. *IEEE Trans. Signal Processing*, 56(8):4020–4030, August 2008.

[92] Qingyang Song and A. Jamalipour. Network selection in an integrated wireless LAN and UMTS environment using mathematical modeling and computing techniques. *IEEE Trans. Wireless Commun.*, 12(3):42–48, June 2005.

[93] Q.H. Spencer, A.L. Swindlehurst, and M. Haardt. Zero-forcing methods for downlink spatial multiplexing in multiuser MIMO channels. *IEEE Trans. Signal Processing*, 52(2):461–471, Feb 2004.

[94] M. Stojnic, H. Vikalo, and B. Hassibi. Rate maximization in multi-antenna broadcast channels with linear preprocessing. *IEEE Trans. Wireless Commun.*, 5(9):2338–2342, September 2006.

[95] H.-J. Su and E. Geraniotis. Maximum signal-to-noise array processing for space-time coded systems. *IEEE Trans. Commun.*, 50(8):1419–1422, Sep. 2002.

[96] Kazuki Takeda, Hiromichi Tomeba, and Fumiyuki Adachi. Theoretical analysis of joint THP/pre-FDE for single-carrier signal transmissions. In *Proc. of IEEE Wireless Comm. and Netw. Conf. (WCNC)*, 2009.

[97] C. Tekin, Mingyan Liu, R. Southwell, Jianwei Huang, and S.H.A. Ahmad. Atomic congestion games on graphs and their applications in networking. *IEEE/ACM Trans. Networking*, 20(5):1541–1552, Oct. 2012.

[98] Adam J. Tenenbaum and Raviraj S. Adve. Linear processing and sum throughput in the multiuser MIMO downlink. *IEEE Trans. Wireless Commun.*, 8(5):2652–2661, May 2009.

[99] Martin Tomlinson. New automatic equaliser employing modulo arithmetic. *Electronics letters*, 7(5):138–139, 1971.

[100] D. Tse and P. Viswanath. Downlink-uplink duality and effective bandwidths. In *Proc. IEEE Int. Symp. Inf. Theory (ISIT)*, Jul. 2002.

[101] C. Tuduce and T. Gross. A mobility model based on WLAN traces and its validation. In *IEEE INFOCOM*, volume 1, pages 664–674, 2005.

[102] R.V. Vohra. *Mechanism Design: A Linear Programming Approach*. Cambridge University Press, 2011.

[103] B. Wang, Y. Wu, F. Han, Y.-H. Yang, and K. J. R. Liu. Green wireless communications: A time-reversal paradigm. *IEEE Journal of Selected Areas in Communications, special issue on Energy-Efficient Wireless Communications*, 29(8):1698–1710, September 2011.

[104] Beibei Wang, Zhu Han, and K. J. R. Liu. Distributed relay selection and power control for multiuser cooperative communication networks using stackelberg game. *IEEE Trans. Mobile Comput.*, 8(7):975–990, July 2009.

[105] Beibei Wang, Yongle Wu, Feng Han, Yu-Han Yang, and K. J. Ray Liu. Green wireless communications: a time-reversal paradigm. *IEEE J. Select. Areas Commun.*, 29(8):1698–1710, Sept 2011.

[106] Beibei Wang, Yongle Wu, and K. J. R. Liu. Game theory for cognitive radio networks: An overview. *Comput. Netw.*, 54(14):2537–2561, October 2010.

[107] Chih-Yu Wang, Yan Chen, and K. J. Ray Liu. Chinese restaurant game. *IEEE Signal Processing Lett.*, 19(12):898–901, Dec. 2012.

[108] Chih-Yu Wang, Yan Chen, and K. J. Ray Liu. Sequential chinese restaurant game. *IEEE Trans. Signal Processing*, 61(3):571–584, Feb. 2013.

[109] Jin-long Wang, Yu-hua Xu, Zhan Gao, and Qi-hui Wu. Discrete-time queuing analysis of opportunistic spectrum access: Single user case. *Frequenz*, 65(11-12):335–341, 2011.

[110] Lusheng Wang and G.-S. Kuo. Mathematical modeling for network selection in heterogeneous wireless networks - a tutorial. *IEEE Communications Surveys Tutorials*, 15(1):271–292, 2013.

[111] Wei Wei, Sharad Jaiswal, Jim Kurose, Don Towsley, Kyoungwon Suh, and Bing Wang. Identifying 802.11 traffic from passive measurements using iterative Bayesian inference. *IEEE/ACM Trans. Netw.*, 20(2):325–338, April 2012.

[112] R.D. Wesel and J.M. Cioffi. Achievable rates for tomlinson-harashima precoding. *IEEE Trans. Inform. Theory*, 44(2):824–831, 1998.

[113] M. B. WILK and R. GNANADESIKAN. Probability plotting methods for the analysis for the analysis of data. *Biometrika*, 55(1):1–17, 1968.

[114] C. Windpassinger, R. F H Fischer, T. Vencel, and J.B. Huber. Precoding in multiantenna and multiuser communications. *IEEE Trans. Wireless Commun.*, 3(4):1305–1316, 2004.

[115] Yongle Wu, Beibei Wang, K. J. R. Liu, and T.C. Clancy. Repeated open spectrum sharing game with cheat-proof strategies. *IEEE Trans. Wireless Commun.*, 8(4):1922–1933, 2009.

[116] Liang Xiao, Yan Chen, W.S. Lin, and K. J. R. Liu. Indirect reciprocity security game for large-scale wireless networks. *IEEE Trans. Inf. Forensics Security*, 7(4):1368–1380, August 2012.

[117] Fengyuan Xu, C.C. Tan, Qun Li, Guanhua Yan, and Jie Wu. Designing a practical access point association protocol. In *Proc. of IEEE INFOCOM*, Mar. 2010.

[118] Y. Xu, A. Anpalagan, Q. Wu, L. Shen, Z. Gao, and J. Wang. Decision-theoretic distributed channel selection for opportunistic spectrum access: Strategies, challenges and solutions. *IEEE Communications Surveys Tutorials*, 2013.

[119] Yuhua Xu, Jinlong Wang, Qihui Wu, A. Anpalagan, and Yu-Dong Yao. Opportunistic spectrum access in cognitive radio networks: Global optimization using local interaction games. *IEEE J. Select. Areas Commun.*, 6(2):180–194, Apr 2012.

[120] Yuhua Xu, Jinlong Wang, Qihui Wu, A. Anpalagan, and Yu-Dong Yao. Opportunistic spectrum access in unknown dynamic environment: A game-theoretic stochastic learning solution. *IEEE Trans. Wireless Commun.*, 11(4):1380–1391, Apr. 2012.

[121] Yu-Han Yang, Y. Chen, C. Jiang, C.-Y. Wang, and K. J. Ray Liu. Wireless access network selection game with negative network externality. *IEEE Trans. Wireless Commun.*, 2013.

[122] Yu-Han Yang, Beibei Wang, W. S. Lin, and K. J. R. Liu. Near-optimal waveform design for sum rate optimization in time-reversal multiuser downlink systems. *IEEE Trans. Wireless Commun.*, 12(1):346–357, Jan 2013.

[123] Qiaoyang Ye, Beiyu Rong, Yudong Chen, M. Al-Shalash, C. Caramanis, and J.G. Andrews. User association for load balancing in heterogeneous cellular networks. *IEEE Trans. Wireless Commun.*, 12(6):2706–2716, 2013.

[124] Wei Yu. Multiuser water-filling in the presence of crosstalk. In *Information Theory and Applications Workshop*, pages 414–420, January 2007.

[125] Wei Yu, Zhu Ji, and K.J.R. Liu. Securing cooperative ad-hoc networks under noise and imperfect monitoring: Strategies and game theoretic analysis. *IEEE Transactions on Information Forensics and Security*, 2(2):240–253, 2007.

[126] Wei Yu and K. J. R. Liu. Game theoretic analysis of cooperation stimulation and security in autonomous mobile ad hoc networks. *IEEE Trans. Mobile Comput.*, 6(5):507–521, 2007.

[127] Wei Yu, David P Varodayan, and John M Cioffi. Trellis and convolutional precoding for transmitter-based interference presubtraction. *IEEE Trans. Commun.*, 53(7):1220–1230, 2005.

[128] Wei Yu, D.P. Varodayan, and J.M. Cioffi. Trellis and convolutional precoding for transmitter-based interference presubtraction. *IEEE Trans. Commun.*, 53(7):1220–1230, 2005.

[129] J. Zander. Performance of optimum transmitter power control in cellular radio systems. *IEEE Trans. Veh. Technol.*, 41(1):57–62, 1992.